UiT
THE ARCTIC UNIVERSITY OF NORWAY

Faculty of Science and Technology

Environmental response to past and recent climate variability in the Trondheimsfjord region, central Norway

A multiproxy geochemical approach

—

Johan C. Faust

A dissertation for the degree of Philosophiae Doctor – July 2014

"Keep your head up,

keep your heart strong"

- Ben Howard

Preface

This thesis is the result of a three year PhD study at the Department of Geology at the University of Tromsø, Norway. It compromises three scientific papers, which were prepared in the period between November 2011 and April 2014 at the Geological Survey of Norway (NGU) in Trondheim. The project was funded by the European Union and was part of the Marie Curie Initial Training Network *CASE* "The Changing Arctic and Subarctic Environment". In addition to intensive training sessions and progress meetings the CASE Network provided close collaboration with eleven other PhD students from nine different European countries at the Universities of Bordeaux, Amsterdam, Plymouth, Tromsø and Kiel. The existent work was also presented at the Goldschmidt conference in Montreal and Florence as well as at the EGU in Vienna. Additionally, The Geological Society provided a travel and accommodation grant for a conference presentation in London, a research award from Iso-Analytical Ltd. supported isotopic analysis, the Research Council of Norway provided a Marie Curie "toppfinansiering" and the Stiftung Mercator, part of the European Campus of Excellence (ECE), offered the participation in the summer school "Climate Change in the Marine Realm" in Bremen and Sylt, Germany.

Acknowledgment

I would like to thank all people who helped and supported me during the last four years. Foremost, I would like to thank my supervisor Dr. Jochen Knies for his great guidance and allowing the freedom to pursue an interesting topic. Thank you for giving me the chance to attend various cruises, conferences and courses. I am very grateful for the opportunity to continue working with you, it will be great!

I would like to express my gratitude to the CASE group for unforgettable days and adventures. Our meetings have always been very inspiring and encouraging. A special thanks goes to Michi, Danish dynamite Christian and Patricia for intense discussions not only about science. Diane and Sarah, of course, big thanks also to you not only for all your help with my Tromsø University organisation problems. Thanks to the principal investigators: Jacques Giraudeau, Simon Belt, Hans Renssen, Katrine Husum, Jochen Knies, Robert Spielhagen, for providing these wonderful and exciting stays, progress meetings and training courses at your institutes. There was always a smile in your face providing support and the confidence that we will all manage to succeed. It was great with all of you.

This PhD study would not have been possible without the help of the NGU and the marine geology group; in particular I have to express my gratitude to Ola Magne Sæther, Rolf Tore Ottesen, Reidulv Bøe, Martin Klug, Anne Liinamaa-Dehls, Karl Fabian, John Naliboff, Benjamin Snook, Magne Vik Bjørkøy, Alenka Černe and Julian Schilling for their interest, stimulating discussions, and many useful comments. Furthermore, I would like to thank Anne Nordtømme, Bjørn Willemoes-Wissing, Clea Elisatbeth Fabian, Melanie Mesli, and Wieslawa Koziel for the great laboratory assistance, their patience, help and support and captain Oddvar Longva, and the crew of the RV Seisma for their professional support during our expeditions.

The group of "young" scientists at the NGU is acknowledged for being such a likable and sociable lot. For sharing numerous fantastic ski trips, bike rides, mountain and fishing tours and social get-togethers that successfully distracted me from my PhD. I would like to thank my local friends and colleagues. I would also like to mention the NGU football team providing so often the highlight of the week. To all my friends I left behind in Germany and elsewhere in Europe thank you very much indeed for not losing the connection and for your constant support.

Thank you Simone for all the help and the hours you spent listening to all my ideas and problems and for reading my stuff, this thesis is also your thesis. And, of course, I wish to

thank my supportive family, Susanne Moebus, Michael Faust, Susanne Würth, Dieter Mazur, Wolfgang Bödecker, Astrid Nahrmann and my brothers Steffen and Anton who provided support and motivation, patiently listened through difficult times during the “PhD race" and making it such a pleasure to come back home.

At last, this work is a contribution to the CASE Initial Training Network funded by the European Community’s 7th Framework Programme FP7 2007/2013, Marie-Curie Actions, under Grant Agreement No. 238111.

Trondheim April 2014

Johan Faust

Table of Contents

1 Introduction

How do natural climate variations affect the environmental conditions on Earth`s different regions? And how sensitive is Earth`s climate to the alteration of its surface and atmosphere by human activity? To answer these basic questions a profound knowledge of the climate system is required which can only be developed by studying long term past climatic changes. However, since climate is the statistical evidence of the average weather over a longer period of time (decades to millions of years) at a certain point (IPCC, 2007) it is not possible to see, feel or directly measure climate. Hence, to estimate climate variabilities over long time scales changes of the internal components of the climate system (air, water, ice, land surfaces and vegetation (Ruddiman, 2001)) are reconstructed by using climate proxies. Thus, it is crucial to identify high-resolution proxy data from key areas characterized by specific climate phenomena where instrumental record data are available to estimate the relative magnitude of past climatic changes (Abrantes et al., 2009).

Norwegian fjords meet all these requirements to decipher past climate signals. Their sediments contain information regarding environmental changes of the hinterland and oceanographic variability on the adjacent continental margins and shelves through water mass exchange (Schafer et al., 1983; Syvitski and Schafer, 1985; Hald et al., 2003; Husum and Hald, 2004; Forwick and Vorren, 2007; Howe et al., 2010; Hald et al., 2011). Moreover, biogenic sedimentation generated in-situ in the fjord through biogeochemical processes and primary productivity can also reflect local and global influences on the environment (Knies et al., 2003; Knies, 2005). General high sedimentation together with the possibility to quantify environmental parameters such as water exchange and freshwater input offer an excellent opportunity for studying land-ocean interactions and can provide ultra-high-resolution records of local responses to short-term variability in the earth's climate (Mikalsen et al., 2001; Kristensen et al., 2004; Paetzel and Dale, 2010).

Apart from the relatively warm northward flowing North Atlantic Current, the Norwegian coastal climate is strongly influenced by the North Atlantic Oscillation (NAO) (e.g. Hurrell, 1995; Dickson et al., 2000; Cherry et al., 2005). This dominant mode of the atmospheric circulation is most pronounced during winter times (Dec-Mar) and is defined as the difference in atmospheric pressure at sea level between the Icelandic low and the Azorean high (Hurrell, 1995). It controls the strength and direction of westerly winds and storm tracks across the North Atlantic (Olsen et al., 2012) and swings between two phases: A positive (negative) NAO generates periods of warmer and wetter (colder and dryer) climate condi-

tions in north-western Europe (e.g. Wanner et al., 2001; Fig. 1). Moreover, its strong impact on precipitation, temperature and wind intensity changes along the Norwegian coast (Ottersen et al., 2001) affects e.g. energy supply and demand, agricultural, fisheries and marine and terrestrial ecological dynamics (Ottersen et al., 2001; Drinkwater et al., 2003; Hurrell et al., 2013).

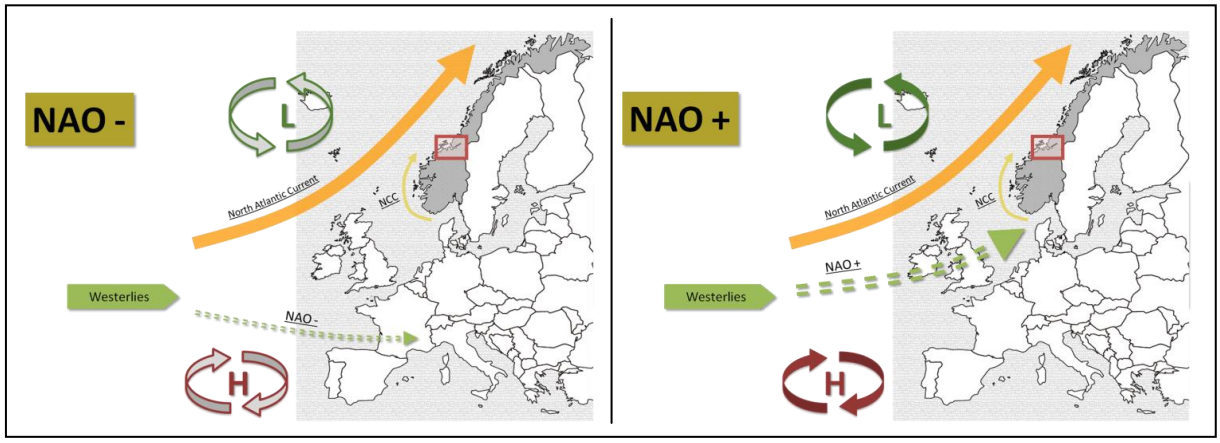

Fig. 1: During a negative NAO phase (left) both, the Azorean high and the Icelandic low are weaker and the Westerlies flow further south which results in colder and drier conditions in Norway. During a positive NAO phase (right), both pressure areas are well developed, the Westerlies are "pushed" further north transporting moisture and heat to Norway resulting in warmer and wetter conditions. The red square is the location of the study area, the Trondheimsfjord. Yellow arrows indicate the North Atlantic Current transporting relative warm water towards the north and the Norwegian Coastal Current (NCC).

To better understand NAO variability and to estimate not only the range of possible fluctuations but also assess their predictability and possible shifts associated with ongoing global warming, long term NAO reconstructions are crucial, but until today rare and often inconsistent (Pinto and Raible, 2012). The general challenges for NAO reconstructions are its possible non-stationarity (a spatial shift of the atmospheric pressure areas) and its strong alteration on very short time scales requiring high resolution (winter) paleoclimatic records which can provide the essential knowledge for its prediction and the quantification of possible anthropogenic induced changes. Reconstructions based on early instrumental and documentary proxy data, tree rings, speleothems, and ice core data gave best results so far (Jones et al., 1997; Appenzeller et al., 1998; Glueck and Stockton, 2001; Luterbacher et al., 2001; Cook et al., 2002; Vinther et al., 2003) but only for the past 950 years (Trouet et al., 2009). Recently, Olsen et al. (2012) extended the NAO record to 5,200 years using a multi-proxy geochemical record from lake sediments in Greenland. However, this record still covers only half the Holocene and needs support from additional studies.

Changes in precipitation and temperature associated with the NAO are assumed to alter the constitution of fluvial sediment flux from land towards ocean basins generated by

weathering and erosion of bedrock and soils (e.g. White and Blum, 1995; Lamy et al., 2001; Govin et al., 2012). Exploring such a relationship between terrigenous input and changes in environmental conditions requires detailed knowledge of the transport mechanisms dominating particle supply (e.g. Zabel et al., 2001). To date no systematic organic and inorganic geochemical investigation of the marine sediments as a basis for long term paleoclimate studies has been conducted in any Norwegian fjord. As for most Norwegian fjords, studies from the Trondheimsfjord in central Norway (Fig. 1 and 2) focus on biological processes (e.g. Haug et al., 1973; Sakshaug and Myklestad, 1973; Børsheim et al., 1999; Sakshaug and Sneli, 2000; Öztürk et al., 2002), sedimentary and mass-wasting processes (Bøe et al., 2003; Bøe et al., 2004; Rise et al., 2006; Lysså et al., 2008; L'Heureux et al., 2009; L'Heureux et al., 2010; Hansen et al., 2011; L'Heureux et al., 2011) and oceanography (Wendelbo, 1970; Jacobson, 1983).

The objective of this PhD project is to (a) detect sources of particular sediment components to identify environmental mechanisms controlling their supply and distribution, (b) to identify geochemical proxies for terrestrial input/river discharge and finally (c) apply these findings on Holocene sequences to reconstruct the variability of the North Atlantic Oscillation (NAO) for the last 2,800 years. For this purpose we establish a multiproxy data set from various sediment cores and surface sediment samples from the Trondheimsfjord and compare the results with instrumental data of air temperature, precipitation and river discharge as well as with geochemical bedrock and overbank sediment data from the adjacent drainage area.

2 Study Area

The Trondheimsfjord

The temperate Trondheimsfjord is located in the central part of Norway (Fig.1 and 2) and, with a length of approximately 135 km, it is the third longest fjord in the country (Jacobson, 1983). Like many fjords, its complex morphology is characterised by relatively wide and shallow areas, narrow trenches and steep slopes, up to 30-40 degrees (Bøe et al., 2003). Three sills, the Agdenes Sill at the entrance (max. 330 m water depth), the Tautra Ridge in the middle section (max. 100 m water depth) and the Skarnsund in the inner part (max. water depth 100 m) divide the Trondheimsfjord into four main basins: Stjørnfjord, Seaward basin, Middle fjord and Beistadfjord (Fig. 2).

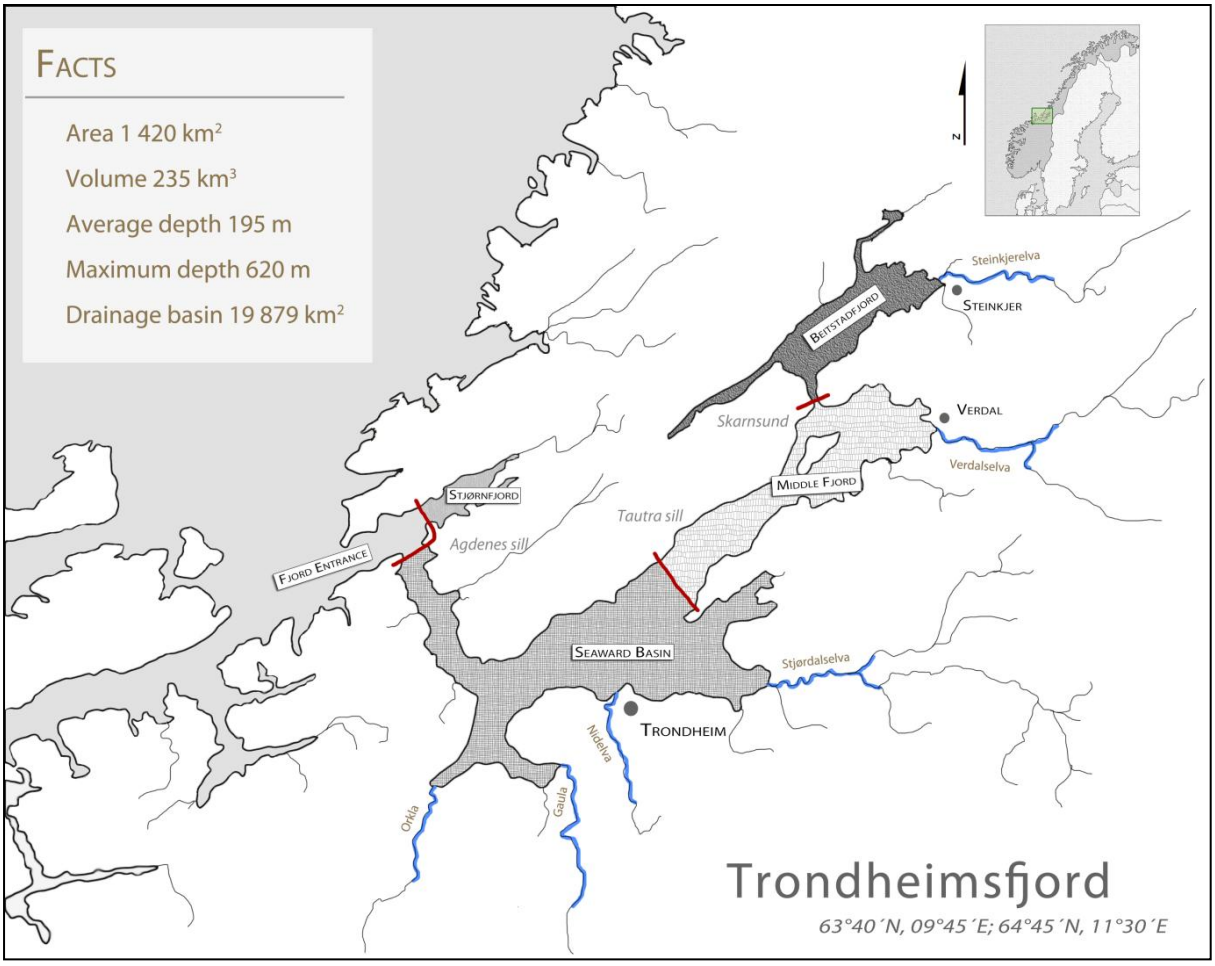

Fig. 2: Map of the Trondheimsfjord showing the three sills (red lines) dividing the fjord into four main basins as well as the six main rivers entering the fjord from the south/southeast. Inset upper right corner: Location of the Trondheimsfjord in central Norway.

The average tide in the Trondheimsfjord is 1.8 m, the average water depth is 165 m and the maximum water depth (620 m) is found at the mouth of the Seaward basin (Sakshaug and Sneli, 2000 and references therein). The total drainage area is approximately 20 000 km^2 (Rise et al., 2006) with a mean precipitation in the north-west area (1700 mm/year) that is twice as high as in the south-east region (855 mm/year). Moreover, the maritime climate in the Trondheimsfjord region is strongly influenced by the North Atlantic Oscillation (NAO) (Wanner et al., 2001), causing warm and wet (+NAO) or cold and dry (-NAO) weather conditions especially during winter times. Additionally, the relative warm (about 7.5°C) Atlantic water flowing into the Trondheimsfjord modulates seasonal air temperatures over the fjord region, resulting in lower (higher) air temperatures in summer (winter) and a strong temperature gradient from the fjord towards the hinterland can be observed, especially during winter months.

Oceanography

In general, interactions between forces governing the fjord circulation, coupled with the complex bottom topography and coastline, result in a complicated flow pattern and distribution of different water masses within the fjord system (Svendsen et al., 2002). The seasonal variation of freshwater supply from the six main rivers entering into the fjord (Gaula, Orkla, Nidelva, Stjørdalselva, Verdalselva and Steinkjerelva; Fig. 2) affect the surface salinity and the three sills hinder a free exchange of water with the open ocean. The water masses in the fjord are, therefore, often stratified and three layers can often be identified (Fig. 3): a brackish water layer on top; an intermediate layer down to the height of the sill

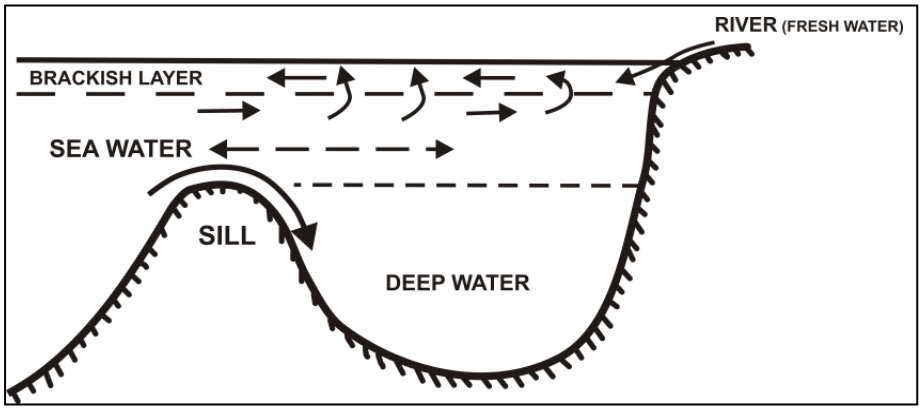

Fig. 3: Sketch of the estuarine circulation of a fjord (modified after Jacobson, 1983)

top and a deep water/basin water layer beneath the sill height which is usually renewed twice a year (Jacobson, 1983). The level of stratification is the balance between the buoyancy flux, set up by the discharge of freshwater, and processes that work to homogenize the water masses such as tidal mixing and wind acting on the surface layer (Syvitski, 1989). The overall water circulation is marked by the outward flowing brackish water above an

inward moving compensating marine current with almost constant temperature and salinity of approximately 7.5°C and 34.8, respectively, around the entire year (Sakshaug and Sneli, 2000). The mixing of these two main currents produces a residual compensating current below the surface layer (Jacobson, 1983). This current system is known as the "estuarine circulation" and is shown schematically in Figure 3.

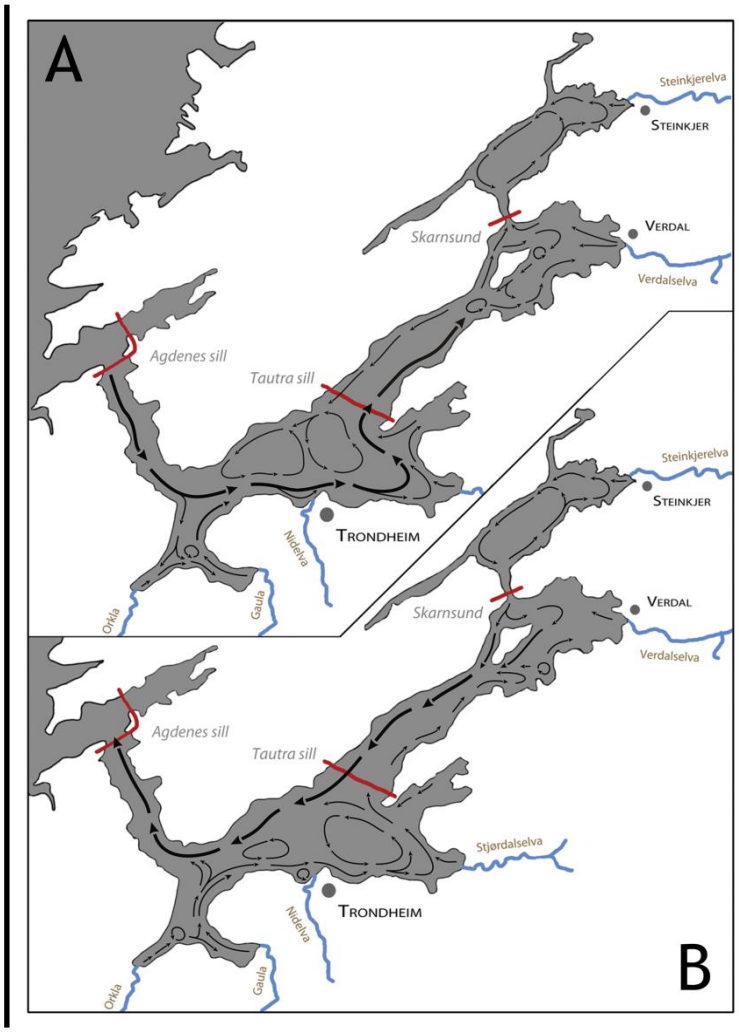

Fig. 4: Surface water circulation pattern during high tide phase A) and low tide phase B) (modified after Jacobson, 1983; and Bierach, 1989).

The Coriolis effect deflects surface currents towards the right, especially in the Seaward basin. Ocean water entering the fjord, therefore, always flows along the south side of the fjord, while outward currents always flow along the north side (Fig. 4). As a result, large volumes of the riverine water recirculate and mix into each basin before leaving the Trondheimsfjord after a residence time of ca. 20 days (Jacobson, 1983).

Sedimentary processes

Depending on the river discharge, which varies with season, rivers can transport all types of grain sizes into the fjords. The coarse component is usually deposited close to the river estuary and the re-sedimentation of these sediments may occur as slide and debris flow

events (Bøe et al., 2003; Bøe et al., 2004; Lyså et al., 2008; L'Heureux et al., 2009; L'Heureux et al., 2010; Hansen et al., 2011; L'Heureux et al., 2011). However, the finest component of the inorganic fraction may be transported over long distances even beyond the fjord. The transport takes place in the brackish surface plume (Fig. 3), above the halocline (Hoskin et al., 1978). Thus, the distance a particle is carried out into the fjord depends on its size, the velocity of the surface current and the stratification of the water column. As mentioned above one of the main causes for the surface-layer velocity is the freshwater discharge. During periods of high discharge e.g. due to the snow melt in spring, the velocity of the fjord's surface water is also high and the water column is well stratified. As a result the suspended material can be transported over long distances. Accordingly, although the fjord is partly very deep, the water masses below the estuarine circulation cell can be described as an energetically relatively low environment and the distribution of sediments within the fjord are, therefore, largely controlled by the circulation in the upper part of the water column (Wendelbo, 1970; Syvitski, 1989).

Geology

The geology in the Trondheimsfjord region is characterised by Caledonian nappes along its south-eastern side, autochthonous Precambrian granitoid gneisses and Caledonian slivers along its north-western side, and a basement window (Tømmerås anticline) exposing Precambrian volcanic rocks near its north-eastern end (Roberts, 1997). The Caledonian nappes belong to the Middle and Upper Allochthon and consist mainly of schist, metagreywacke and ophiolitic greenstone, intruded by gabbroic to tonalitic rocks. During the Quaternary, glaciers eroded deeply into the bedrock, forming a 1100-1300 m deep basin between Trondheim and the Agdenes sill (Rise et al., 2006). The hemipelagic sediments of mostly pre-Holocene age have a maximum thickness of up to 750 m (Bøe et al., 2003; Rise et al., 2006).

3 Materials and methods

The results presented and discussed in this thesis were obtained by extensive, mostly geochemical but also mineralogical and sedimentological analyses of sixty surface sediment samples collected across the entire Trondheimsfjord, plus one entire multicore (MC99-3) and the first five meter of a giant piston core (MD99-2292; see also Bøe et al., 2003) both recovered from the same location in the fjords Seaward Basin (Fig. 2).

Organic carbon, bulk elemental geochemistry and grain size analyses

The elemental composition of the surface- and the multicore sediment samples, retrieved from different multicores sliced in 1 cm intervals, were analysed at the ACME Ltd. laboratory in Vancouver, British Columbia Canada. Determination was performed by inductively coupled plasma atomic emission spectroscopy (ICP-AES) following a four-acid digestion, which is considered to be a total digestion method. Prior to sediment sampling the elemental composition of the sediment core MD99-2292 was measured in 0.5 cm steps using an Avaatech X-ray fluorescence (XRF) core scanner at EPOC, CNRS/University of Bordeaux 1, France. Subsequently, sediment slices (1 cm deep, 1.5 cm wide, 7 cm long) were taken in a 4 cm interval for further analyses.

Analyses for total carbon (TC), total organic carbon (C_{org}) and grain size were performed at the Laboratory of the Geological Survey of Norway (NGU). Weight percentages (wt. %) of C_{org} and TC were determined with a LECO SC-444 and Carbonate content was calculated as $CaCO_3 = (TC - C_{org}) \times 8.33$. The determination of grain size distribution was performed by laser diffraction using a Coulter LS 200 instrument. The analysis was carried out on material within a particle diameter range of 0.4–2000 µm.

Total nitrogen and stable carbon isotope analyses

Total nitrogen (N_{tot} in wt%) was determined using a Carlo Erba NC2500 Isoprime elemental analyzer isotope ratio mass spectrometer at EPOC, CNRS/University of Bordeaux 1, France. The inorganic nitrogen (N_{inorg}) content was analysed on sediment subsamples treated with KOBr-KOH solution to remove organic nitrogen (see Knies et al. (2007) for details) using an EA-IRMS (Iso-Analytical Ltd., UK). The organic proportion of the total nitrogen content was calculated by subtracting the N_{inorg} fraction from N_{tot}. Stable carbon isotopes of the C_{org} fraction ($\delta^{13}C_{org}$) were measured on decarbonated (10 % HCl) aliquots using an EA-IRMS (Iso-Analytical Ltd., UK). $\delta^{13}C_{org}$ values are given in per mil vs. Vienna-PDB.

Bulk mineral assemblage analyses

Bulk mineral assemblages were measured via X-ray diffraction (XRD) using a Philips X'Pert Pro MD, Cu-radiation (k(alpha) 1.541, 45 kV, 40 mA) and X'Celerator detector system at the Central Laboratory for Crystallography and Applied Material Sciences (ZEKAM), University of Bremen, Germany. Quantification of the mineral content was carried out with Quantitative Phase-Analysis with X-ray Powder Diffraction (QUAX) (details are given in Vogt et al., 2002).

Chronology

The chronology of the multicore MC99-3 is based on ^{210}Pb and ^{137}Cs content on neighbouring sediment core in the multi-corer rack (MC99-1). ^{210}Pb and ^{137}Cs measurements were performed in a low background, high efficiency, well-shaped γ-detector at EPOC, CNRS/University of Bordeaux 1, France. According to the age model of Milzer et al. (2013), the sedimentation rate is 0.49 cm/year and the core base age is 1959. The dating error increases gradually down core from ±0.07 to ±3.53 years. As changes in sedimentation rate, degree of sediment compaction, sediment remobilisation as well as biological activity and diffusion can influence the accuracy of the ^{210}Pb analysis, the artificial nuclide ^{137}Cs was used to validate the chronology. Distinct ^{137}Cs increases have been found at core depths of 12.5 cm and 36.5 cm. According to the age model these depths correspond to 1986 (±1.7 yr) and 1963 (±3.4 yr), respectively (Milzer et al., 2013). Hence they are in good agreement with the nuclear weapon tests fallouts (max. in 1963) and the power plant accident of Chernobyl in 1986.

The age model of the upper five meters of the MD99-2292 is based on eight accelerator mass spectrometry (AMS) radiocarbon (^{14}C) date measurements and polynomial regression between the dates. The ^{14}C-AMS dates were determined on carbonate shell material at the Leibniz Laboratory (University of Kiel, Germany) and at the Laboratoire de Mesure du Carbone 14 (Gif sur Yvette Cedex, France). We applied a reservoir correction of 400 years ($\Delta R = 0$) and converted the radiocarbon dates into calibrated years with the Calib 6.0.1 software (Stuiver and Reimer, 1993).

Additional geochemical and instrumental data used

To identify geochemical proxies for terrestrial input and river discharge in the Trondheimsfjord we used two additional geochemical data sets including overbank sediments and bedrock analyses from the drainage area. The bedrock analyses reflects the chemical composition of geological units. Overbank sediments (also called alluvial soil, levée or floodplain sediments) accumulate during active widespread erosion related to flooding episodes. They

are considered to represent the average lithological input of a whole catchment area upstream from the sampling site (Ottesen et al., 1989).

In order to compare our results with the recent climate variability, seasonal and annual mean air temperature and precipitation records for the Trondheimsfjord region since 1900 were obtained from the Norwegian Meteorological Institute (www.eklima.no). Moreover, time series (1963 - present) of river discharge for the six largest rivers entering the Trondheimsfjord, Gaula, Orkla, Nidelva, Stjørdalselva, Verdalselva and Steinkjerelva (Fig. 2) were obtained from the Norwegian Water Resource and Energy Directorate (www.nve.no).

4 Summary of papers

Paper I

Faust, J.C., Knies, J., Slagstad, T., Vogt, C., Milzer, G., Giraudeau, J., (in review). **Geochemical composition of Trondheimsfjord surface sediments: Sources and spatial variability of marine and terrigenous components.** *Continental Shelf Research*

This first paper aims to investigate the inorganic/organic geochemistry of surface sediments and to identify geochemical proxies for terrestrial input and river discharge in the Trondheimsfjord, central Norway. Sixty evenly distributed surface sediment samples were analysed for their elemental composition, total organic carbon (C_{org}), nitrogen (N_{org}) and organic carbon stable isotopes ($\delta^{13}C_{org}$), bulk mineral composition and grain size distribution. The results indicate carbonate marine productivity to be the main $CaCO_3$ source. A strong decreasing gradient of marine-derived organic matter from the entrance towards the fjord inner part is consistent with modern primary production data. We show that the origin of the organic matter, as well as the distribution of $CaCO_3$ in Trondheimsfjord sediments can be used as a proxy for the variable inflow of Atlantic water and changes in river runoff. Furthermore, the comparison of grain size independent Al-based trace element ratios with geochemical analyses from terrigenous sediments and bedrocks provides evidence that the distribution of K/Al, Ni/Al and K/Ni in the fjord sediments reflecte regional sources of K and Ni in the northern and southern drainage basin of the Trondheimsfjord, respectively. We propose that the application of these findings to temporally well-constrained sediment records will provide a robust reconstruction of past climate changes in central Norway and potentially illuminate both the variability of the North Atlantic Current and the North Atlantic Oscillation since the last deglaciation.

Paper II

Faust, J.C., Knies, J., Milzer, G., Giraudeau, J., (in review). **Terrigenous input to a fjord in central Norway records the environmental response to the North Atlantic Oscillation over the past 50 years**. *The Holocene*

In the second paper we examine instrumental time series and show that the dominant mode of the atmospheric circulation in the North Atlantic region, the North Atlantic Oscillation (NAO), has a strong impact on river discharge, temperature, and precipitation in central Norway. In addition, elemental composition analysis of a short sediment core re-

veals that from 1959 to 2010 winter precipitation and temperature changes are recorded by changes in the inorganic geochemical composition of Trondheimsfjord sediments. Elemental ratios of Al/Zr and K/Ni in the sediment core MC99-3 show a close relation to small scale, high frequency climate variations and large-scale changes in the Northern Hemisphere climate. Thus, terrigenous input and related erosional processes in the fjord hinterland are highly sensitive to atmospheric circulation variability in the North Atlantic region. A comparison between the elemental ratio of Al/Zr and NAO records derived from ice accumulation rates of Norwegian glaciers, western Greenland ice sheets and river discharge anomalies in the Eurasian Arctic, supports our assumption that it is possible to reconstruct long term NAO variations from sedimentary archives in central Norwegian fjords.

Paper III

Faust, J.C., Fabian, K., Milzer, G., Giraudeau, J. Knies, J., (in prep.). **North Atlantic Oscillation dynamics recorded in central Norwegian fjord sediments during the past 2800 years**. To be submitted to Nature Geos*cience*

The objective of the third paper is to establish the first reconstruction of the North Atlantic Oscillation from marine sediments. By comparing geochemical measurements from a short sediment core from the Trondheimsfjord, central Norway with instrumental data we show that marine primary productivity proxies are sensitive to NAO changes during the past 50 years. This result is used to link a 2800 years paleoproductivity record to a reliable 500-year long winter NAO reconstruction based on early instrumental and documentary proxy data and establish a late Holocene high resolution NAO record. We show that NAO variabilities coincide with climatically associated changes in paleo-demographics, northern hemisphere (NH) glacier advances and compared to the recent (300 years or so) NAO variabilities positive/negative phases are more persistent. Furthermore, a strong volcanic eruption may have induced the onset of the Little Ice Age (LIA), which is marked by a rapid transition from a stable positive to a stable negative NAO phase.

5 Synthesis

Fjord deposits have a great potential for providing high-resolution sedimentary records that reflect local terrestrial and marine processes and, therefore, offer unique opportunities for the investigation of sedimentological and geochemical climatically induced processes. However, the complexity of fjord systems in terms of bathymetry, oceanography and sedimentary processes requires a profound knowledge of the fjord constitution before starting to interpret climatic signals in Holocene sediment sequences. For this reason, we first attempt to provide a comprehensive overview of the Trondheimsfjord environmental system by applying a geochemical multiproxy analysis on sixty surface sediment samples and compare our findings with available geochemical data from the fjords drainage area. Next, we use the gained knowledge to identify possible organic and inorganic geochemical climate proxies. The consistency of these proxies is evident from a fifty year long geochemical record paralleled with instrumental data of regional temperature, precipitation, river discharge and the NAO. The ultimate result is the first high resolution NAO reconstruction established on marine sediments based on a 2,800 year long paleoproductivity record.

The main conclusions of this study are:

- The inorganic geochemical composition of Trondheimsfjord sediments reflects regional differences in the geology of the terrestrial source area. Specifically, greenstones and metagreywackes located along the southern side of the fjord are the main Ni source in Trondheimsfjord sediments. Thus, Ni enters the Trondheimsfjord mainly via the rivers Orkla, Gaula and Nidelva directly into the Seaward Basin. On the other hand, K and Zr originate largely from Precambrian felsic volcanic rocks related to a tectonic window called *Tømmerås anticline* (see Roberts, 1997 for details) in the north-eastern hinterland.
- Changes in the inorganic geochemical composition of the Trondheimsfjord sediments are closely related to the variability of Trondheimsfjord regional winter-spring river runoff, winter air temperature and precipitation which in turn are strongly related to changes of the NAO. In particular, K, Ni, Zr and Al are proxies for temporal changes in the supply of terrigenous material induced by river runoff, air temperature and precipitation and record both small scale, high frequency, and large scale long term shifts in Northern Hemisphere climate.

- Due to its strong impact on changes of wind, temperature and precipitation in Norway the NAO strongly affects marine primary productivity changes within the Trondheimsfjord. Hence, marine primary productivity proxies such as Ca and $CaCO_3$ can be used to reconstruct NAO variability.
- Finally, the NAO reconstruction based on marine primary productivity changes reveals that late Holocene NAO variability coincides with climatically associated changes in paleo-demographics, and Northern Hemisphere glacier advances. Furthermore, a strong volcanic eruption may have induced the onset of the Little Ice Age, which is marked by a rapid transition from a stable positive to a stable negative NAO phase.

6 Outlook

This study shows that Trondheimsfjord sediments have a great potential for high resolution climate reconstruction. Further investigations should focus on the inorganic geochemical climate proxies presented in this study and test their reliability for long term reconstructions. In this context, a detailed elemental source to sink study in the Trondheimsfjord region could provide important knowledge about the transport mechanisms of individual elements from the hinterland into the fjord. Among others, this would help to identify the response time of the different proxies and provide a better understanding of the seasonal variation of the sediment supply from the main rivers entering the fjord.

Long-term observation of primary productivity in the Trondheimsfjord could reveal seasonal and NAO induced changes in more detail. Furthermore, a detailed study of the connection between planktic and benthic marine productivity and their relation to $CaCO_3$ production and sedimentation could help to provide a better understanding of the proposed link between NAO and $CaCO_3$ in Trondheimsfjord sediments.

Moreover, Trondheimsfjord sediments should be used to expand the NAO record for the entire Holocene. Also, the application of physical modeling studies of the NAO could help to constrain potential triggers and main amplifiers for the reconstructed large scale climatic changes.

As shown in this study, fjord sediments provide the possibility to unveil past atmospheric processes. Hence, further investigations of fjord sediments from other parts of the world may reveal other atmospheric modes for example the NAO related Arctic Oscillation (AO). By combining the findings from different fjords from different continents past atmospheric changes can be revealed on a global scale.

7 References

Abrantes F., Lopes C., Rodrigues T., Gil I., Witt L., Grimalt J. and Harris I. (2009) Proxy calibration to instrumental data set: Implications for paleoceanographic reconstructions. *Geochemistry, Geophysics, Geosystems* **10**.

Appenzeller C., Stocker T.F. and Anklin M. (1998) North Atlantic oscillation dynamics recorded in Greenland ice cores. *Science* **282**, 446-449.

Bøe R., Rise L., Blikra L.H., Longva O. and Eide A. (2003) Holocene mass-movement processes in Trondheimsfjorden, Central Norway. *Norw J Geol* **83**, 3-22.

Bøe R., Bugge T., Rise L., Eidnes G., Eide A. and Mauring E. (2004) Erosional channel incision and the origin of large sediment waves in Trondheimsfjorden, central Norway. *Geo-Mar Lett* **24**, 225-240.

Børsheim K.Y., Myklestad S.M. and Sneli J.-A. (1999) Monthly profiles of DOC, mono- and polysaccharides at two locations in the Trondheimsfjord (Norway) during two years. *Mar Chem* **63**, 255-272.

Cherry J., Cullen H., Visbeck M., Small A. and Uvo C. (2005) Impacts of the North Atlantic Oscillation on Scandinavian hydropower production and energy markets. *Water Resour Manag* **19**, 673-691.

Cook E.R., D'Arrigo R.D. and Mann M.E. (2002) A Well-Verified, Multiproxy Reconstruction of the Winter North Atlantic Oscillation Index since a.d. 1400*. *J Climate* **15**, 1754-1764.

Dickson R.R., Osborn T.J., Hurrell J.W., Meincke J., Blindheim J., Adlandsvik B., Vinje T., Alekseev G. and Maslowski W. (2000) The Arctic Ocean response to the North Atlantic oscillation. *J Climate* **13**, 2671-2696.

Drinkwater K.F., Belgrano A., Borja A., Conversi A., Edwards M., Greene C.H., Ottersen G., Pershing A.J. and Walker H. (2003) the response of marine ecosystems to climate variability associated with the North Atlantic Oscillation. The North Atlantic Oscillation: Climatic Significance and Environmental Impact. *AGU*, Washington, DC, pp. 211-234.

Forwick M. and Vorren T.O. (2007) Holocene mass-transport activity and climate in outer Isfjorden, Spitsbergen: marine and subsurface evidence. *Holocene* **17**, 707-716.

Glueck M.F. and Stockton C.W. (2001) Reconstruction of the North Atlantic Oscillation, 1429-1983. *Int J Climatol* **21**, 1453-1465.

Govin A., Holzwarth U., Heslop D., Ford Keeling L., Zabel M., Mulitza S., Collins J.A. and Chiessi C.M. (2012) Distribution of major elements in Atlantic surface sediments (36°N–49°S): Imprint of terrigenous input and continental weathering. *Geochem Geophy Geosy* **13**.

Hald M., Husum K., Vorren T.O., Grosfjeld K., Jensen H.B. and Sharapova A. (2003) Holocene climate in the subarctic fjord Malangen, northern Norway: a multi-proxy study. *Boreas* **32**, 543-559.

Hald M., Salomonsen G.R., Husum K. and Wilson L.J. (2011) A 2000 year record of Atlantic Water temperature variability from the Malangen Fjord, northeastern North Atlantic. *The Holocene* **21**, 1049-1059.

Hansen L., L'Heureux J.S. and Longva O. (2011) Turbiditic, clay-rich event beds in fjord-marine deposits caused by landslides in emerging clay deposits -

palaeoenvironmental interpretation and role for submarine mass-wasting. *Sedimentology* **58**, 890-915.

Haug A., Myklestad S. and Sakshaug E. (1973) Studies on the phytoplankton ecology of the Trondheimsfjord. I. The chemical composition of phytoplankton populations. *Journal of Experimental Marine Biology and Ecology* **11**, 15-26.

Hoskin C.M., Burrell D.C. and Freitag G.R. (1978) Suspended sediment dynamics in Blue Fjord, western Prince William Sound, Alaska. *Estuarine and Coastal Marine Science* **7**, 1-16.

Howe J.A., Austin W.E.N., Forwick M., Paetzel M., Harland R. and Cage A.G. (2010) Fjord systems and archives: a review. *Geological Society, London, Special Publications* **344**, 5-15.

Hurrell J.W. (1995) Decadal Trends in the North-Atlantic Oscillation - Regional Temperatures and Precipitation. *Science* **269**, 676-679.

Hurrell J.W., Kushnir Y., Ottersen G. and Visbeck M. (2013) An Overview of the North Atlantic Oscillation. The North Atlantic Oscillation: Climatic Significance and Environmental Impact. *American Geophysical Union*, pp. 1-35.

Husum K. and Hald M. (2004) A continuous marine record 8000-1600 cal. yr BP from the Malangenfjord, north Norway: foraminiferal and isotopic evidence. *Holocene* **14**, 877-887.

IPCC (2007) Summary for Policymakers. in: Solomon, S., D. Qin, M. Manning, Z. Chen, M. Marquis, K.B. Averyt, M.Tignor and H.L. Miller (Ed.), Climate Change 2007: The Physical Science Basis. Contribution of Working Group I to the Fourth Assessment Report of the Intergovernmental Panel on Climate Change. *Cambridge University Press*, Cambridge, United Kingdom and New York, NY, USA.

Jacobson P. (1983) Physical oceanography of the Trondheimsfjord. *Geophysical & Astrophysical Fluid Dynamics* **26**, 3-26.

Jones P.D., Jonsson T. and Wheeler D. (1997) Extension to the North Atlantic Oscillation using early instrumental pressure observations from Gibraltar and south-west Iceland. *Int J Climatol* **17**, 1433-1450.

Knies J., Hald M., Ebbesen H., Mann U. and Vogt C. (2003) A deglacial–middle Holocene record of biogenic sedimentation and paleoproductivity changes from the northern Norwegian continental shelf. *Paleoceanography* **18**, 1096.

Knies J. (2005) Climate-induced changes in sedimentary regimes for organic matter supply on the continental shelf off northern Norway. *Geochim Cosmochim Ac* **69**, 4631-4647.

Knies J., Brookes S. and Schubert C.J. (2007) Re-assessing the nitrogen signal in continental margin sediments: New insights from the high northern latitudes. *Earth Planet Sc Lett* **253**, 471-484.

Koistinen T., Stephens M.B., Bogatchev V., Nordgulen Ø., Wennerström M. and Korhonen J. (2001) Geological Map of the Fennoscandian Shield, scale: 1: 2,000,000. *Geological Survey of Finland, Norway and Sweden and the North-West Department of Natural Resources of Russia*.

Kristensen D.K., Sejrup H.P., Haflidason H., Berstad I.M. and Mikalsen G. (2004) Eight-hundred-year temperature variability from the Norwegian continental margin and the North Atlantic thermohaline circulation. *Paleoceanography* **19**.

L'Heureux J.S., Hansen L. and Longva O. (2009) Development of the submarine channel in front of the Nidelva River, Trondheimsfjorden, Norway. *Mar Geol* **260**, 30-44.

L'Heureux J.S., Hansen L., Longva O., Emdal A. and Grande L.O. (2010) A multidisciplinary study of submarine landslides at the Nidelva fjord delta, Central Norway - Implications for geohazard assessment. *Norw J Geol* **90**, 1-20.

L'Heureux J.S., Glimsdal S., Longva O., Hansen L. and Harbitz C.B. (2011) The 1888 shoreline landslide and tsunami in Trondheimsfjorden, central Norway. *Mar Geophys Res* **32**, 313-329.

Lamy F., Hebbeln D., Rohl U. and Wefer G. (2001) Holocene rainfall variability in southern Chile: a marine record of latitudinal shifts of the Southern Westerlies. *Earth Planet Sc Lett* **185**, 369-382.

Luterbacher J., Xoplaki E., Dietrich D., Jones P.D., Davies T.D., Portis D., Gonzalez-Rouco J.F., von Storch H., Gyalistras D., Casty C. and Wanner H. (2001) Extending North Atlantic Oscillation reconstructions back to 1500. *Atmos Sci Lett* **2**, 114-124.

Lyså A., Hansen L., Christensen O., L'Heureux J.S., Longva O., Olsen H.A. and Sveian H. (2008) Landscape evolution and slide processes in a glacioisostatic rebound area; a combined marine and terrestrial approach. *Mar Geol* **248**, 53-73.

Mikalsen G., Sejrup H.P. and Aarseth I. (2001) Late-Holocene changes in ocean circulation and climate: foraminiferal and isotopic evidence from Sulafjord, western Norway. *Holocene* **11**, 437-446.

Milzer G., Giraudeau J., Schmidt S., Eynaud F. and Faust J. (2013) Qualitative and quantitative reconstruction of surface water characteristics and recent hydrographic changes in the Trondheimsfjord, central Norway. *Clim. Past Discuss.* **9**, 4553-4598.

Olsen J., Anderson N.J. and Knudsen M.F. (2012) Variability of the North Atlantic Oscillation over the past 5,200 years. *Nat Geosci* **5**, 808-812.

Ottersen G., Planque B., Belgrano A., Post E., Reid P. and Stenseth N. (2001) Ecological effects of the North Atlantic Oscillation. *Oecologia* **128**, 1-14.

Ottesen R.T., Bogen J., Bølviken B. and Volden T. (1989) Overbank sediment: a representative sample medium for regional geochemical mapping. *Journal of Geochemical Exploration* **32**, 257-277.

Paetzel M. and Dale T. (2010) Climate proxies for recent fjord sediments in the inner Sognefjord region, western Norway. *Geological Society, London, Special Publications* **344**, 271-288.

Pinto J.G. and Raible C.C. (2012) Past and recent changes in the North Atlantic oscillation. *Wires Clim Change* **3**, 79-90.

Rise L., Bøe R., Sveian H., Lyså A. and Olsen H.A. (2006) The deglaciation history of Trondheimsfjorden and Trondheimsleia, Central Norway. *Norw J Geol* **86**, 415-434.

Roberts D. (1997) Geochemistry of Palaeoproterozoic porphyritic felsic volcanites from the olden and Tømmerås windows, central Norway. *GFF* **119**, 141-148.

Ruddiman W.F. (2001) Earth's Climate: Past and Future. *W. H. Freeman and Company*, New York.

Sakshaug E. and Myklestad S. (1973) Studies on the phytoplankton ecology of the trondheimsfjord. III. Dynamics of phytoplankton blooms in relation to environmental factors, bioassay experiments and parameters for the physiological state of the populations. *Journal of Experimental Marine Biology and Ecology* **11**, 157-188.

Sakshaug E. and Sneli J.-A. (2000) Trondheimsfjorden. *Tapir Forlag*, Trondheim.

Schafer C.T., Smith J.N. and Seibert G. (1983) Significance of natural and anthropogenic sediment inputs to the saguenay Fjord, Quebec. *Sediment Geol* **36**, 177-194.

Stuiver M. and Reimer P.J. (1993) Extended 14C data base and revised CALIB 3.0 14C age calibration program. *Radiocarbon* **35**, 215-230.

Svendsen H., Beszczynska-Møller A., Hagen J.O., Lefauconnier B., Tverberg V., Gerland S., Ørbøk J.B., Bischof K., Papucci C., Zajaczkowski M., Azzolini R., Bruland O., Wiencke C., Winther J.-G. and Dallmann W. (2002) The physical environment of Kongsfjorden–Krossfjorden, an Arctic fjord system in Svalbard. *Polar Res* **21**, 133-166.

Syvitski J. and Schafer C.T. (1985) Sedimentology of Arctic Fjords Experiment (SAFE): Project Introduction. *Arctic* **38**, 264-270.

Syvitski J.P.M. (1989) On the deposition of sediment within glacier-influenced fjords: Oceanographic controls. *Mar Geol* **85**, 301-329.

Trouet V., Esper J., Graham N.E., Baker A., Scourse J.D. and Frank D.C. (2009) Persistent Positive North Atlantic Oscillation Mode Dominated the Medieval Climate Anomaly. *Science* **324**, 78-80.

Vinther B.M., Johnsen S.J., Andersen K.K., Clausen H.B. and Hansen A.W. (2003) NAO signal recorded in the stable isotopes of Greenland ice cores. *Geophys Res Lett* **30**.

Vogt C., Lauterjung J. and Fischer R.X. (2002) Investigation of the Clay Fraction (<2µm) of the Clay Minerals Society Reference Clays. *Clays and Clay Minerals* **50**, 388-400.

Wanner H., Brönnimann S., Casty C., Gyalistras D., Luterbacher J., Schmutz C., Stephenson D. and Xoplaki E. (2001) North Atlantic Oscillation – Concepts And Studies. *Surveys in Geophysics* **22**, 321-381.

Wendelbo P.S. (1970) Hydrografiske forhold i Trondheimsfjorden 1963-66. PhD Thesis, University of Oslo

White A.F. and Blum A.E. (1995) Effects of Climate on Chemical-Weathering in Watersheds. *Geochim Cosmochim Ac* **59**, 1729-1747.

Zabel M., Schneider R.R., Wagner T., Adegbie A.T., de Vries U. and Kolonic S. (2001) Late Quaternary climate changes in central Africa as inferred from terrigenous input to the Niger fan. *Quaternary Res* **56**, 207-217.

Öztürk M., Steinnes E. and Sakshaug E. (2002) Iron speciation in the Trondheim fjord from the perspective of iron limitation for phytoplankton. *Estuar Coast Shelf S* **55**, 197-212.

Paper I

Faust, J.C., Knies, J., Slagstad, T., Vogt, C., Milzer, G., Giraudeau, J., (in review). Geochemical composition of Trondheimsfjord surface sediments: Sources and spatial variability of marine and terrigenous components. Submitted to Continental Shelf Research, 01.03.2014

Geochemical composition of Trondheimsfjord surface sediments: Sources and spatial variability of marine and terrigenous components

Johan C. Faust [a, b, *], Jochen Knies [a], Trond Slagstad [a], Christoph Vogt [c], Gesa Milzer [d], Jacques Giraudeau [d]

[a] Geological Survey of Norway, 7491 Trondheim, Norway
[b] University of Tromsø, Department of Geology, 9011 Tromsø, Norway
[c] Crystallography/ZEKAM, Geosciences, University of Bremen, 28334 Bremen, Germany
[d] Universite Bordeaux 1 UMR CNRS 5805 EPOC, 33405 Talence cedex , France

*Corresponding author: Norges geologiske undersøkelse /Geological Survey of Norway (NGU), Marine Geology, Postboks 6315 Sluppen, 7491 Trondheim, Norway. Tel.: +47 7390 4000. E-mail address: jfaust@uni-bremen.de (J. Faust).

Keywords: Trondheimsfjord, surface sediments, Norway, fjord environment, stable isotopes, carbon, nitrogen, elemental composition, terrigenous input, marine input, inorganic organic geochemistry

Abstract

High sedimentation rates in fjords provide excellent possibilities for high resolution sedimentary and geochemical records over the Holocene. As a baseline for an improved interpretation of geochemical data from fjord sediment cores, this study aims to investigate the inorganic/organic geochemistry of surface sediments and to identify geochemical proxies for terrestrial input and river discharge in the Trondheimsfjord, central Norway. Sixty evenly distributed surface sediment samples were analysed for their elemental composition, total organic carbon (C_{org}), nitrogen (N_{org}) and organic carbon stable isotopes ($\delta^{13}C_{org}$), bulk mineral composition and grain size distribution. Our results indicate carbonate marine productivity to be the main $CaCO_3$ source. Also, a strong decreasing gradient of marine-derived organic matter from the entrance towards the fjord inner part is consistent with modern primary production data. We show that the origin of the organic matter as well as the distribution of $CaCO_3$ in Trondheimsfjord sediments can be used as a proxy for the variable inflow of Atlantic water and changes in river runoff. Furthermore, the comparison of

grain size independent Al-based trace element ratios with geochemical analysis from terrigenous sediments and bedrocks provides evidence that the distribution of K/Al, Ni/Al and K/Ni in the fjord sediments reflect regional sources of K and Ni in the northern and southern drainage basin of the Trondheimsfjord. Applying these findings to temporally well-constrained sediment records will provide important insights into both the palaeoenvironmental changes of the hinterland and the palaeoceanographic modifications in the Norwegian Sea as response to rapid climate changes and associated feedback mechanisms.

1. Introduction

In general, fjords are ideal places to study modern and past environmental and climate changes (Syvitski et al., 1987). The sediments delivered to fjords contain information regarding environmental changes of the hinterland and oceanographic variability on the adjacent continental margins and shelves through water mass exchange (e.g. Schafer et al., 1983; Syvitski and Schafer, 1985; Howe et al., 2010). Moreover, biogenic sedimentation generated in-situ in the fjord through biogeochemical processes and primary productivity can also reflect local and global influences on the environment. As such, sediments accumulating in fjords offer an excellent opportunity for studying land-ocean interactions and can provide ultra-high-resolution records of local responses to short-term variability in the earth's climate.

Before deciphering the past climate signals in the sedimentary record, however, it is important to understand the modern depositional environment within the fjords (Inall and Gillibrand, 2010). Here, we investigate the environmental constraints in the

Trondheimsfjord, central Norway, based on sixty surface sediment samples from the entire Trondheimsfjord (Fig. 1). We used these samples to study the modern geochemical and sedimentological processes that occur within the fjord and to identify possible proxies for past environmental changes. For these purposes, we analysed all surface sediment samples for elemental composition, total organic carbon (C_{org}) and total organic nitrogen (N_{org}) content, organic carbon stable isotopes ($\delta^{13}C_{org}$), bulk mineral composition and grain size distribution. To the best of our knowledge, no similar systematic organic and inorganic geochemical investigation of fjord surface sediments as a basis for long term palaeoclimate studies has been conducted in the Trondheimsfjord or in any other Norwegian fjord.

To gain a better understanding of the modern environmental system, numerous studies have focused on the contribution of organic carbon (e.g. Sargent et al., 1983; Goñi et al., 1997; Winkelmann and Knies, 2005; Knies and Martinez, 2009) and trace elements (Hirst, 1962; Calvert et al., 1993; Hayes, 1993; Cho et al., 1999; Karageorgis et al., 2005; Govin et al., 2012) to identify marine/terrigenous sources of shelf and open ocean surface sediments. In particular, Sepúlveda et al. (2011) and Bertrand et al. (2012) conducted inorganic and organic geochemical surveys on surface sediments obtained from fjords in northern Patagonia, Chile. They reported a significant influence from freshwater inflow on their geochemical composition and a decreasing gradient of terrigenous-derived organic- and inorganic material from the inner fjords towards the open ocean. Further, Sepúlveda et al. (2011) and Bertrand et al. (2012) argued that fjords may be an important CO_2 sink and that Al-based elemental ratios are suitable proxies for estimating temporal variations in river discharge. In the current study, we took a high spatial surface sediment sample distribution and combined our results with geochemical and geological field mapping datasets from the

drainage area of the Trondheimsfjord. We aim to detect sources of particular sediment components and to better identify environmental mechanisms controlling their supply and distribution in the Trondheimsfjord. Further, by using this multiproxy approach to obtain a better understanding of the modern environmental conditions in the Trondheimsfjord area, new baseline knowledge is provided for future applications on Holocene sequences to reconstruct the variability of the North Atlantic Oscillation (NAO) and the North Atlantic Current (NAC) for the last 10,000 years.

2. Study area

The temperate Trondheimsfjord is located in the central part of Norway (Fig.1) and, with a length of approximately 135 km, it is the third longest fjord in the country (Jacobson, 1983). Like many fjords, its complex morphology is characterised by relatively wide and shallow areas, narrow trenches and steep slopes, up to 30-40 degrees (Bøe et al., 2003). Three sills, the Agdenes Sill at the entrance (max. 330 m water depth), the Tautra Ridge in the middle section (max. 100 m water depth) and the Skarnsund in the inner part (max. water depth 100 m) divide the Trondheimsfjord into four main basins: Stjørnfjord, Seaward basin, Middle fjord and Beistadfjord (Fig. 1) (For detailed maps of bathymetry and topography of the drainage area, we refer to http://kart.statkart.no). The average tide in the Trondheimsfjord is 1.8 m, the average water depth is 165 m and the maximum water depth (620 m) is found at the mouth of the Seaward basin (Sakshaug and Sneli, 2000 and references therein).

The maritime climate in the Trondheimsfjord region is strongly influenced by the NAO (Wanner et al., 2001), causing warm and wet (+NAO) or cold and dry (-NAO) weather

conditions especially during winter times. The Atlantic water flowing into Trondheimsfjord display temperatures and salinity of approximately 7.5°C and 34.8, respectively, around the entire year (Sakshaug and Sneli, 2000). It modulates seasonal air temperatures over the fjord region, resulting in lower (higher) air temperatures in summer (winter) and a strong temperature gradient from the fjord towards the hinterland is observed, especially during winter months. The total drainage area is approximately 20 000 km^2 (Rise et al., 2006) with a mean precipitation in the north-west area (1700 mm/year) that is twice as high as in the south-east region (855 mm/year). Glaciers are not present in the drainage area and the annual precipitation is strongly correlated to the river discharge (Sakshaug and Sneli, 2000) of the six main rivers enter into the fjord: Gaula, Orkla, Nidelva, Stjørdalselva, Verdalselva and Steinkjerelva (Fig. 1). The freshwater supply from these rivers decreases the surface salinity and initiates an estuarine circulation, which is a typical surface circulation system for fjords (Jacobson, 1983). The Coriolis effect deflects surface currents towards the right, especially in the Seaward basin. Ocean water entering the fjord, therefore, always flows along the south side of the fjord, while outward currents always flow along the north side (Fig. 1). As a result large volumes of the riverine water recirculate and mix into each basin before leaving the Trondheimsfjord after a residence time of ca. 20 days (Jacobson, 1983). Although the fjord is partly very deep, the water masses below the estuarine circulation cell can be described as an energetically relatively low environment and the distributions of sediments within the fjord are, therefore, largely controlled by the circulation in the upper part of the water column (Wendelbo, 1970; Syvitski, 1989). Deeper water masses are usually renewed twice a year (Jacobson, 1983) and there is no observation of sub- or anoxic conditions in the fjord.

The geology in the Trondheimsfjord region (Fig. 2) is characterized by Caledonian nappes along its southeastern side, autochthonous Precambrian granitoid gneisses and Caledonian slivers along its northwestern side, and a basement window (Tømmerås anticline) exposing Precambrian volcanic rocks near its northeastern end (Roberts, 1997). The Caledonian nappes belong to the Middle and Upper Allochthon and consist mainly of schist, metagreywacke and ophiolitic greenstone, intruded by gabbroic to tonalitic rocks. During the Quaternary, glaciers eroded deeply into the bedrock, forming a 1100-1300 m deep basin between Trondheim and the Agdenes sill (Rise et al., 2006). The hemipelagic sediments of mostly pre-Holocene age have a maximum thickness of up to 750 m (Bøe et al., 2003; Rise et al., 2006). Moreover, numerous slide and debris flow events have affected the fjord during the Holocene (Bøe et al., 2003; Bøe et al., 2004; Lyså et al., 2008; L'Heureux et al., 2009; L'Heureux et al., 2010; Hansen et al., 2011; L'Heureux et al., 2011).

3. Material and Methods

3.1 Fjord surface sediments: Sampling and preparation

In April 2011, sixty surface sediment samples were collected at water depths between 25 and 605 m across the entire Trondheimsfjord (63°40´N, 09°45´E, 64°45´N, 11°30´E) (Fig. 1 and Tab. S1). The first centimetre of multicores (5.5 cm diameter) collected from each sampling location was sampled aboard the research vessel "FF Seisma" and stored in plastic bags at -18°C. Prior to further analyses, all samples were freeze-dried and, except for grain size measurements, homogenised through grinding using a Fritsch Micro Mill PULVERISETTE 7 with agate grinding bowls and balls for 1-2 minutes at a speed of 250 rotations per minute.

3.2. Organic carbon, bulk elemental geochemistry and grain size analyses

35 elements (Al, Ti, Na, Mg, Ba, Ca, Zr, Ni, Fe, Cu, Pb, Sr, Zn, Ag, Co, Mn, As, U, Th, Cd, Sb, Bi, V, P, La, Cr, K, W, Sn, Y, Nb, Mo, Be, Sc, S) were analysed at the ACME Ltd laboratory in Vancouver, British Columbia Canada. Determination was performed by inductively coupled plasma atomic emission spectroscopy (ICP-AES) following a four-acid digestion which is considered to be a total digestion method. 250 mg of each sample is heated (200°C) in a mixture of H_2O-HF-$HClO_4$-HNO_3 (2:2:1:1) to fuming and taken to dryness. The residue is dissolved in hydrochloric acid (50 %). The analytical quality was calculated by duplicate analyses of every 20 samples (Tab. S1) and further controlled by using the certified multi-element soil standard OREAS 45e and the certified multi-element basalt standard OREAS 24p.

Analyses for total carbon (TC), total organic carbon (C_{org}) and grain size were performed at the Laboratory of the Geological Survey of Norway (NGU). Weight percentages (wt. %) of C_{org} and TC were determined with a LECO SC-444 (Tab. S2). Prior to the analysis for C_{org}, sediment subsamples (ca. 200 mg) were transferred into carbon-free pervious ceramic combustion boats. To remove inorganic carbon (carbonate) combustion boats were placed on a heating plate with 50°C (±5°C) and samples were treated with 10 % (vol.) hydrochloric acid (HCl). Subsequently, samples were rinsed 10 times with distilled water (water was withdrawn by vacuum attached to the combustion boats). The certified reference material Leco 501-034, blanks and sample replicates were included in every batch. Results are given in weight percentage and the analytical error for TC and TOC was ±2.3 % rel. (n = 28) and ±2.0 % rel. (n = 26), respectively. Carbonate content was calculated as $CaCO_3 = (TC - C_{org}) \times 8.33$. The determination of grain size distribution was performed by laser diffraction

using a Coulter LS 200 instrument. The analysis was carried out on material within a particle diameter range of 0.4–2000 µm and the results are presented on the basis of volume, as cumulative volume percentage (Tab. S3). Prior to the grain size analyses, sediment samples (0.12-0.58 g) were treated with 5 % sodium pyrophosphate ($Na_4P_4O_7 \bullet 10H_2O$, Merck PA) to prevent particles becoming charged and agglomerated and afterwards placed in an ultrasonic bath (5-6 min). At least one duplicate of each sample with the same net weight were analysed and the uncertainty was ±10% cumulative mass volume percentage. We assume biogenic silica and $CaCO_3$ to have only a minor effect on the grain size measurement because: (a) Biogenic silica analysis of 10 surface sediments from the Trondheimsfjord applying the method from Mortlock and Froelich (1989) (unpublished data, Geological Survey of Norway) reveal very low content of biogenic silica (< 0.8 %). (b) The grain size distribution is consistent with previous studies (e.g. Bøe et al., 2004) and our own observation during sampling. Furthermore, (c) the $CaCO_3$ content in 73 % of all samples within the Trondheimsfjord reveal values lower than 4.5 wt. % of the total sediment.

3.3. Total nitrogen and stable carbon isotope analyses

Total nitrogen (N_{tot} in wt%) was determined using a Carlo Erba NC2500 Isoprime elemental analyzer isotope ratio mass spectrometer (EA-IRMS) at EPOC, CNRS/University of Bordeaux 1, France. Duplicate measurements of all samples and additional triple measurements of ~25% of all samples produced a standard deviation of 0.002 % for N_{tot} (sigma 1, n = 60). The inorganic nitrogen (N_{inorg}) content was analysed on 20 mg sediment subsamples treated with KOBr-KOH solution to remove organic nitrogen (see Knies et al. (2007) for details) using an EA-IRMS (Iso-Analytical Ltd., UK). Precision of the measurement was 3.48 % (n = 10). The organic proportion of the total nitrogen content was calculated by

subtracting the N_{inorg} fraction from N_{tot}. The results from the nitrogen analyses are shown in the supplementary information Tab. S2.

Stable carbon isotopes of the C_{org} fraction ($\delta^{13}C_{org}$) were measured on decarbonated (10 % HCl) aliquots using an EA-IRMS (Iso-Analytical Ltd., UK). $\delta^{13}C_{org}$ values are given in per mil vs. Vienna-PDB (Tab. S2). The applied reference standards were IA-R005 (Beet sugar) with a $\delta^{13}C_{V\text{-}PDB}$ value of -26.03 ‰, IA-R001 (wheat flour) with a $\delta^{13}C_{V\text{-}PDB}$ value of -26.43 ‰ and IA-R006 (sugar from cane) with a $\delta^{13}C_{V\text{-}PDB}$ value of -11.64 ‰ The mean standard deviation for $\delta^{13}C$ of IA-R005, IA-R001 and IA-R006 is 0.14 % (n = 10), 0.23 % (n = 10) and 0.53 % (n = 10), respectively.

3.4. MT index

An index for the variable input of marine versus terrigenous organic matter (MT index) was designed applying a modified version of the method described in Bertrand et al. (2012) and Sepúlveda et al. (2009). In brief, the MT index is calculated by a linear regression between the score of the first axis of a principle component analysis (observation scores F1: 93.06 %; F2: 6.94 %, Tab. S4) and its variables: $\delta^{13}C_{org}$ and the fraction of terrestrial organic carbon (F_{terr}), which is calculated from the N_{org}/C_{org} ratio (Perdue and Koprivnjak, 2007; data in the Tab. S2). To calculate F_{terr}, the lowest and highest N_{org}/C_{org} ratios (0.052; Site 314, 0.113; Site 502) were used to define the terrestrial and the marine end member, respectively. The resulting equation is MT index = 16.68 - 0.034 * F_{terr} + 0.65 * $\delta^{13}C_{org}$ and positive (negative) MT index values indicate higher (lower) marine OM input. The MT index does not consider lacustrine components. We ultimately apply the MT index on the surface set of samples as a baseline for an improved evaluation of changes in marine versus terrigenous OM supply into the fjord on longer time scales. By using the end members for

N_{org}/C_{org} given in this paper, the MT index can be calculated not only for any surface sediment samples but also for long sediment cores retrieved in the Trondheimsfjord for follow up studies. Instead of interpreting relative variation of raw $\delta^{13}C_{org}$ and N_{org}/C_{org} data, the MT index combines both parameters and provides the possibility to compare past changes of marine versus terrigenous OM with the modern distribution of the OM in the Trondheimsfjord.

3.5 Bulk mineral assemblage analyses

Bulk mineral assemblages were measured via X-ray diffraction (XRD) using a Philips X'Pert Pro MD, Cu-radiation (k(alpha) 1.541, 45 kV, 40 mA) and X'Celerator detector system at the Central Laboratory for Crystallography and Applied Material Sciences (ZEKAM), University of Bremen, Germany. Samples were prepared by means of the Philips/Panalytical back loading system and a fixed divergence slit (1/4°2θ) with a detection angle from 3°-85° 2θ and a step size of 0.0168° 2θ was used. The calculated time was 100 s per step. Quantification of the mineral content was carried out with Quantitative Phase-Analysis with X-ray Powder Diffraction (QUAX) (details are given in Vogt et al., 2002). Results and error (rel. %) are shown in Tab. S3.

3.6 Elemental composition of terrestrial material

In order to compare our results with geochemical studies from the terrestrial area surrounding the Trondheimsfjord, we used two data sets including overbanked sediments and bedrock analyses. The bedrock analysis reflects the chemical composition of geological units. Overbanked sediments (also called alluvial soil, levée or floodplain sediments) accumulate during active widespread erosion related to flooding episodes. They are

considered to represent the average lithological input of a whole catchment area upstream from the sampling site (Ottesen et al., 1989).

Ottesen et al. (2000) reported the natural chemical composition of 38 overbanked sediments samples (< 63 μm) collected across Trondheimsfjord drainage area using X-ray fluorescence analyses at the Geological Survey of Sweden.

Finally, 183 bedrock samples were available from the Trondheimsfjord drainage area as part of the regional mapping program at the NGU. The chemical composition of these samples (Tab. S5) were determined on a Philips PW 1480 X-ray spectrometer (XRF) at the Geological Survey of Norway (NGU). The locations of the samples are plotted in the simplified geological map (Fig. 2).

4. Results and Discussion

4.1. Mineral assemblages and grain size

The mineral assemblages of surface sediments from Trondheimsfjord are characterized, generally, by high concentrations of metamorphic minerals consistent with the local geology (Fig. 2 and section 2.1), indicating the material to be of local origin and freshly weathered. The XRD analyses reveal that, on average, more than one third of the sediment is composed of phyllosilicates (34.2 %), followed by quartz (22 %), plagioclase (19.5 %) and illite+mica (18.2 %). Calcite (2.2 %), aragonite (0.4 %) and other carbonates (1.9 %) are, on average, only poorly represented in Trondheimsfjord sediments (Tab. S3).

Previously, Howe et al. (2010) reported that the distribution of sediments within fjords depends on its bathymetry and the hydrographic regime. In the Trondheimsfjord, mineral

assemblages and grain sizes were, in some cases, highly variable, even over relatively short distances, most likely due to the inflow of rivers and rapid changes in water depth; however, no correlation between water depth and any grain size fraction was found ($r^2 = < 0.09$), although a general pattern of increasing grain size from the inner fjord to the fjord mouth could be observed (Fig. 3).

This observation is consistent with the XRD analyses, which also shows an increasing trend in the amount of quartz (17.3 % to 26.1 %) and a decrease in illite/mica (21.5 % to 7.9 %) and phyllosilicates (42.9 % to 16.3 %) (Tab. S3), on going from the inside to the outer parts of the fjord. We suggest that the increase in grain size is mainly related to current speed, especially due to tidal currents. This is particularly well illustrated at the fjord entrance where the in- and outflowing (tidal) currents are forced through the narrow passage and above the Agdenes sill (Fig. 1). The high mean current velocity (0.2 m/s) results in sediment winnowing (Jacobson, 1983) and thus enrichment in the coarser grain fractions. Since the velocity of the tidal current decreases towards the inner fjord (less water has to be transported), the proportion of fine grained material increases in that area.

4.2. Sources of organic matter

In order to estimate the relative contributions of marine versus terrigenous organic matter (OM) to the surface sediments in Trondheimsfjord, we examined the stable isotope composition of organic carbon ($\delta^{13}C_{org}$) and the ratio of total organic carbon (C_{org}) to total organic nitrogen (N_{org}) (Fig. 4). In contrast to C_{org} only, these parameters are independent of changes in sedimentation rate and their differences for marine and terrigenous OM have been investigated and utilised extensively in previous studies (Goñi et al., 1997; Stein and MacDonald, 2004 and references therein; Karageorgis et al., 2005; Winkelmann and Knies,

2005; Perdue and Koprivnjak, 2007; Knies and Martinez, 2009; Sepúlveda et al., 2009; Knudson et al., 2011; Sepúlveda et al., 2011; Bertrand et al., 2012). Terrigenous OM is relatively depleted in nitrogen, and characterized by C_{org}/N_{org} ratios >15, compared to marine OM with a significantly lower C/N signature (e.g. Bordovskiy, 1965; Stein and MacDonald, 2004; Rullkötter, 2006). The stable isotope composition ($\delta^{13}C_{org}$) of OM reflects the isotope composition of the different carbon sources and the fractionation of ^{12}C and ^{13}C during photosynthesis (e.g. Hayes, 1993). In general, the carbon source for marine organisms is enriched in ^{13}C compared to atmospheric CO_2 (carbon source for land plants) and the fractionation factor for plants using the C_3 pathway for carbon fixation, typical for high latitude regions (Collins and Jones, 1986; Still et al., 2003), is also larger than for marine organisms (O'Leary, 1981; Schubert and Calvert, 2001; Rullkötter, 2006) which results in higher $\delta^{13}C_{org}$ values for marine OM compared to terrigenous OM (e.g. Schubert and Calvert, 2001).

The C_{org}/N_{org} ratios of the surface sediment samples from Trondheimsfjord show an increase from the entrance of the fjord (e.g. C_{org}/N_{org} = 8.8; Site 502) towards the inner fjord (e.g. C_{org}/N_{org} = 14.3; Site 201) (Fig. 4) with highest values occurring in the samples closest to river inlets (e.g. C_{org}/N_{org} = 19.1; Site 314). In contrast to the C_{org}/N_{org} ratios the $\delta^{13}C_{org}$ values in the surface sediments show the opposite trend (Fig. 4), decreasing from the outside towards the inside of the fjord. Highest (-21.2 ‰; Site 502) and lowest values (-26 ‰; Site 324) values were found for sites corresponding to the entrance of the fjord and river deltas, respectively. Furthermore, as expected from the spatial distribution $\delta^{13}C_{org}$ and N_{org}/C_{org} correlates well (r^2 = 0.74, Fig. 5).

The systematic relationship between $\delta^{13}C_{org}$ signatures and the N_{org}/C_{org} ratio have been used to establish a two end member mixing model (for mathematical reasons we use the N_{org}/C_{org} ratio here, seePerdue and Koprivnjak (2007)). All data show that the composition of sedimentary organic matter in surface sediments is consistent with mixing of marine and terrigenous C3-photosynthetic organic matter. As discussed previously, the admixture of C4 plant types is insignificant in the study region (Collins and Jones, 1986; Still et al., 2003) and does not influence the binary system of the two end members (terrestrial vegetation/soil and marine organic matter). Furthermore, the regression of N_{org}/C_{org} vs $\delta^{13}C_{org}$ (Fig. 5) for the studied sample set indicates that the proposed N_{org}/C_{org} end member values (0.052; 0,113) corroborate typical $\delta^{13}C_{org}$ based end members for terrestrial (-27 ‰) and marine OM (-21 ‰ - -20 ‰) in the study region (Knies, 2005; Winkelmann and Knies, 2005; Knies and Martinez, 2009).

The resulting MT index (Fig. 6), which builds on the overall good regression of N_{org}/C_{org} vs. $\delta^{13}C_{org}$ (Fig. 5), trace the change from more terrigenous OM in the inner fjord towards higher relative abundances of marine OM in the sediments towards the entrance. Thus, the MT index is sensitive for evaluating the origin of the OM (Jasper and Gagosian, 1990) and this is demonstrated convincingly for the locations studied here (Fig. 6).

Bøe et al. (2003) reported sedimentation rates between 0.4 and 2.5 mm/year over the past 6000 years in the Seaward and Middle fjord basin based on eleven sediment cores. Assuming these sedimentation rates our surface sediments contain a record of 25 to 4 years. Most of our samples, however, were very fluffy due to a high content of water and furthermore ^{210}Pb-dating results of four multicores from different basins (Entrance, Seaward, Middle fjord) reveal sedimentation rates of 5-7 mm/year for the past 60 years

(Milzer et al., 2013b). We assume therefore, that our results mirror modern environmental conditions.

The reliability of the MT index as a proxy for the origin of the OM can be demonstrated further by comparison with the modern primary production in the Trondheimsfjord. Volent et al. (2011) studied the spatial and temporal evolution of phytoplankton blooms in the Trondheimsfjord from March to October 2004 by combining the analysis of water samples, and data from a ship-mounted automatic flow through sensor system, Ferrybox (measuring Chlorophyll a and turbidity) with red, green, blue (RGB) colour satellite images and remotely sensed total suspended matter (TSM) from the MERIS instrument aboard the satellite ENVISAT (ENVIronmental SATellite, European Space Agency). Volent et al. (2011) reported that high turbidity (cloudy water in the RGB images and high TSM concentrations) was not related to suspended minerals of nonbiological origin, but was caused by loose coccoliths (calcium carbonate plates of coccolithophores) as well as by large cells with high pigment content. Thus, the measured turbidity was interpreted as reflecting primary production in the fjord. Even though the images from Volent et al. (2011) only reveal a snapshot of the annual primary production in the Trondheimsfjord, a strong visual correlation with our MT index data is clear (Fig. 6). According to the MT index values, the turbidity (phytoplankton) concentration is highest at the fjord entrance and in the centre part of the Seaward basin and decreases towards the river deltas and the inner part of the fjord. In addition, the distribution of phytoplankton in Trondheimsfjord is related to river runoff and surface water circulation (Sakshaug and Myklestad, 1973; Volent et al., 2011) and is most obvious in the channel behind the Tautra sill. In this region, we find high MT index values on the south side compared to the north side. Satellite images (Volent et al., 2011) reveal that turbid,

coccolith-rich, inward flowing surface water from the Seaward basin crosses the Tautra sill on the southern side whereas the outward flowing surface water on the north side is clearer. The distribution of phytoplankton, therefore, potentially helps to explain the variations in MT indices over short distances near the Tautra sill and illustrates the important role of the inflow pattern of oceanic water for the distribution of marine OM versus terrigenous OM in Trondheimsfjord sediments. Finally, the distribution of $\delta^{13}C$ in benthic foraminifera from the Trondheimsfjord is very similar to the MT index. Milzer et al (2013a) found a general increasing trend of $\delta^{13}C$ in benthic foraminifera from the inner Trondheimsfjord towards the open ocean with lowest values close to river deltas. In accordance to our findings, Milzer et al. (2013a) assume terrigenous derived C_{org} to be responsible for lower $\delta^{13}C$ values at river deltas and the inner part of the fjord marine derived C_{org} for the increasing $\delta^{13}C$ values towards the fjord entrance.

Only two samples sites (Site 329, south of the Agdenes sill and Site 214, northeast of the Tautra sill) fail to fit into the observed pattern (Fig. 6). Analysis from the deepest part at the entrance of the fjord (Site 329; water depth 605 m; MT index = -0.75) indicates a more terrestrial source of the OM compared to the surrounding sample sites. Site 329 is close to a disposal place for ships and explosives and, therefore, the OM could be anthropogenically influenced; although, we do not find any other indication for contamination in this area from the inorganic analyses and currently have no firm explanation for this discrepancy. In contrast, data from Site 214 indicates a more marine source of the OM compared to the surrounding stations, with a MT index value of 1.54. This area is a well-known fishing ground (O. Longva, pers. comm. 2012), as supported by numerous fish bones in the sample and the hinterland region is used intensively for agriculture. Thus, the OM is probably altered by

marine organic waste and nitrogen-rich fertilizer. This is supported by a $\delta^{13}C_{org}$ value (-22.35 ‰) which is in line with the values of the surrounding samples (Fig. 4).

To summarise the organic geochemical analyses, the MT Index appears to represent an excellent tool for distinguishing, semi-quantitatively, between marine and terrigenous OM for the majority of the surface sediments from the fjord. The clear proximal to distal trend of the MT index is in agreement with previous investigations of fjords in northern Patagonia. The terrestrial index based on $\delta^{13}C_{org}$ and salinity (Bertrand et al., 2012), for example, shows a decreasing trend from the fjord inner part towards the open ocean. Similarly, Sepúlveda et al. (2011) found a strong gradient (84 % difference) of organic carbon sources between open ocean areas and those located towards inner fjords and/or river outlets using a combination of C_{org}/N_{tot}, $\delta^{13}C_{org}$ and $\delta^{15}N$ data. Collectively, these findings reveal that changes in the terrigenous vs. marine OM input in fjords are mostly controlled by two opposing and fundamental processes: (1) the inflow of freshwater transporting terrigenous OM and (2) the inflow of oceanic waters supporting marine organisms e.g. through higher salinities. In the Trondheimsfjord, the freshwater supply is controlled by continental precipitation and temperature (snowmelt), while the inflow of Atlantic water is mainly controlled by the strength of tides, bathymetry, the amount of river run-off, as well as the strength of the NAC flowing along the Norwegian coast. On a smaller scale, the fjord surface circulation may also play an important role in the distribution of marine versus terrigenous OM in fjord sediments, as illustrated by the variations in the MT index in the Middle fjord basin close to the Tautra sill (Fig. 6). Since the inflow of Atlantic water and precipitation pattern in central Norway are linked via NAO and NAC to large-scale climate systems (Hald et al., 2011; Pinto and Raible, 2012), well-constrained (temporally) MT index records from the Trondheimsfjord

may be used as a proxy-based method for further Holocene climate change studies in the future.

4.3. Bulk inorganic sediment composition

4.3.1. Marine source

Ca and $CaCO_3$ in Trondheimsfjord sediments are strongly correlated (r^2=0.97, n = 60) and corroborate the spatial pattern of the MT index data (Fig.7 and 8). Both parameter (Ca and $CaCO_3$) show a clear proximal to distal trend in the Trondheimsfjord sediments with highest values at the entrance and lowest values in the inner part of the fjord and river deltas (Fig 7 and 8). However, the overall regression of the MT index vs. Ca and $CaCO_3$, respectively, is relatively poor (both r^2 = 0.3, n = 60). One possible explanation for this discrepancy lies in the extremely high Ca and $CaCO_3$ concentrations for five sampling locations (mean Ca = 7.9 %; mean $CaCO_3$ = 18.3 %) compared to the mean value for the entire dataset (Ca = 2.9 %; $CaCO_3$ = 4.6 %; n=60). Samples from these locations are the only samples where aragonite (1.6 - 6.0 %) was present (Tab. S3). This indicates that eroded remnants of the deep water coral *Lophelia pertusa,* which grows at the entrance of the fjord and on the Tautra sill (Mortensen et al., 2001 and reference therein) are the source for the carbonate enrichments. By excluding these five samples (Sites 500, 501, 502, 329 & 217) the overall regression between the MT index increases significantly for $CaCO_3$ (r^2 = 0.6, n = 60) but only slightly for Ca (r^2 = 0.4, n = 60). Our findings show that the latter is likely explained by the dilution of marine produced carbonates with terrigenous Ca bearing minerals (e.g. amphibole). Indeed, alluvial soil samples show a fairly homogenous distribution of Ca in the catchment area of the fjord (Fig. 7), with mean Ca concentration of 2.5 % (Ottesen et al.

2000). Moreover, samples recovered along the shore and in river deltas with a negative MT index show no relation between Ca and the MT index (Fig 9). $CaCO_3$ is only slightly related to the negative MT index values ($r^2 = 0.2$) and also Ca and $CaCO_3$ show no connection in samples with a negative MT index ($r^2 = 0.04$, n= 29). These findings express the influence of a terrestrial Ca source on biogenic components in samples close to the shore and in river deltas.

Samples with MT index values > -0.7 (Fig. 9) reveal a good correlation of Ca and the MT index ($r^2 = 0.57$, n =43). The regression becomes even stronger ($r^2 = 0.77$, n = 39) by excluding the samples enriched in aragonite from eroded deep water corals (Fig. 9). Also the regression between $CaCO_3$ and Ca in samples with MT index values > -0.7 increases significantly, $r^2 = 0.98$ (n = 43). The strong correlation between Ca and $CaCO_3$ points to biogenic calcite as the main Ca source in samples with positive MT index values. This assumption is further supported by clear negative correlations (r = -0.6 to -0.8) of Ca and $CaCO_3$ with any terrigenous element (e.g. Al, Fe, Ti, and Zr).

As a result, variations in the concentrations of Ca and $CaCO_3$ in samples with positive MT index values can be treated as a proxy for carbonate marine productivity and may serve as an indicator for the variable inflow of North Atlantic water masses versus river discharge.

4.3.2. Terrestrial sources

In the following section, we discuss the changes in the geochemical composition of the terrigenous fraction in the surface sediments and identify possible land sources by studying the behaviour of Al-based ratios. From the 35 analysed elements, we focus on the elements Ni and K as their spatial distribution can be directly related to the available bedrock and

alluvial soil measurements in the hinterland. The variation in grain size and mineral assemblage may have contributed to some trace element variability (e.g. Loring, 1990 and references therein). Elemental ratios are insensitive to dilution effects and by using a normaliser incorporating mainly in a single grain size fraction the grain size effect can be minimized. Al is a conservative element, showing a strong correlation ($r^2 = 0.8$) with grain size fraction < 63 µm in our study area and Bertrand et al. (2012) found that Al is relatively insensitive to changes in the nature of sediment sources, catchment size, and hydrodynamic sorting in fjords of northern Patagonia.

4.3.2.1. Proxies for terrestrial sediment supply from the southern hinterland

Ni/Al ratios show highest values close to the river deltas of Orkla, Gaula and Nidelva in the southwest and decrease towards the inner and outer part of the Trondheimsfjord (Fig. 10). Alluvial soil which are assumed to represent the overall geochemical signature of the catchment areas (Ottesen et al., 1989) show elevated Ni values in the southern hinterland (Fig. 10; Ottesen et al., 2000). Ottesen et al. (2000) also found that Ni in alluvial soil correlated well with Cr and Mg, suggesting that the main sources for Ni were iron-magnesium minerals e.g. olivine, amphibole and pyroxene. Consistent with the observations of Ottesen et al. (2000), Ni correlates best with Mg ($r^2 = 0.9$) and Cr ($r^2 = 0.9$) in the fjord surface sediments, pointing to a distinct Ni source located in the southern hinterland. This conclusion is supported further by the bedrock analyses, that reveals high Ni concentrations in the greenstones and metagreywackes located along the southern side of the fjord (Fig. 10). Other geochemical investigations of urban surface soil from Ottesen and Langedal (2001) and Andersson et al. (2010) exhibit no anthropogenic Ni contamination by the city of Trondheim and attributed elevated Ni concentration by the presence of greenstone

bedrocks. This suggests that the elevated Ni/Al values are natural and related to changes in the terrestrial sediment supply from the southern hinterland. Furthermore, temporal changes in Ni/Al are, thus, likely the result of changes in erosion and runoff in the southern hinterland that, in turn, are controlled by precipitation and temperature variability.

4.3.2.2. Proxies for terrestrial sediment supply from the northern hinterland

A precise association of K to a specific mineral does not exist. Several studies (e.g. Shimmield, 1992; Martinez et al., 1999) reported potassium feldspar ($K[ALSi_3O_8]$) and illite ($(K,H_3O)Al[(OH)_2Si_3AlO_{10}]$) (e.g. Yarincik et al., 2000) as the dominant K source in marine sediments deposited in upwelling regions or restricted basins (Cariaco Basin). In the Trondheimsfjord surface sediments K is not related to the amount of potassium feldspar ($r = -0.44$) and like Al, K correlates well with the clay fraction ($r^2 = 0.8$). As a result, the distribution of K in the Trondheimsfjord sediments is related to the concentration of phyllosilicates ($r^2 = 0.6$), however, K has no affiliation to a specific clay mineral. Best regression was found with illite $r^2 = 0.2$. These findings suggest that the analysed K originates potentially from a mixture of different (clay) minerals and maybe also from K ions adsorbed to clay minerals (Müller, 1977). Additional analyses are necessary to define the specific K source in the Trondheimsfjord sediments. Nevertheless, K/Al values in the surface sediments are highest in inner fjord (Beitstadfjord and Middle fjord) and at the mouth of the Steinkjerelva river (Fig. 11). They decrease continuously towards the fjord entrance suggesting a K source in the northern drainage area of the Trondheimsfjord. The comparison of these findings with geochemical investigations of bedrock and overbanked sediments on land, further confirms this suggestion. Precambrian felsic volcanic rocks related to a tectonic window called *Tømmerås anticline* (see Roberts, 1997 for details) in the north-eastern

hinterland (Fig. 2) show highest K concentration (average > 4 %) in the hinterland bedrock (Fig. 11). Ottesen et al. (2000) found highest K concentration in samples from the *Tømmeråsanticline* region compared to the rest of the fjord catchment area (Fig. 11). Depending on the freshwater discharge, fine grained K-rich material can be transported over large distances above the halocline in the brackish surface layer (Hoskin et al., 1978). As such, we suggest that temporal changes of K/Al are an indicator of the variable supply of sediments from the northern hinterland of the Trondheimsfjord.

To summarise, we show that the inorganic geochemical composition of surface sediment from the Trondheimsfjord reflect regional differences in the geology of the terrestrial source area. Specifically, K is transported from the northern hinterland into the Middle fjord and Ni enters into the Seaward basin from a separate region in the southern hinterland (Fig. 10 and 11). Compared to other Al-based elemental ratios K/Al and Ni/Al show a distinct spatial distribution which is related to the spatial distribution of K und Ni in bedrock and alluvial soil measurements in the hinterland. Thus, the grain size independent distribution of Ni/Al and K/Al in the Trondheimsfjord sedimentary records might be used to investigate past changes in terrestrial input and, thus, reconstruct variable freshwater inflow from separated provinces. Moreover, the distribution of K/Al and Ni/Al are strongly influenced by the fjord bathymetry. The Tautra sill forms the boundary between the Seaward basin and the Middle fjord (Fig. 1) and prevents a free water exchange between these deep basins. By forming a ratio between K (northern province) and Ni (southern province), the strong effect of the sill on circulation and sedimentation in the fjord can be demonstrated (Fig. 12).

It should be noted that in drainage areas with generally lower content of K or Ni, temporal and spatial variations of transport and storage processes, for example due to faster

erosion or variable run-off, could significantly alter the spatial distribution of K/Al and Ni/Al. To exclude this possibility and to finally confirm our findings it is necessary to study the flux rates of production, transport, and discharge of detritus for every drainage basin over longer time periods. Unfortunately, to our knowledge no such data set are available yet and accumulation rates cannot be calculated. However, the strong relation between the spatial variation of elemental concentrations in Trondheimsfjord sediments with their distribution in the drainage area bedrock and overbanked sediments is a strong indicator that hinterland areas with low Ni and low K concentration have a negligible effect on K and Ni concentration in Trondheimsfjord surface sediments. In addition, overbanked sediments are formed along the streams during flood events (Ottesen et al., 1989) and, therefore, they reflect to some extent the river loads. Further investigations of short sediment cores covering the last century will prove the capability of the proxies by comparing K/Al and Ni/Al records to instrumental data such as temperature and precipitation, and thus the erosional capacity of the fjord catchment area.

5. Conclusions and Implications

The geochemical composition of sixty surface sediment samples from the Trondheimsfjord, central Norway, show that the distribution of carbonate and marine C_{org} follow related patterns of primary production within the fjord which are related to the inflow of salty oceanic waters. As such, we propose that a combined marine-terrestrial (MT) index and the carbonate content can be used to recognise past changes in the inflow of North Atlantic derived ocean waters. Furthermore, by analysis of grain size independent elemental ratios such as K/Al, Ni/Al and K/Ni, distinct Ni and K sources in bedrocks and alluvial soil in the southern and northern hinterland, respectively, can be identified in fjord

sediments. In applying this approach for reconstructing past climate in the region, we assume that temporal variations of these ratios are mainly controlled by continental precipitation and the resulting river discharge transporting the material into the fjord. Ultimately, the application of these organic and inorganic proxies on longer time scales will provide a robust reconstruction of past climate changes in central Norway and potentially illuminate both the variability of the North Atlantic Current and the North Atlantic Oscillation since the last deglaciation.

Acknowledgments

We thank the captain Oddvar Longva, and the crew of the RV Seisma for their professional support during our expeditions. Further we would like to express our gratitude to Karine Charlier and Philippe Martinez (EPOC, CNRS/University of Bordeaux 1), Anne Nordtømme, Bjørn Willemoes-Wissing, Clea Elisatbeth Fabian, Melanie Mesli, and Wieslawa Koziel (NGU) for their help with the laboratory work. For their interest, stimulating discussions, and many useful comments we thank our colleagues Simon Belt, Ola Magne Sæther, Rolf Tore Ottesen, Simone Sauer and Anne Liinamaa-Dehls. This work is a contribution to the CASE Initial Training Network funded by the European Community's 7th Framework Programme FP7 2007/2013, Marie-Curie Actions, under Grant Agreement No. 238111.

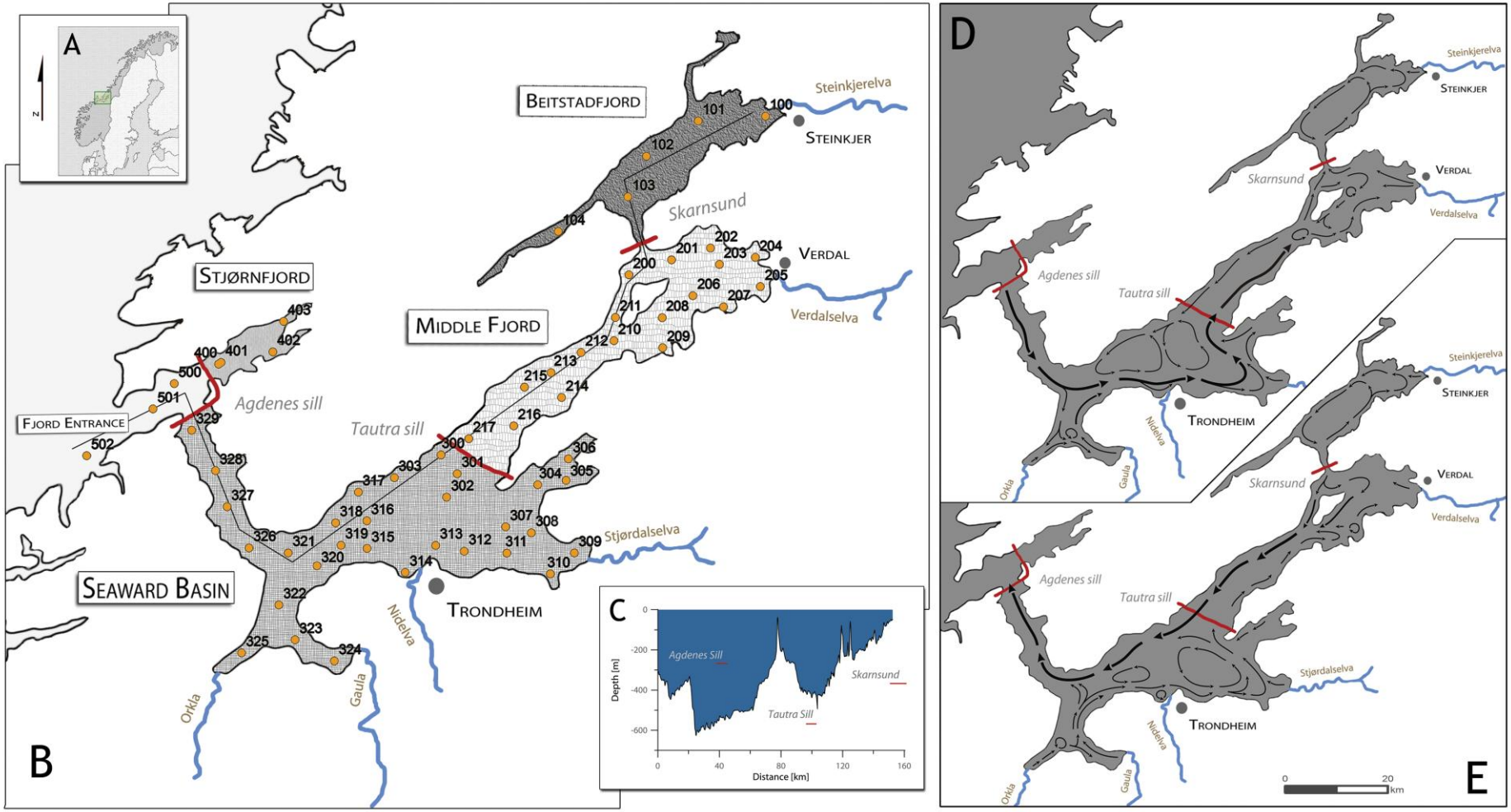

Figure 1: A) Location of the study area. B) Map of the Trondheimsfjord showing the sampling positions (yellow circles. Tab. S1) and the three sills (red lines) dividing the fjord into four main basins as well as the six main rivers entering the fjord from the south/southeast. The thin black line is the path of the bathymetry profile C). Inset: Surface water circulation pattern during high tide phase D) and low tide phase E) (modified after Jacobson, 1983; and Bierach, 1989).

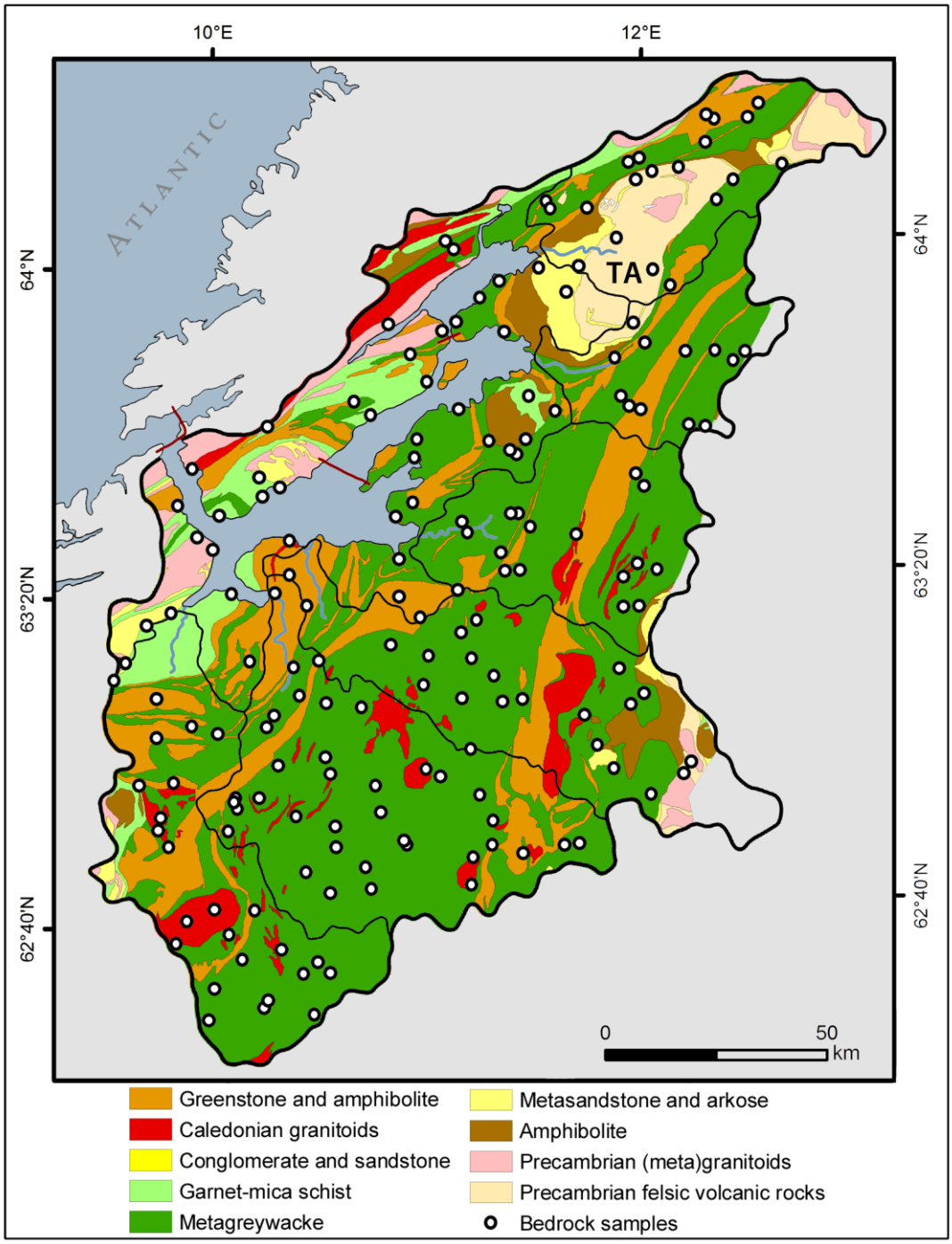

Figure 2: Simplified geological map of the Trondheimsfjord drainage area modified after Koistinen et al. (2001) shows the main lithology and bedrock sampling positions (circles) for the geochemical analyses. *TA* indicates the Tømmerås anticline, see section 2 for details. Coordinates are presented in Tab. S5.

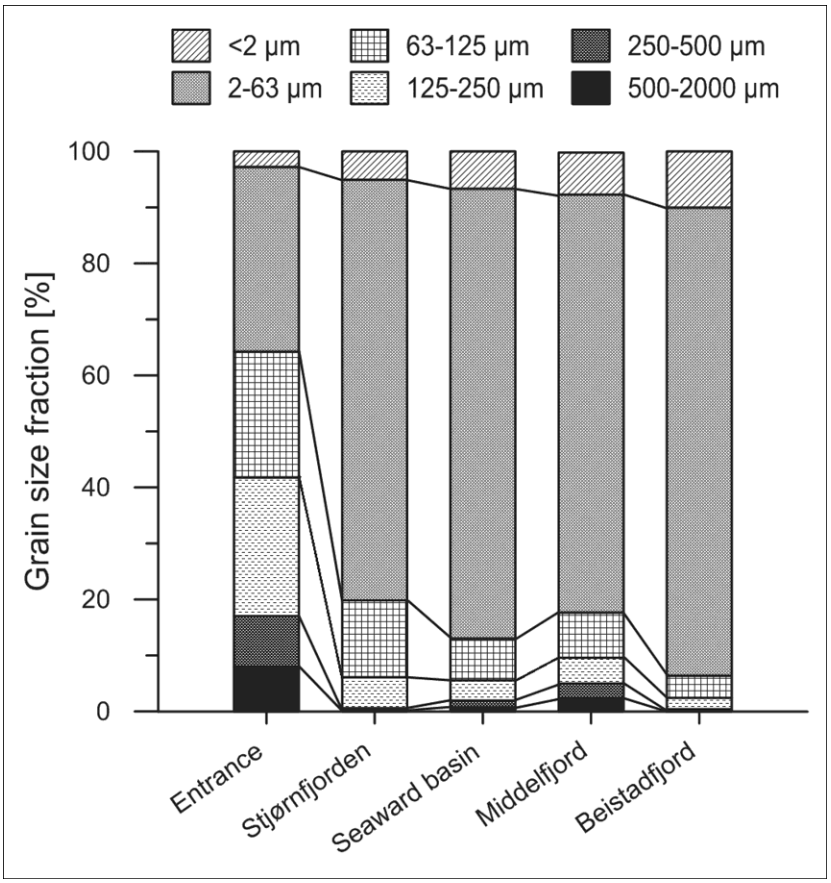

Figure 3: Average grain size distribution for each basin revelling an increase of the fine- and a decrease of the coarse grained fraction from the inside to the outer parts of the Trondheimsfjord. Data are presented in Tab. S3.

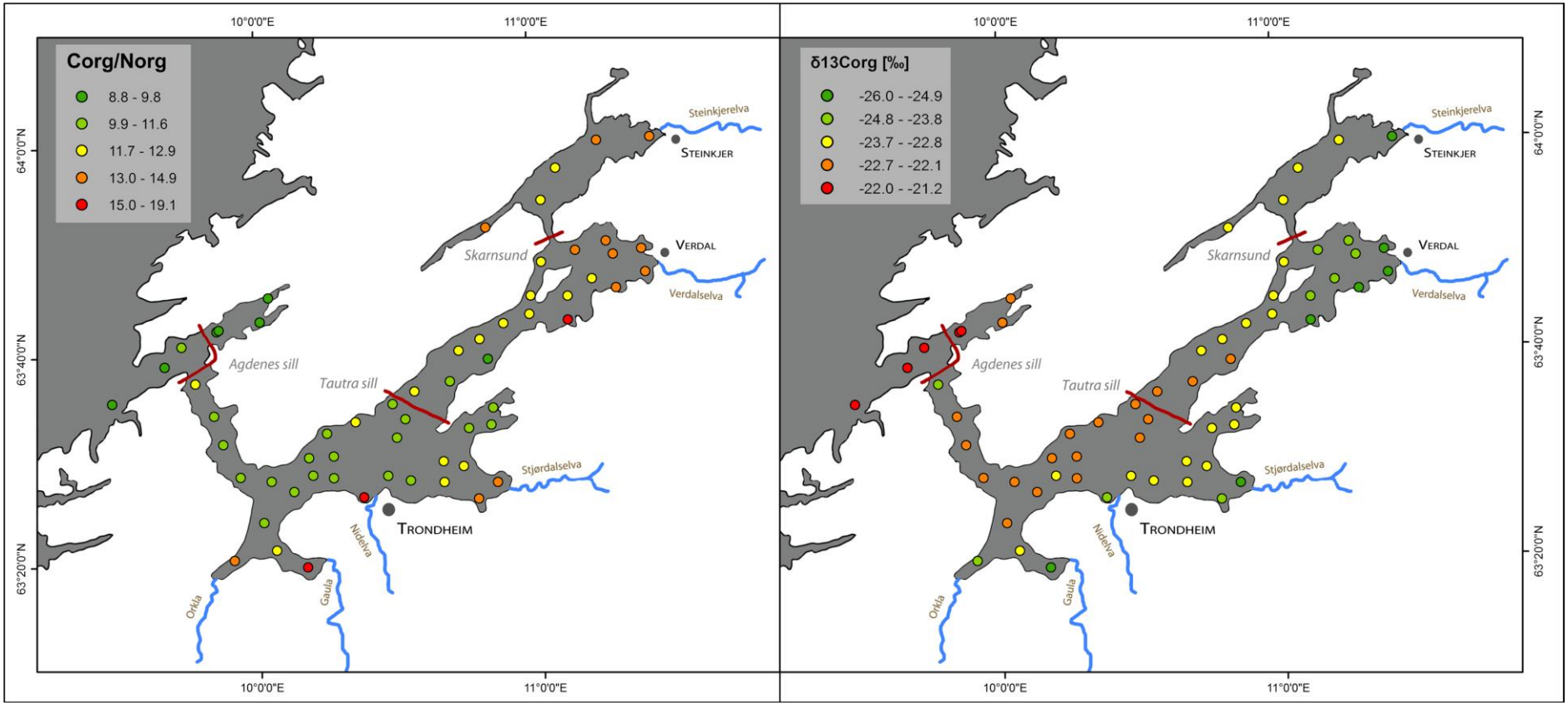

Figure 4: Distribution of C_{org}/N_{org} ratios (left) and $\delta^{13}C_{org}$ (right) of the surface sediments samples. Both parameters show a clear trend from more terrigenous OM at the river deltas and the inner part of the fjord towards more marine OM at the fjord entrance. Data are presented in Tab. S2.

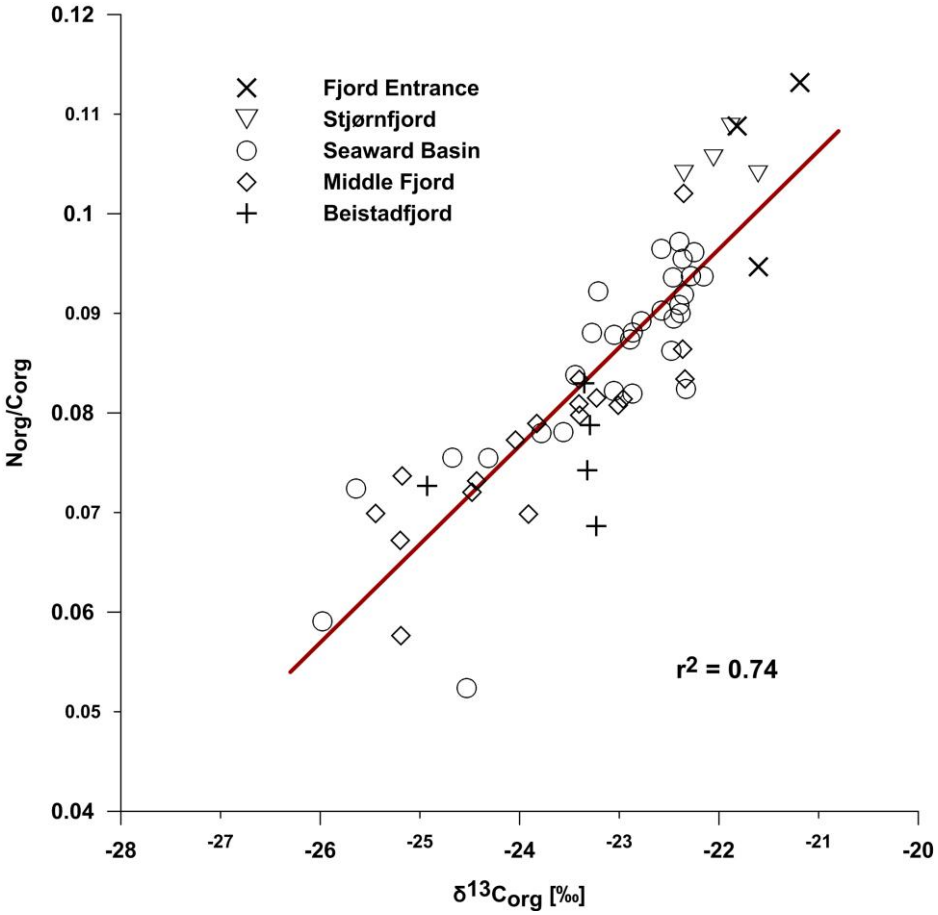

Figure 5: Correlation between N_{org}/C_{org} ratios and $\delta^{13}C_{org}$ in the surface sediments.

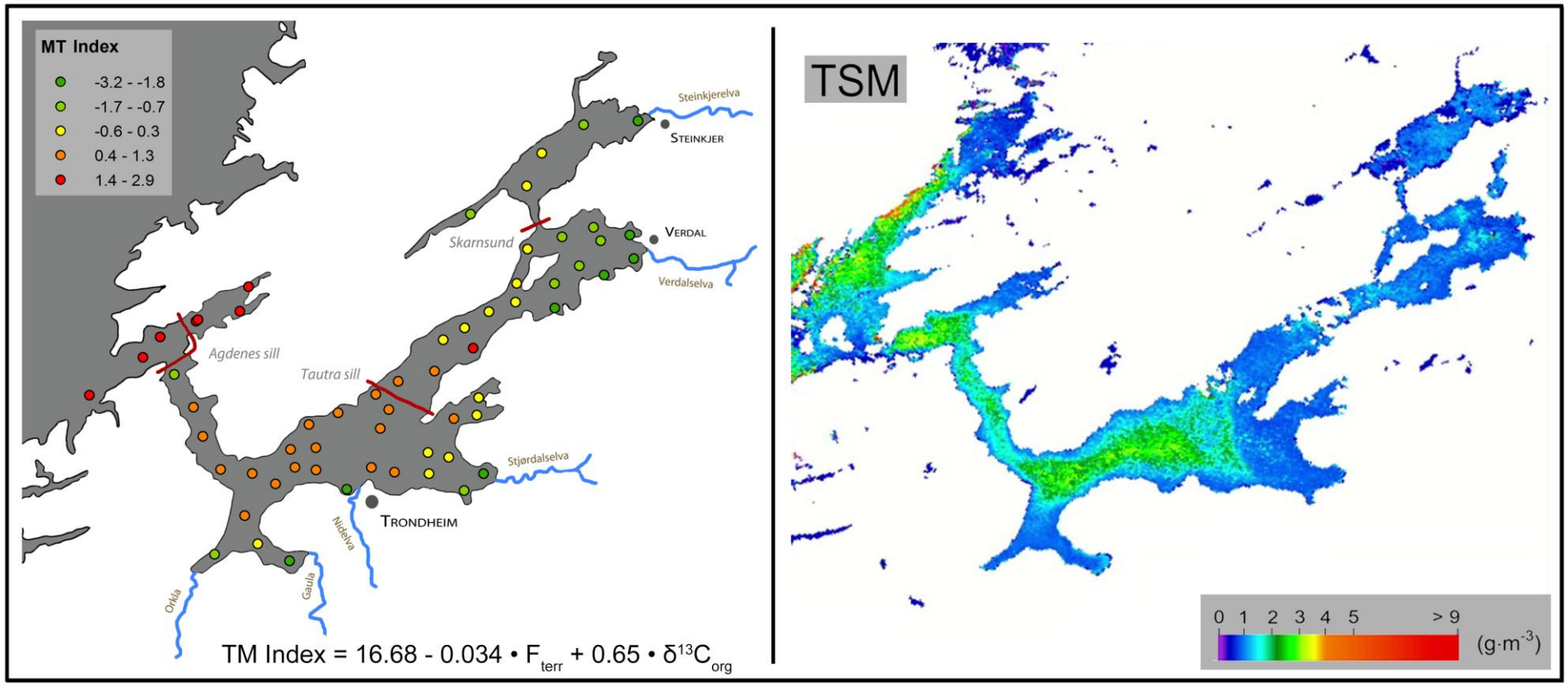

Figure 6: Left: The TM Index combines N_{org}/C_{org} and $\delta^{13}C_{org}$ and can be calculated with F_{terr} in % and $\delta^{13}C_{org}$ in ‰ for any location using the equation displayed at the lower part of the figure. Right: The inside-outside trend of the terrigenous vs. marine OM is in accordance with occurrence of coccoliths and large cells with high pigment content revealed by satellite measurements of the total suspended matter (TSM in g/m^3) recorded on 11.08.2004 and published by Volent et al. (2001).

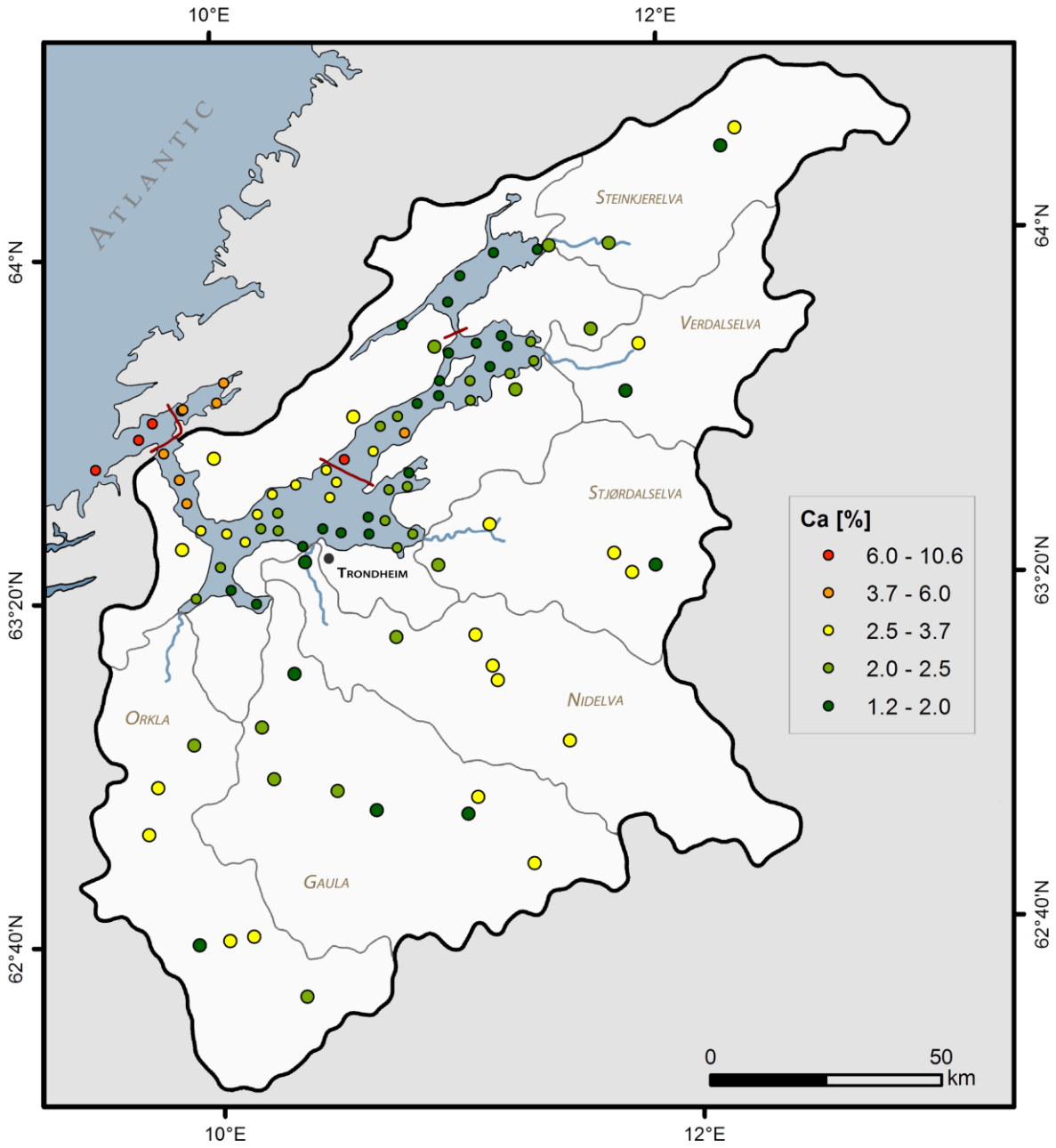

Figure 7: Results of calcium measurements in the surface sediment samples (this study, Tab. S1) and in overbank sediments from Ottesen et al. (2000) in the Trondheimsfjord drainage area. The drainage areas of the six main rivers are indicated by grey lines. The Ca concentrations in the surface sediments show a clear decreasing trend from the entrance towards the fjord inside.

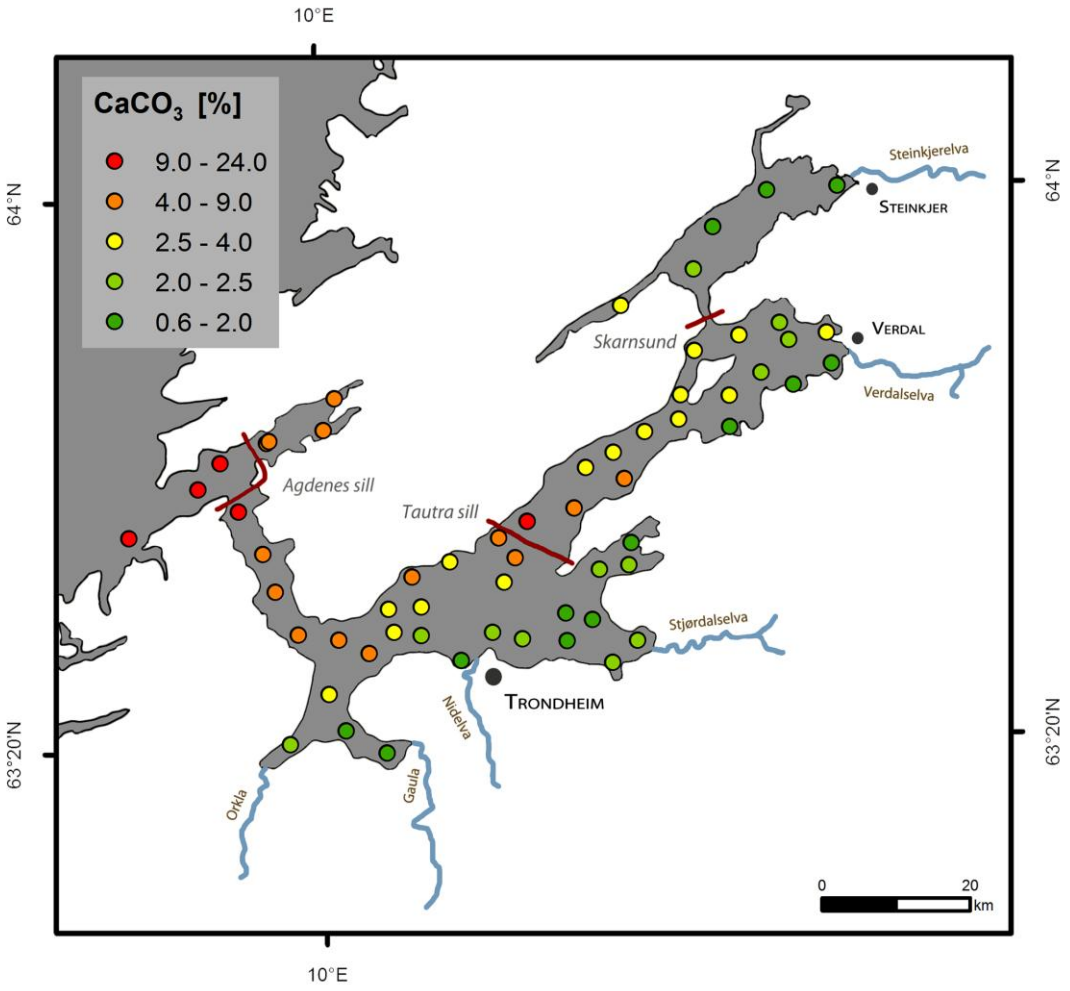

Figure 8: Results of $CaCO_3$ measurements in the surface sediment samples (this study, Tab. S2). The $CaCO_3$ concentrations show a clear decreasing trend from the entrance towards the inner part of the fjord.

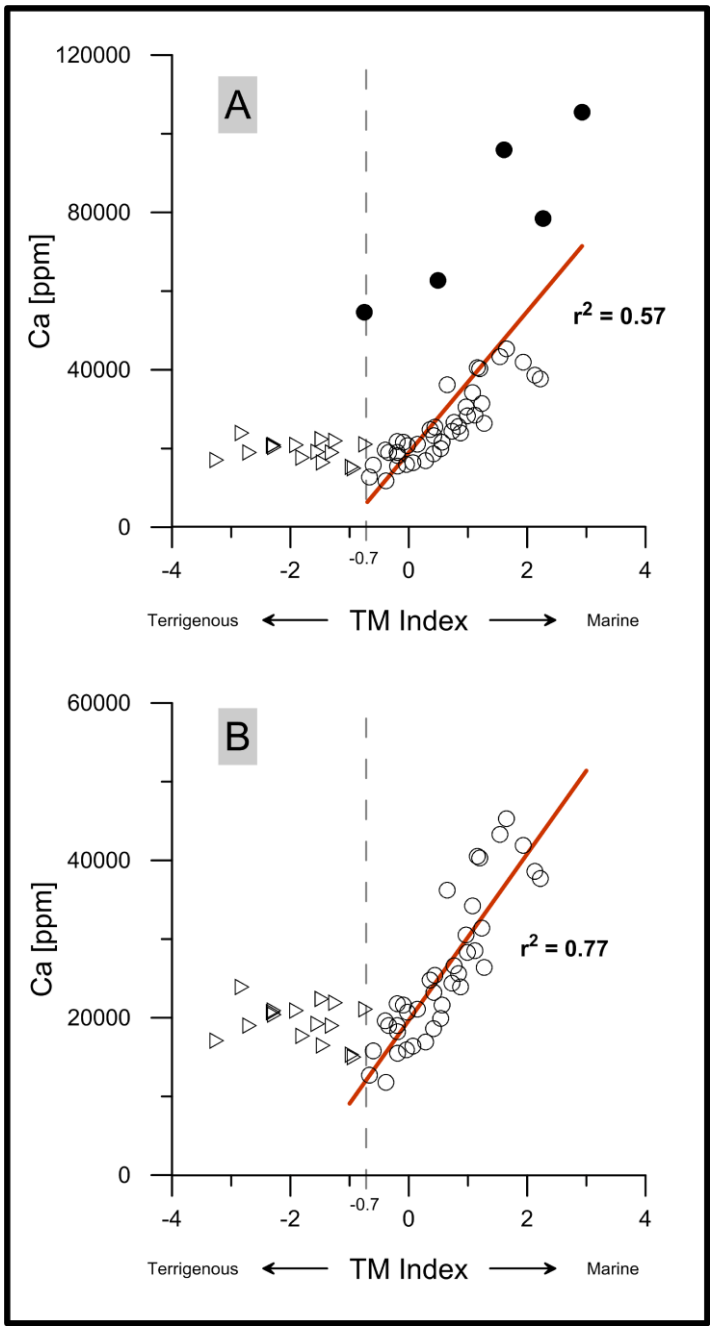

Figure 9: A) Cross correlation between calcium and the MT index for all surface sediments. The red line indicates the regression for samples with a MT index value > -0.7 (circles). Five samples (filled circles) show very high calcium concentration most likely due to abundant coral remains. B) By excluding these samples the relation between calcium and samples with a MT index value > -0.7 (open circles) is much more pronounced indicating large supply of calcium by marine organisms.

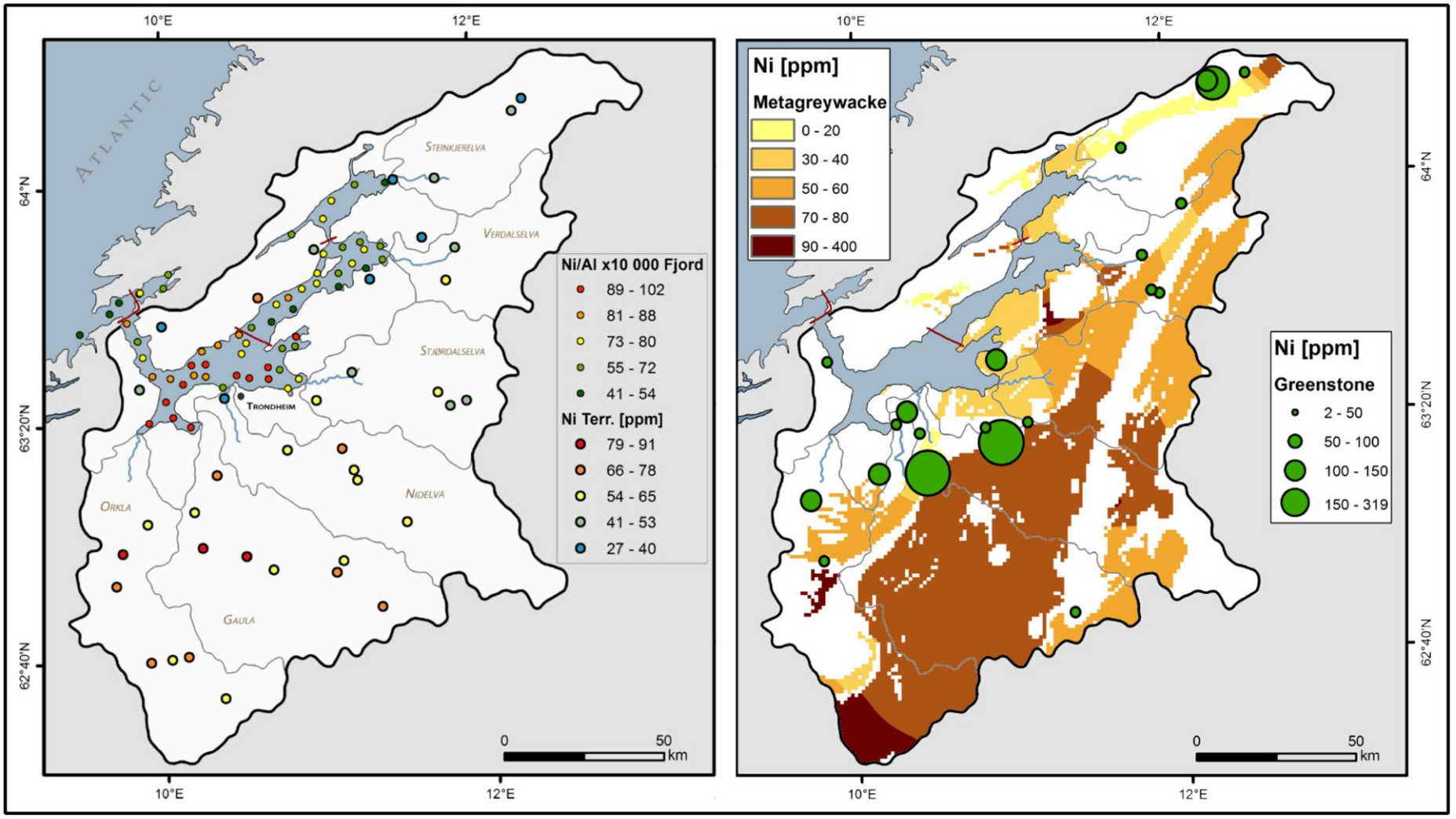

Figure 10: Left: Comparison of the Ni concentration from Ottesen et al. (2000) in the Trondheimsfjord drainage area and Ni/Al in the fjord sediments (this study, Tab. S1). The drainage areas of the six main rivers are indicated by grey lines. Ni/Al in fjord sediments shows highest values close to the river deltas of Orkla, Gaula and Nidelva in the south and decreases towards the inner and outer fjord. This pattern is in accordance with the distribution of Ni in the hinterland. Right: In general our analyses reveal metagreywackes and greenstones to contain highest Ni concentration in the terrestrial bedrock. In accordance with Ottesen et al. (2000) interpolated Ni concentrations within the metagreywackes area (sampling positions are shown in figure 2, data are presented in Tab. S5) and Ni contents in the greenstones samples are highest in the southern hinterland of the fjord.

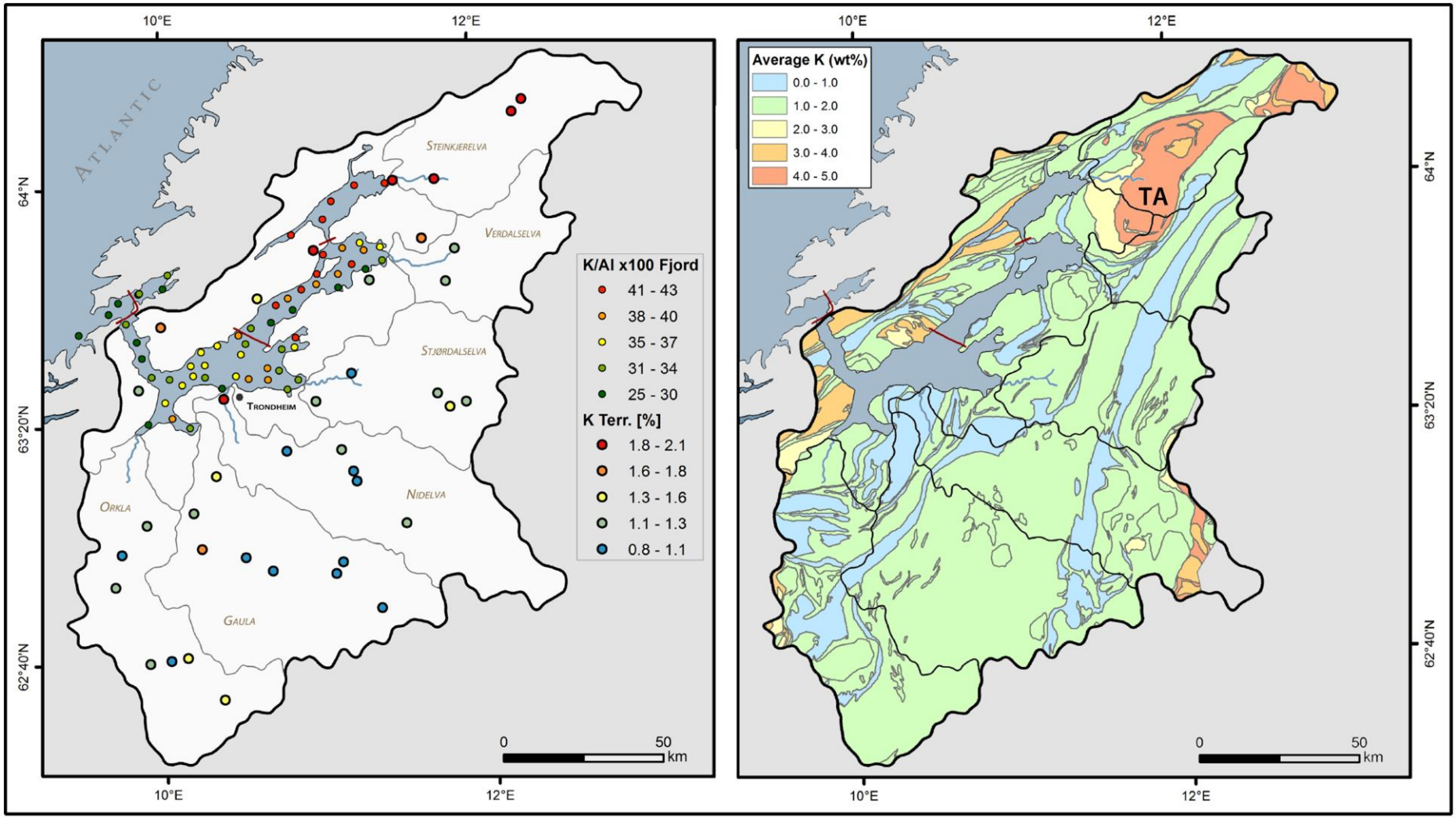

Figure 11: Left: Comparison of the K concentration from Ottesen et al. (2000) in the Trondheimsfjord drainage area and K/Al in the fjord sediments (this study, Tab. S1). The drainage areas of the six main rivers are indicated by grey lines. K/Al in fjord sediments shows highest values close to the Steinkjerelva river delta the in the north and decreases towards the outer fjord. This pattern is in accordance with the distribution of Ni in the hinterland. Right: The chemical data (sampling positions are shown in figure 2, data are presented in Tab. S5) from the various geological units are used to calculate the units' average K concentration. The Tømmerås anticline (TA) in the northern drainage area show highest K concentration (average > 4 %).

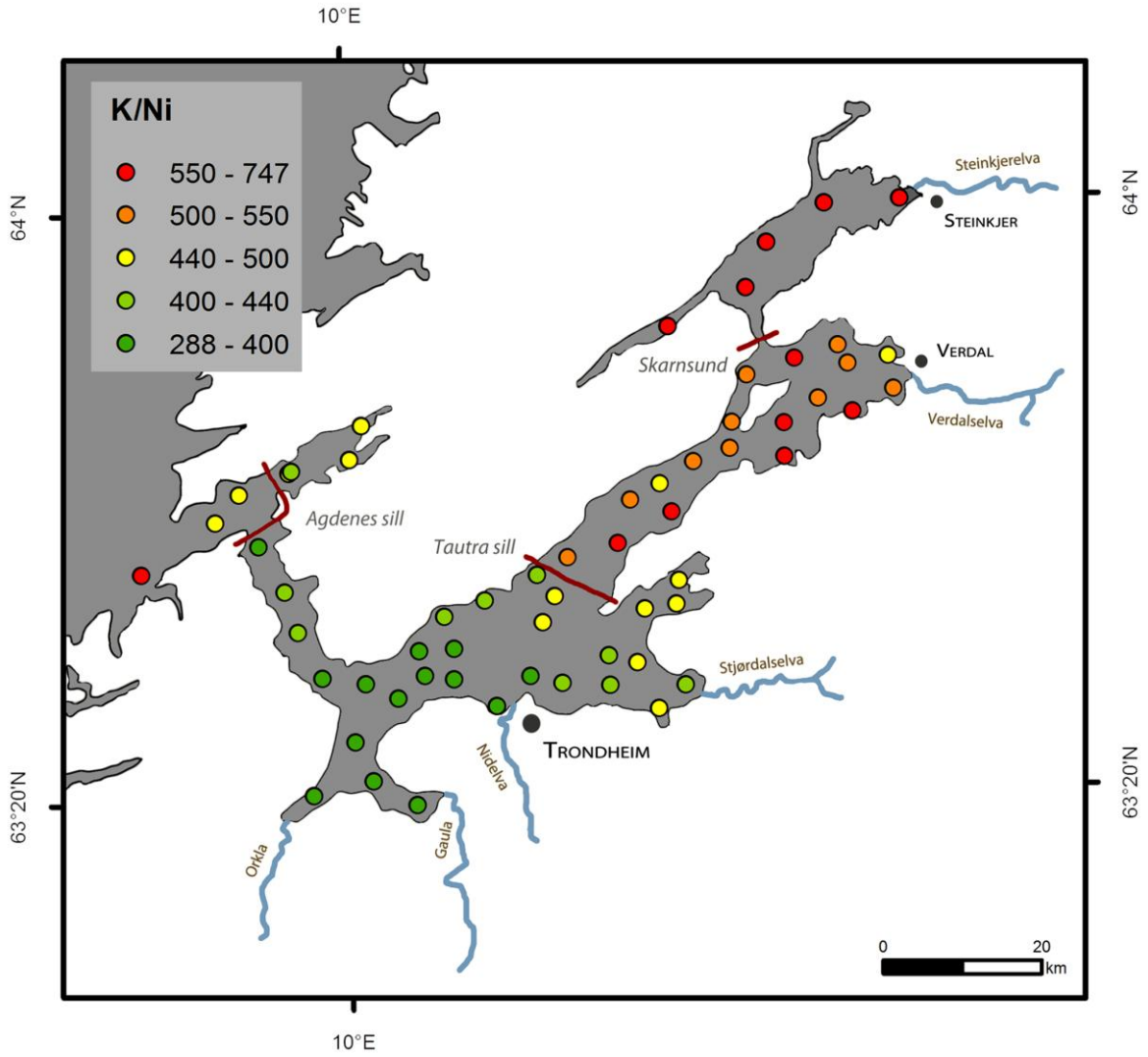

Figure 12: K/Ni in the surface sediments (Tab. S1). The Tautra sill in the middle of the fjord has a strong influence on the water circulation. As a result the K/Ni values are low in the southern and high in the northern part of the fjord.

References

Andersson M., Ottesen R.T. and Langedal M. (2010) Geochemistry of urban surface soils - Monitoring in Trondheim, Norway. *Geoderma* **156**, 112-118.

Bertrand S., Hughen K.A., Sepulveda J. and Pantoja S. (2012) Geochemistry of surface sediments from the fjords of Northern Chilean Patagonia (44-47°S): Spatial variability and implications for paleoclimate reconstructions. *Geochim Cosmochim Ac* **76**, 125-146.

Bordovskiy O.K. (1965) Sources of organic matter in marine basins. *Mar Geol* **3**, 5-31.

Bøe R., Rise L., Blikra L.H., Longva O. and Eide A. (2003) Holocene mass-movement processes in Trondheimsfjorden, Central Norway. *Norw J Geol* **83**, 3-22.

Bøe R., Bugge T., Rise L., Eidnes G., Eide A. and Mauring E. (2004) Erosional channel incision and the origin of large sediment waves in Trondheimsfjorden, central Norway. *Geo-Mar Lett* **24**, 225-240.

Calvert S.E., Pedersen T.F. and Thunell R.C. (1993) Geochemistry of the surface sediments of the Sulu and South China Seas. *Mar Geol* **114**, 207-231.

Cho Y.-G., Lee C.-B. and Choi M.-S. (1999) Geochemistry of surface sediments off the southern and western coasts of Korea. *Mar Geol* **159**, 111-129.

Collins R.P. and Jones M.B. (1986) The influence of climatic factors on the distribution of C4 species in Europe. *Vegetatio* **64**, 121-129.

Goñi M.A., Ruttenberg K.C. and Eglinton T.I. (1997) Sources and contribution of terrigenous organic carbon to surface sediments in the Gulf of Mexico. *Nature* **389**, 275-278.

Govin A., Holzwarth U., Heslop D., Ford Keeling L., Zabel M., Mulitza S., Collins J.A. and Chiessi C.M. (2012) Distribution of major elements in Atlantic surface sediments (36°N–49°S): Imprint of terrigenous input and continental weathering. *Geochem Geophy Geosy* **13**.

Hald M., Salomonsen G.R., Husum K. and Wilson L.J. (2011) A 2000 year record of Atlantic Water temperature variability from the Malangen Fjord, northeastern North Atlantic. *The Holocene*.

Hansen L., L'Heureux J.S. and Longva O. (2011) Turbiditic, clay-rich event beds in fjord-marine deposits caused by landslides in emerging clay deposits - palaeoenvironmental interpretation and role for submarine mass-wasting. *Sedimentology* **58**, 890-915.

Hayes J.M. (1993) Factors controlling 13C contents of sedimentary organic compounds: Principles and evidence. *Mar Geol* **113**, 111-125.

Hirst D.M. (1962) The geochemistry of modern sediments from the Gulf of Paria—II The location and distribution of trace elements. *Geochim Cosmochim Ac* **26**, 1147-1187.

Hoskin C.M., Burrell D.C. and Freitag G.R. (1978) Suspended sediment dynamics in Blue Fjord, western Prince William Sound, Alaska. *Estuarine and Coastal Marine Science* **7**, 1-16.

Howe J.A., Austin W.E.N., Forwick M., Paetzel M., Harland R. and Cage A.G. (2010) Fjord systems and archives: a review. *Geological Society, London, Special Publications* **344**, 5-15.

Inall M.E. and Gillibrand P.A. (2010) The physics of mid-latitude fjords: a review. *Geological Society, London, Special Publications* **344**, 17-33.

Jacobson P. (1983) Physical oceanography of the Trondheimsfjord. *Geophysical & Astrophysical Fluid Dynamics* **26**, 3-26.

Jasper J.P. and Gagosian R.B. (1990) The sources and deposition of organic matter in the Late Quaternary Pigmy Basin, Gulf of Mexico. *Geochim Cosmochim Ac* **54**, 1117-1132.

Karageorgis A.P., Anagnostou C.L. and Kaberi H. (2005) Geochemistry and mineralogy of the NW Aegean Sea surface sediments: implications for river runoff and anthropogenic impact. *Appl Geochem* **20**, 69-88.

Knies J. (2005) Climate-induced changes in sedimentary regimes for organic matter supply on the continental shelf off northern Norway. *Geochim Cosmochim Ac* **69**, 4631-4647.

Knies J., Brookes S. and Schubert C.J. (2007) Re-assessing the nitrogen signal in continental margin sediments: New insights from the high northern latitudes. *Earth Planet Sc Lett* **253**, 471-484.

Knies J. and Martinez P. (2009) Organic matter sedimentation in the western Barents Sea region: Terrestrial and marine contribution based on isotopic composition and organic nitrogen content. *Norw J Geol* **89**, 79-89.

Knudson K.P., Hendy I.L. and Neil H.L. (2011) Re-examining Southern Hemisphere westerly wind behavior: insights from a late Holocene precipitation reconstruction using New Zealand fjord sediments. *Quaternary Sci Rev* **30**, 3124-3138.

Koistinen T., Stephens M.B., Bogatchev V., Nordgulen Ø., Wennerström M. and Korhonen J. (2001) Geological Map of the Fennoscandian Shield, scale: 1: 2,000,000. *Geological Survey of Finland, Norway and Sweden and the North-West Department of Natural Resources of Russia.*

L'Heureux J.S., Hansen L. and Longva O. (2009) Development of the submarine channel in front of the Nidelva River, Trondheimsfjorden, Norway. *Mar Geol* **260**, 30-44.

L'Heureux J.S., Hansen L., Longva O., Emdal A. and Grande L.O. (2010) A multidisciplinary study of submarine landslides at the Nidelva fjord delta, Central Norway - Implications for geohazard assessment. *Norw J Geol* **90**, 1-20.

L'Heureux J.S., Glimsdal S., Longva O., Hansen L. and Harbitz C.B. (2011) The 1888 shoreline landslide and tsunami in Trondheimsfjorden, central Norway. *Mar Geophys Res* **32**, 313-329.

Loring D.H. (1990) Lithium — a new approach for the granulometric normalization of trace metal data. *Mar Chem* **29**, 155-168.

Lyså A., Hansen L., Christensen O., L'Heureux J.S., Longva O., Olsen H.A. and Sveian H. (2008) Landscape evolution and slide processes in a glacioisostatic rebound area; a combined marine and terrestrial approach. *Mar Geol* **248**, 53-73.

Martinez P., Bertrand P., Shimmield G.B., Karen C., Jorissen F.J., Foster J. and Dignan M. (1999) Upwelling intensity and ocean productivity changes off Cape Blanc (northwest Africa) during the last 70,000 years: geochemical and micropalaeontological evidence. *Mar Geol* **158**, 57-74.

Milzer G., Giraudeau J., Faust J., Knies J., Eynaud F. and Rühlemann C. (2013a) Spatial distribution of benthic foraminiferal stable isotopes and dinocyst assemblages in surface sediments of the Trondheimsfjord, central Norway. *Biogeosciences Discuss.* **10**, 5889-5921.

Milzer G., Giraudeau J., Schmidt S., Eynaud F. and Faust J. (2013b) Qualitative and quantitative reconstruction of surface water characteristics and recent hydrographic changes in the Trondheimsfjord, central Norway. *Clim. Past Discuss.* **9**, 4553-4598.

Mortensen P., aring, B. l., Hovland T., Fosså J.H. and Furevik D.M. (2001) Distribution, abundance and size of Lophelia pertusa coral reefs in mid-Norway in relation to seabed characteristics. *Journal of the Marine Biological Association of the United Kingdom* **81**, 581-597.

Mortlock R.A. and Froelich P.N. (1989) A simple method for the rapid determination of biogenic opal in pelagic marine sediments. *Deep Sea Research Part A. Oceanographic Research Papers* **36**, 1415-1426.

Müller P.J. (1977) CN ratios in Pacific deep-sea sediments: Effect of inorganic ammonium and organic nitrogen compounds sorbed by clays. *Geochim Cosmochim Ac* **41**, 765-776.

O'Leary M.H. (1981) Carbon isotope fractionation in plants. *Phytochemistry* **20**, 553-567.

Ottesen R.T., Bogen J., Bølviken B. and Volden T. (1989) Overbank sediment: a representative sample medium for regional geochemical mapping. *Journal of Geochemical Exploration* **32**, 257-277.

Ottesen R.T., Bogen J., Bølviken B., Volden T. and Haugland T. (2000) Geokjemisk atlas for Norge, del 1: Kjemisk sammensetning av flomsedimenter. *Geological survey of Norway (NGU), Norwegian Water Resources and Energy Directorate (NVE)*, Trondheim.

Ottesen R.T. and Langedal M. (2001) Urban geochemistry in Trondheim, Norway. *Norges Geologiske Undersokelse* **438**, 63-69.

Perdue E.M. and Koprivnjak J.F. (2007) Using the C/N ratio to estimate terrigenous inputs of organic matter to aquatic environments. *Estuar Coast Shelf S* **73**, 65-72.

Pinto J.G. and Raible C.C. (2012) Past and recent changes in the North Atlantic oscillation. *Wires Clim Change* **3**, 79-90.

Rise L., Bøe R., Sveian H., Lyså A. and Olsen H.A. (2006) The deglaciation history of Trondheimsfjorden and Trondheimsleia, Central Norway. *Norw J Geol* **86**, 415-434.

Roberts D. (1997) Geochemistry of Palaeoproterozoic porphyritic felsic volcanites from the olden and Tømmerås windows, central Norway. *GFF* **119**, 141-148.

Rullkötter J. (2006) Organic Matter: The Driving Force for Early Diagenesis. in: Schulz, H.D., Zabel, M. (Eds.), Marine Geochmistry, 2 ed. *Springer*, Berlin Heidelberg New York, pp. 125-168.

Sakshaug E. and Myklestad S. (1973) Studies on the phytoplankton ecology of the trondheimsfjord. III. Dynamics of phytoplankton blooms in relation to environmental factors, bioassay experiments and parameters for the physiological state of the populations. *Journal of Experimental Marine Biology and Ecology* **11**, 157-188.

Sakshaug E. and Sneli J.-A. (2000) Trondheimsfjorden. *Tapir Forlag*, Trondheim.

Sargent J.R., Hopkins C.C.E., Seiring J.V. and Youngson A. (1983) Partial characterization of organic material in surface sediments from Balsfjorden, northern Norway, in relation to its origin and nutritional value for sediment-ingesting animals. *Mar Biol* **76**, 87-94.

Schafer C.T., Smith J.N. and Seibert G. (1983) Significance of natural and anthropogenic sediment inputs to the saguenay Fjord, Quebec. *Sediment Geol* **36**, 177-194.

Schubert C.J. and Calvert S.E. (2001) Nitrogen and carbon isotopic composition of marine and terrestrial organic matter in Arctic Ocean sediments:: implications for nutrient utilization and organic matter composition. *Deep Sea Research Part I: Oceanographic Research Papers* **48**, 789-810.

Sepúlveda J., Pantoja S., Hughen K.A., Bertrand S., Figueroa D., León T., Drenzek N.J. and Lange C. (2009) Late Holocene sea-surface temperature and precipitation variability in northern Patagonia, Chile (Jacaf Fjord, 44°S). *Quaternary Res* **72**, 400-409.

Sepúlveda J., Pantoja S. and Hughen K.A. (2011) Sources and distribution of organic matter in northern Patagonia fjords, Chile (~44-47°S): A multi-tracer approach for carbon cycling assessment. *Cont Shelf Res* **31**, 315-329.

Shimmield G.B. (1992) Can sediment geochemistry record changes in coastal upwelling palaeoproductivity? Evidence from northwest Africa and the Arabian Sea. *Geological Society, London, Special Publications* **64**, 29-46.

Stein R. and MacDonald R.W. (2004) The Organic Carbon Cycle in the Arctic Ocean. *Springer*, Berlin Heidelberg.

Still C.J., Berry J.A., Collatz G.J. and DeFries R.S. (2003) Global distribution of C3 and C4 vegetation: Carbon cycle implications. *Global Biogeochem Cy* **17**, 1006.

Syvitski J. and Schafer C.T. (1985) Sedimentology of Arctic Fjords Experiment (SAFE): Project Introduction. *Arctic* **38**, 264-270.

Syvitski J.P.M., Burrell D.C. and Skei J.M. (1987) Fjords: Processes and Products. *Springer-Verlag*, New York.

Syvitski J.P.M. (1989) On the Deposition of Sediment within Glacier-Influenced Fjords - Oceanographic Controls. *Mar Geol* **85**, 301-329.

Vogt C., Lauterjung J. and Fischer R.X. (2002) Investigation of the Clay Fraction (<2µm) of the Clay Minerals Society Reference Clays. *Clays and Clay Minerals* **50**, 388-400.

Volent Z., Johnsen G., Hovland E.K., Folkestad A., Olsen L.M., Tangen K. and Sørensen K. (2011) Improved monitoring of phytoplankton bloom dynamics in a Norwegian fjord by integrating satellite data, pigment analysis, and Ferrybox data with a coastal observation network. *Journal of Applied Remote Sensing* **5**.

Wanner H., Brönnimann S., Casty C., Gyalistras D., Luterbacher J., Schmutz C., Stephenson D. and Xoplaki E. (2001) North Atlantic Oscillation – Concepts And Studies. *Surveys in Geophysics* **22**, 321-381.

Wendelbo P.S. (1970) Hydrografiske forhold i Trondheimsfjorden 1963-66. PhD Thesis, University of Oslo

Winkelmann D. and Knies J. (2005) Recent distribution and accumulation of organic carbon on the continental margin west off Spitsbergen. *Geochem Geophy Geosy* **6**.

Yarincik K.M., Murray R.W. and Peterson L.C. (2000) Climatically sensitive eolian and hemipelagic deposition in the Cariaco Basin, Venezuela, over the past 578,000 years: Results from Al/Ti and K/Al. *Paleoceanography* **15**, 210-228.

Supplementary Paper I

Table S1: Location of sampling stations and list of the presented elements measured by 4 Acid digestion ICP-AES

Sampling station	Latitude (DD)	Longitude (DD)	Water depth (m)	Al (%)	Ca (%)	K (%)	Ni (ppm)	Mg (%)	Cr (ppm)
100	64.0031	11.4382	57	6.68	1.77	2.69	36	1.77	86
101	64.0002	11.2442	157	7.62	1.27	3.2	53	2.29	105
102	63.9580	11.0923	222	7.69	1.18	3.28	59	2.45	110
103	63.9075	11.0352	252	7.73	1.55	3.26	58	2.36	112
104	63.8664	10.8323	128	7.11	1.5	2.92	47	2.05	91
200	63.8090	11.0305	325	7.41	1.96	2.98	57	2.35	113
201	63.8262	11.1542	110	7.27	1.9	2.86	50	2.15	105
202	63.8393	11.2666	82	7.39	1.92	2.73	50	2.19	108
203	63.8183	11.2904	402	7.46	1.65	2.98	56	2.33	114
204	63.8255	11.3938	300	6.68	2.07	2.35	47	2.01	99
205	63.7883	11.4052	81	7.11	2.09	2.37	47	2.05	98
206	63.7801	11.2117	422	7.61	1.53	3.12	57	2.39	112
207	63.7644	11.2976	25	5.7	2.09	1.51	27	1.25	60
208	63.7537	11.1220	421	6.94	2.11	2.7	49	2.13	103
209	63.7157	11.1205	30	5.57	2.39	1.52	23	1.29	65
210	63.7266	10.9822	425	7.65	1.9	3.03	59	2.41	118
211	63.7559	10.9887	416	7.53	1.82	3.12	60	2.48	113
212	63.7129	10.8874	426	7.5	1.9	3.06	60	2.49	114
213	63.6887	10.8005	412	7.78	2.16	3.1	63	2.48	119
214	63.6568	10.8284	72	5.65	4.33	1.39	24	1.27	55
215	63.6711	10.7238	370	7.53	2.07	3.06	60	2.48	114
216	63.6227	10.6901	175	5.88	3.62	1.73	31	1.5	65
217	63.6080	10.5619	212	5.27	6.27	1.63	32	1.41	70
300	63.5885	10.4822	253	7.7	2.83	2.94	68	2.68	124
301	63.5641	10.5268	176	6.55	3.14	2.17	48	1.98	94
302	63.5349	10.4954	165	6.81	2.66	2.4	54	2.12	107
303	63.5610	10.3484	240	6.99	2.54	2.54	58	2.26	118
304	63.5475	10.7542	63	5.97	2.32	1.95	39	1.76	88
305	63.5521	10.8345	62	6.7	2.11	2.31	48	2.05	97
306	63.5791	10.8429	117	7.65	1.69	3.23	70	2.8	134
307	63.4956	10.6603	173	7.56	1.64	3.03	69	2.7	124
308	63.4872	10.7320	82	6.6	2.18	2.19	46	2.02	98
309	63.4602	10.8520	77	6.86	2.04	2.24	54	2.09	115
310	63.4346	10.7829	58	6.44	2.19	2.17	49	2.02	109
311	63.4624	10.6616	177	7.22	1.59	2.89	67	2.57	139
312	63.4661	10.5415	254	7.27	1.86	2.82	69	2.59	138
313	63.4743	10.4608	316	7.32	1.99	2.72	69	2.48	137
314	63.4411	10.3736	71	5.74	1.9	1.57	40	1.63	99
315	63.4723	10.2674	492	6.15	2.16	2.03	51	1.96	114

Table S1 - continued

Sampling station	Latitude (DD)	Longitude (DD)	Water depth (m)	Al (%)	Ca (%)	K (%)	Ni (ppm)	Mg (%)	Cr (ppm)
315	63.4723	10.2674	492	6.15	2.16	2.03	51	1.96	114
316	63.5072	10.2681	483	7.81	2.39	2.83	72	2.72	147
317	63.5436	10.2457	292	7.57	2.64	2.68	64	2.4	132
318	63.5052	10.1794	500	7.73	2.56	2.82	72	2.65	149
319	63.4771	10.1936	504	7.35	2.48	2.51	65	2.46	137
320	63.4517	10.1248	500	7.43	2.85	2.72	71	2.58	150
321	63.4686	10.0443	512	7.1	3.05	2.34	60	2.29	129
322	63.4029	10.0158	433	7.51	2.44	2.68	72	2.61	146
323	63.3586	10.0596	335	7.24	1.58	2.8	74	2.59	151
324	63.3311	10.1693	170	6.31	1.71	2.04	60	1.95	114
325	63.3432	9.9087	301	6.99	2.24	1.9	66	2.38	150
326	63.4755	9.9337	530	6.98	3.42	2.18	57	2.14	119
327	63.5279	9.8733	546	6.21	4.03	1.83	45	1.86	101
328	63.5736	9.8417	566	6.96	4.05	2.02	48	1.95	107
329	63.6251	9.7759	605	5.95	5.46	1.78	48	1.94	116
400	63.7080	9.8546	225	5.75	4.53	1.68	37	1.62	85
401	63.7101	9.8621	225	6.88	4.19	2.25	53	2.22	112
402	63.7226	10.0101	83	6.53	3.77	1.86	42	1.91	95
403	63.7607	10.0419	94	6.9	3.86	2.13	48	2.04	101
500	63.6841	9.7277	115	4.3	9.59	1.09	22	1.07	50
501	63.6525	9.6666	389	4.94	7.84	1.27	26	1.24	57
502	63.5941	9.4771	350	4.59	10.55	1.25	22	1.08	52
			mean	6.8	2.9	2.4	52.1	2.1	108.1
			s.d.[(a)]	0.8	1.8	0.6	14.1	0.4	25.6
			Analytical uncertainty (rel.%) [(b)]	0.6	0.5	1.4	0.8	0.9	2.2
			Lower detection limit (ppm)	100	100	100	2	100	2

[(a)] s.d. = standard deviation (1 sigma)

[(b)] The analytical uncertainty was calculated as 1 s.d. of repeated analyses of every 20th sample

Table S2: Organic geochemistry and calculated MT index

Sampling station	Latitude (DD)	Longitude (DD)	Water depth (m)	TOC (wt%)	TC (wt%)	N_{inorg} (%)	N_{tot} (%)	$\delta^{13}C_{org}$ (‰)	F_{terr} [(a)] (wt%)	MT Index [(b)]
100	64.0031	11.4382	57	1.52	1.75	0.02	0.13	-24.93	66.62	-1.79
101	64.0002	11.2442	157	1.19	1.36	0.04	0.13	-23.32	64.00	-0.66
102	63.9580	11.0923	222	1.24	1.47	0.04	0.14	-23.29	56.57	-0.39
103	63.9075	11.0352	252	1.07	1.35	0.04	0.13	-23.35	49.67	-0.19
104	63.8664	10.8323	128	1.36	1.67	0.04	0.13	-23.23	73.26	-0.92
200	63.8090	11.0305	325	1.03	1.44	0.04	0.12	-23.40	54.91	-0.40
201	63.8262	11.1542	110	0.94	1.24	0.04	0.10	-23.91	71.28	-1.29
202	63.8393	11.2666	82	0.82	1.12	0.04	0.10	-24.48	67.67	-1.54
203	63.8183	11.2904	402	0.94	1.22	0.04	0.11	-24.43	65.78	-1.44
204	63.8255	11.3938	300	0.92	1.27	0.03	0.09	-25.45	71.16	-2.29
205	63.7883	11.4052	81	0.82	1.02	0.03	0.08	-25.20	75.57	-2.28
206	63.7801	11.2117	422	0.97	1.25	0.04	0.12	-24.04	59.04	-0.96
207	63.7644	11.2976	25	0.78	1.00	0.02	0.07	-25.18	64.94	-1.90
208	63.7537	11.1220	421	0.87	1.18	0.03	0.10	-23.83	56.32	-0.73
209	63.7157	11.1205	30	1.11	1.35	0.01	0.08	-25.19	91.31	-2.81
210	63.7266	10.9822	425	1.03	1.43	0.04	0.13	-23.40	49.01	-0.20
211	63.7559	10.9887	416	1.12	1.50	0.04	0.13	-23.23	52.11	-0.19
212	63.7129	10.8874	426	0.97	1.31	0.04	0.12	-23.40	53.06	-0.34
213	63.6887	10.8005	412	1.10	1.47	0.04	0.13	-23.01	53.28	-0.09
214	63.6568	10.8284	72	0.50	1.32	0.01	0.06	-22.35	18.32	1.54
215	63.6711	10.7238	370	1.10	1.49	0.04	0.12	-22.96	52.24	-0.02
216	63.6227	10.6901	175	0.55	1.19	0.01	0.06	-22.36	44.00	0.65
217	63.6080	10.5619	212	0.35	2.17	0.02	0.04	-22.34	48.96	0.49
300	63.5885	10.4822	253	0.97	1.50	0.03	0.12	-22.46	32.19	0.99
301	63.5641	10.5268	176	0.73	1.27	0.02	0.09	-22.40	26.32	1.24
302	63.5349	10.4954	165	0.75	1.18	0.02	0.09	-22.45	38.98	0.76
303	63.5610	10.3484	240	0.80	1.16	0.02	0.09	-22.33	50.59	0.44
304	63.5475	10.7542	63	0.65	0.94	0.01	0.07	-23.21	34.50	0.43
305	63.5521	10.8345	62	0.84	1.10	0.02	0.09	-23.28	41.35	0.15
306	63.5791	10.8429	117	1.25	1.47	0.03	0.14	-23.05	41.66	0.28
307	63.4956	10.6603	173	0.93	1.12	0.03	0.10	-22.87	51.37	0.07
308	63.4872	10.7320	82	0.74	0.93	0.02	0.08	-23.44	48.29	-0.20
309	63.4602	10.8520	77	1.23	1.50	0.02	0.11	-25.64	67.03	-2.27
310	63.4346	10.7829	58	1.02	1.27	0.02	0.09	-24.31	62.01	-1.24
311	63.4624	10.6616	177	0.90	1.06	0.02	0.10	-23.05	50.94	-0.04
312	63.4661	10.5415	254	0.99	1.28	0.02	0.11	-22.87	41.26	0.42
313	63.4743	10.4608	316	0.97	1.25	0.02	0.11	-22.78	39.42	0.54
314	63.4411	10.3736	71	1.20	1.27	0.01	0.08	-24.53	100.00	-2.69
315	63.4723	10.2674	492	0.85	1.13	0.02	0.09	-22.48	44.33	0.56

Table S2 - continued

Sampling station	Latitude (DD)	Longitude (DD)	Water depth (m)	TOC (wt%)	TC (wt%)	N_{inorg} (%)	N_{tot} (%)	$\delta^{13}C_{org}$ (‰)	F_{terr} [(a)] (wt%)	MT Index [(b)]
316	63.5072	10.2681	483	1.01	1.39	0.02	0.11	-22.40	36.72	0.88
317	63.5436	10.2457	292	0.98	1.47	0.03	0.12	-22.25	28.02	1.27
318	63.5052	10.1794	500	1.13	1.57	0.02	0.13	-22.38	38.11	0.84
319	63.4771	10.1936	504	1.08	1.50	0.02	0.12	-22.89	42.43	0.36
320	63.4517	10.1248	500	1.31	1.86	0.02	0.15	-22.28	31.97	1.12
321	63.4686	10.0443	512	1.20	1.79	0.02	0.13	-22.35	35.03	0.97
322	63.4029	10.0158	433	1.11	1.50	0.02	0.12	-22.57	37.68	0.73
323	63.3586	10.0596	335	1.01	1.23	0.02	0.10	-23.56	57.71	-0.60
324	63.3311	10.1693	170	1.02	1.22	0.01	0.07	-25.98	88.96	-3.25
325	63.3432	9.9087	301	1.31	1.56	0.02	0.12	-24.67	61.94	-1.47
326	63.4755	9.9337	530	1.34	2.05	0.02	0.15	-22.58	27.45	1.08
327	63.5279	9.8733	546	0.95	1.73	0.02	0.10	-22.15	32.04	1.20
328	63.5736	9.8417	566	1.19	1.99	0.02	0.13	-22.36	29.12	1.16
329	63.6251	9.7759	605	1.04	2.51	0.02	0.10	-23.78	57.88	-0.75
400	63.7080	9.8546	225	1.19	2.17	0.01	0.14	-21.61	15.13	1.65
401	63.7101	9.8621	225	1.48	2.47	0.02	0.18	-21.88	7.30	1.93
402	63.7226	10.0101	83	1.75	2.49	0.01	0.20	-22.05	12.53	2.23
403	63.7607	10.0419	94	1.87	2.68	0.02	0.21	-22.35	15.09	2.13
500	63.6841	9.7277	115	0.54	3.24	0.01	0.06	-21.60	30.40	1.61
501	63.6525	9.6666	389	0.80	2.91	0.01	0.10	-21.82	7.21	2.27
502	63.5941	9.4771	350	0.71	3.59	0.01	0.09	-21.19	0.00	2.93
			mean	1.0	1.4	0.02	0.11	-23.0	49.0	0.11
			s.d. [(c)]	0.3	0.6	0.01	0.03	1.1	20.7	1.38

[(a)] F_{terr} = fraction of terrestrial organic carbon (Fterr), which is calculated from the Norg/Corg ratio

[(b)] MT Index = index for the variable input of terrigenous versus marine organic matter

[(c)] s.d. = standard deviaton (1 sigma)

Table S3: Mineralogical and sedimentological data

Sampling station	Latitude	Longitude	Water depth	< 2 µm	2-63 µm	63-125 µm	125-250 µm	250-500 µm	500-2000 µm	Calcite	Aragonite	Sum Illit + Mica	Sum Phyllosilicates	Quartz	Plagioclase	K-feldspar
	(DD)	(DD)	(m)	(%)	(%)	(%)	(%)	(%)	(%)	(%)	(%)	(%)	(%)	(%)	(%)	(%)
100	64.0031	11.4382	57	4.9	83.9	5.6	3.9	1.3	0.4	0.5	0.0	15.6	28.3	24.9	28.6	3.5
101	64.0002	11.2442	157	11.5	87.3	1.2	0.0	0.0	0.0	0.4	0.0	14.3	39.0	16.1	18.2	4.0
102	63.9580	11.0923	222	13.1	85.7	1.2	0.0	0.0	0.0	0.3	0.0	23.5	46.9	15.1	18.5	2.9
103	63.9075	11.0352	252	11.2	80.8	4.4	3.5	0.1	0.0	0.5	0.0	31.1	56.6	12.6	18.3	1.4
104	63.8664	10.8323	128	9.5	80.2	7.3	2.9	0.1	0.0	0.4	0.0	22.9	43.6	17.9	22.2	2.9
200	63.8090	11.0305	325	10.7	86.6	2.7	0.0	0.0	0.0	0.7	0.0	13.8	43.4	15.9	16.1	2.1
201	63.8262	11.1542	110	8.3	88.7	3.0	0.0	0.0	0.0	0.6	0.0	24.0	42.6	18.6	18.2	2.2
202	63.8393	11.2666	82	5.9	90.8	3.4	0.0	0.0	0.0	0.5	0.0	23.9	53.1	18.7	15.8	2.1
203	63.8183	11.2904	402	9.6	84.7	3.7	2.0	0.0	0.0	0.4	0.0	34.0	45.1	15.7	16.0	2.4
204	63.8255	11.3938	300	5.9	83.0	8.8	2.3	0.0	0.0	0.8	0.0	21.1	39.0	21.9	21.1	2.6
205	63.7883	11.4052	81	5.0	86.5	6.4	2.1	0.0	0.0	0.4	0.0	20.8	36.7	25.3	22.3	2.2
206	63.7801	11.2117	422	10.0	87.8	2.2	0.0	0.0	0.0	0.5	0.0	33.1	47.2	12.9	17.5	2.1
207	63.7644	11.2976	25	2.6	44.9	13.3	15.9	14.9	8.4	1.3	0.0	19.7	34.7	31.8	20.3	1.8
208	63.7537	11.1220	421	8.7	80.2	8.7	2.4	0.0	0.0	1.4	0.0	19.3	41.3	24.8	16.5	3.0
209	63.7157	11.1205	30	2.9	57.9	22.3	10.9	2.5	3.5	0.4	0.0	6.3	14.5	42.5	22.6	3.6
210	63.7266	10.9822	425	9.8	88.1	2.1	0.0	0.0	0.0	0.8	0.0	20.9	37.5	19.1	19.0	4.2
211	63.7559	10.9887	416	11.5	87.1	1.4	0.0	0.0	0.0	1.0	0.0	33.1	46.1	16.3	15.6	4.3
212	63.7129	10.8874	426	10.7	87.7	1.6	0.0	0.0	0.0	1.1	0.0	23.5	47.4	17.4	13.6	2.7
213	63.6887	10.8005	412	10.6	87.3	2.1	0.0	0.0	0.0	1.9	0.0	25.5	42.5	17.0	15.2	4.4
214	63.6568	10.8284	72	2.6	41.4	36.2	14.6	2.2	3.1	3.8	0.0	6.9	19.3	33.2	19.6	6.5
215	63.6711	10.7238	370	11.1	87.4	1.5	0.0	0.0	0.0	2.2	0.0	20.8	47.0	20.2	16.0	3.0
216	63.6227	10.6901	175	4.5	47.9	25.9	13.1	4.5	4.1	3.7	0.0	20.1	30.7	30.5	16.2	3.5
217	63.6080	10.5619	212	2.3	17.0	4.3	20.5	27.7	24.1	14.5	4.4	6.3	15.9	19.5	27.3	4.6

Table S3 - continued

Sampling station	Latitude	Longitude	Water depth	< 2 µm	2-63 µm	63-125 µm	125-250 µm	250-500 µm	500-2000 µm	Calcite	Aragonite	Sum Illit + Mica	Sum Phyllosilicates	Quartz	Plagioclase	K-feldspar
	(DD)	(DD)	(m)	(%)	(%)	(%)	(%)	(%)	(%)	(%)	(%)	(%)	(%)	(%)	(%)	(%)
300	63.5885	10.4822	253	9.7	83.2	4.0	3.0	0.1	0.0	3.0	0.0	21.3	39.3	20.0	16.6	3.6
301	63.5641	10.5268	176	7.4	71.4	12.7	6.0	2.1	0.5	2.8	0.0	17.4	28.5	22.9	25.9	2.9
302	63.5349	10.4954	165	8.0	79.4	9.9	2.7	0.0	0.0	1.2	0.0	20.4	32.0	21.7	22.4	2.3
303	63.5610	10.3484	240	8.7	78.2	9.6	3.4	0.1	0.0	1.7	0.0	12.3	36.0	21.6	15.8	6.0
304	63.5475	10.7542	63	5.8	74.5	14.9	4.8	0.0	0.0	0.6	0.0	10.0	20.9	26.8	26.8	4.9
305	63.5521	10.8345	62	5.7	85.7	6.4	2.2	0.0	0.0	0.6	0.0	22.8	34.7	22.7	15.1	2.4
306	63.5791	10.8429	117	10.5	88.8	0.7	0.0	0.0	0.0	0.5	0.0	21.0	47.9	14.3	14.7	2.8
307	63.4956	10.6603	173	8.8	90.4	0.8	0.0	0.0	0.0	0.4	0.0	29.5	44.8	12.8	16.0	2.6
308	63.4872	10.7320	82	4.4	87.0	6.1	2.5	0.0	0.0	0.9	0.0	13.6	30.5	27.1	22.1	5.1
309	63.4602	10.8520	77	4.7	87.5	5.6	2.2	0.0	0.0	0.9	0.0	15.5	31.4	26.2	25.3	3.1
310	63.4346	10.7829	58	5.1	88.3	5.0	1.7	0.0	0.0	0.5	0.0	9.0	24.6	28.3	27.2	4.2
311	63.4624	10.6616	177	8.1	90.8	1.1	0.0	0.0	0.0	0.4	0.0	11.7	33.9	20.0	23.4	1.0
312	63.4661	10.5415	254	9.0	89.5	1.5	0.0	0.0	0.0	0.7	0.0	15.2	30.9	18.5	24.4	3.7
313	63.4743	10.4608	316	8.4	84.3	4.7	2.6	0.0	0.0	0.0	0.0	14.0	32.9	19.8	19.8	3.1
314	63.4411	10.3736	71	3.1	49.4	16.5	14.9	8.6	7.5	0.4	0.0	11.7	29.9	32.1	20.1	4.7
315	63.4723	10.2674	492	6.6	71.2	15.6	6.6	0.0	0.0	0.7	0.0	17.8	35.0	28.4	18.4	5.1
316	63.5072	10.2681	483	9.0	89.0	2.0	0.0	0.0	0.0	1.5	0.0	22.5	35.8	17.2	16.4	3.5
317	63.5436	10.2457	292	8.8	74.8	6.5	8.0	1.6	0.3	1.4	0.0	16.4	41.8	17.2	19.8	2.9
318	63.5052	10.1794	500	7.9	89.7	2.4	0.0	0.0	0.0	1.8	0.0	19.6	39.7	19.2	17.6	4.1
319	63.4771	10.1936	504	7.4	85.4	5.6	1.6	0.0	0.0	2.9	0.0	5.8	23.6	26.0	18.3	4.5
320	63.4517	10.1248	500	7.8	90.2	2.1	0.0	0.0	0.0	3.8	0.0	17.7	29.7	23.9	17.2	4.2
321	63.4686	10.0443	512	6.4	77.2	11.7	4.7	0.0	0.0	3.1	0.0	21.4	33.5	21.9	20.0	3.4
322	63.4029	10.0158	433	7.0	90.4	2.6	0.0	0.0	0.0	2.8	0.0	25.2	41.6	20.3	15.8	4.7
323	63.3586	10.0596	335	6.2	92.1	1.7	0.0	0.0	0.0	0.0	0.0	23.5	37.3	21.8	19.7	3.5

Table S3 - continued

Sampling station	Latitude	Longitude	Water depth	< 2 µm	2-63 µm	63-125 µm	125-250 µm	250-500 µm	500-2000 µm	Calcite	Aragonite	Sum Illit + Mica	Sum Phyllosilicates	Quartz	Plagioclase	K-feldspar
	(DD)	(DD)	(m)	(%)	(%)	(%)	(%)	(%)	(%)	(%)	(%)	(%)	(%)	(%)	(%)	(%)
324	63.3311	10.1693	170	3.1	73.0	15.7	7.2	0.7	0.3	0.0	0.0	23.5	36.2	30.5	20.3	2.4
325	63.3432	9.9087	301	4.4	81.0	9.8	4.7	0.1	0.0	0.0	0.0	16.6	32.5	25.0	18.4	3.8
326	63.4755	9.9337	530	6.5	75.8	12.9	4.8	0.0	0.0	1.9	0.0	20.5	39.4	20.7	18.5	2.4
327	63.5279	9.8733	546	5.5	67.1	14.3	11.2	1.7	0.2	4.0	0.0	20.5	31.9	25.6	18.7	5.2
328	63.5736	9.8417	566	5.6	73.9	12.7	6.7	0.9	0.2	3.9	0.0	20.0	32.4	21.2	21.8	5.8
329	63.6251	9.7759	605	3.5	52.9	4.6	8.1	17.3	13.7	3.8	1.6	16.1	30.8	21.7	12.0	2.9
400	63.7080	9.8546	225	5.6	66.1	19.7	8.6	0.0	0.0	3.7	0.0	17.6	31.4	18.7	18.1	3.7
401	63.7101	9.8621	225	6.2	80.3	9.4	3.6	0.4	0.1	4.6	0.0	10.9	20.1	18.9	30.0	7.5
402	63.7226	10.0101	83	3.8	78.1	13.5	4.6	0.0	0.0	4.8	0.0	19.6	34.5	18.2	17.4	3.4
403	63.7607	10.0419	94	4.7	75.9	12.3	5.3	1.1	0.7	3.5	0.0	9.3	23.2	25.2	22.9	3.4
500	63.6841	9.7277	115	2.4	25.0	19.2	26.3	10.6	16.5	10.3	5.9	5.3	11.7	27.7	20.3	5.8
501	63.6525	9.6666	389	2.7	41.8	32.5	20.3	2.5	0.3	9.0	3.8	7.7	18.8	27.8	17.3	5.0
502	63.5941	9.4771	350	3.2	32.2	15.7	27.7	14.0	7.2	9.1	6.0	10.7	18.5	22.8	19.1	5.3
			mean	6.6	83.1	5.9	2.7	0.0	0.0	1.1	0.0	19.6	34.7	21.4	19.5	3.6
			s.d. [(a)]	2.8	17.6	7.8	6.6	5.0	4.4	2.7	1.3	6.9	9.7	5.7	3.8	1.3
									Error (rel.%)	±1	±2-3	±5	±5	±1	±2-5	±2-5

[(a)] s.d. = standard deviation (1 sigma)

[(b)] Samples containing aragonite are mark in grey

Table S4: Results of the PCA used to calculate the TM index. Variables are $\delta^{13}C_{org}$ and the fraction of terrestrial organic carbon (F_{terr})

Sampling station	Factor scores: F1	Factor scores: F2
100	-1.79	-0.45
101	-0.66	0.51
102	-0.39	0.27
103	-0.19	-0.01
104	-0.92	0.88
200	-0.40	0.14
201	-1.29	0.38
202	-1.54	-0.12
203	-1.44	-0.15
204	-2.29	-0.63
205	-2.28	-0.31
206	-0.96	-0.13
207	-1.90	-0.67
208	-0.73	-0.09
209	-2.81	0.23
210	-0.20	-0.06
211	-0.19	0.16
212	-0.34	0.08
213	-0.09	0.34
214	1.54	-0.44
215	-0.02	0.34
216	0.65	0.44
217	0.49	0.63
300	0.99	-0.03
301	1.24	-0.19
302	0.76	0.21
303	0.44	0.69
304	0.43	-0.44
305	0.15	-0.24
306	0.28	-0.09
307	0.07	0.37
308	-0.20	-0.11
309	-2.27	-0.89
310	-1.24	-0.21
311	-0.04	0.23
312	0.42	0.02
313	0.54	0.01
314	-2.69	0.96
315	0.56	0.38
316	0.88	0.17
317	1.27	-0.04
318	0.84	0.22
319	0.36	0.04
320	1.12	0.08
321	0.97	0.14
322	0.73	0.09
323	-0.60	0.14
324	-3.25	-0.36
325	-1.47	-0.44
326	1.08	-0.27
327	1.20	0.17
328	1.16	-0.07
329	-0.75	0.00
400	2.13	-0.06
401	2.23	-0.51
402	1.93	-0.44
403	1.65	-0.55
500	1.61	0.46
501	2.27	-0.47
502	2.93	-0.31

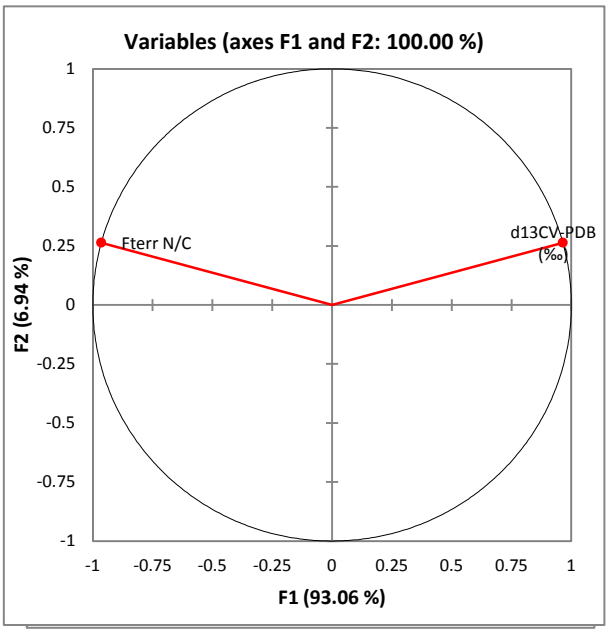

Table S5: Location of the presented bedrock samples and results of the elemental analysis

UTM E	UTM N	Rock type	Ni [ppm]	K_2O [%]	UTM E	UTM N	Rock type	Ni [ppm]	K_2O [%]
645188	7021680	Sandstone, feldspar-bearing	110	2.89	642875	7066809	Greenstone	35	0.44
641558	7021519	Metagreywacke	95	2.73	641030	7068934	Trondhjemite	8	2.63
641632	7028146	Gabbro	160	0.25	614498	7083448	Greenstone	43	0.83
644835	7031285	Gabbro	48	0.24	626138	7065705	Phyllite	61	2.58
649304	7029928	Phyllite	59	2.82	620181	7069009	Garben schist	62	2.24
618189	7029671	Mica schist	37	1.76	619476	7059312	Greenschist	133	1.31
614794	7029506	Quartzite	15	1.26	617342	7055829	Phyllite	17	1.05
613791	7033720	Phyllite	93	1.37	615843	7056711	Phyllite	28	1.19
620595	7039507	Hornblende schist	137	3.32	611108	7058801	Metagreywacke	106	2.15
630851	7037838	Diorite	57	0.16	549438	6992795	Quartz sandstone	67	1.26
617719	7042497	Metagreywacke	58	3.05	543704	6994428	Conglomerate	66	0.84
616119	7042602	Conglomerate	12	0.43	535579	6991720	Metagreywacke	8	3.69
632669	6996987	Trondhjemite	6	0.87	536587	6973767	Trondhjemite	0	3
644458	6976089	Mica schist	81	2.6	535927	6970934	Trondhjemite	0	2.78
647922	6979264	Mica schist	41	2.1	538369	6967138	Hornblende schist	111	2.42
655295	6983875	Granite	0	5.11	539600	6981706	Greenstone	78	0.94
657027	6986490	Granite	0	4.72	531738	6980998	Trondhjemite	0	0.54
639453	6985033	Mica schist	61	2.85	526048	7004681	Mica schist	43	1.28
640705	7007508	Metapelite	69	2.68	528604	7008646	Mica schist	95	2.03
646215	7002010	Mica schist	44	2.07	535578	7000663	Greenstone	70	0.19
643205	6999502	Amphibolite	111	0.2	553653	6978306	Phyllite	11	1.2
635774	6990308	Mica schist	49	1.95	560616	6994257	Quartz sandstone	29	0.45
618618	7000670	Mica schist	177	3.12	562262	6996882	Quartz sandstone	34	1.95
614180	7000104	Mica schist	195	3.31	557922	6952945	Phyllite	39	2.79
612362	7005961	Mica schist	16	3.54	552185	6947400	Metagreywacke	60	2.83
607211	7009906	Hornblende schist	140	2.24	555131	6941829	Mica schist	39	3.02
597507	7010404	Phyllite	42	1.7	560024	6930983	Mica schist	118	1.53
677647	7121405	Sandstone, feldspar-bearing	5	6.13	560929	6932619	Mica schist	22	1.68
683852	7120557	Phyllite	31	4.43	575148	6938832	Mica schist	179	3.51
662781	7113302	Phyllite	84	2.34	572260	6941301	Mica schist	13	2.12
666479	7117786	Phyllite	61	1.77	569079	6938612	Mica schist	53	3.17
654158	7120648	Rhyolite	0	5.26	564056	6944155	Mica schist	78	1.38
660120	7126308	Limestone	0	0.521	571446	6929320	Mica schist	240	4.68
672237	7135177	Greenstone	66	1.71	572397	6926283	Mica schist	67	2.42
662238	7131649	Greenstone	227	0.83	618906	6965795	Amphibolite	12	0.14
565811	7036241	Granitic gneiss	0	1.62	583173	6962655	Mica schist	16	3.14
562423	7024523	Greenstone	63	0.1	584457	6957862	Mica schist	46	2.7
565820	7028590	Greenstone	130	0.05	576426	6967119	Mica schist	24	1.62
585457	6981171	Mica schist	94	0.56	576112	6971793	Mica schist	44	3
612036	6973158	Mica schist	398	3.14	575091	6983736	Mica schist	40	1.9
600025	6983066	Mica schist	38	1.98	631682	6968183	Garben schist	71	2.82
596942	6984770	Diorite	0	2.26	628262	6967686	Mica schist	70	1.76
540060	6945326	Quartzite	11	1.46	609046	6979067	Mica schist	190	3.38
552036	6970756	Quartzite	0	0.84	573986	6987421	Mica schist	112	1.4
548793	6953013	Granodiorite	84	1.08	554034	6975900	Phyllite	42	1.78
542502	6950474	Trondhjemite	15	2.26	553246	6977237	Phyllite	29	2.29
558937	6978263	Phyllite	125	2.28	563141	6985613	Metagreywacke	65	0.91
556885	7009074	Greenstone	110	0.18	594233	7055171	Slate	50	2.31
539034	7019919	Mica schist	11	0.29	594763	7059166	Metagreywacke	8	3.1

Table S5 - continued

UTM E	UTM N	Rock type	Ni [ppm]	K2O [%]	UTM E	UTM N	Rock type	Ni [ppm]	K2O [%]
542960	7051225	Granitic gneiss	0	6.34	566883	7007844	Metagreywacke	10	1.98
560850	7061972	Granitic gneiss	5	3.62	582127	6998738	Mica gneiss	10	1.91
559610	7046353	Mica schist	47	2.02	574096	6999590	Mica gneiss	75	3.05
558886	7050541	Mica schist	98	4.26	568195	7001346	Phyllite	70	1.97
548789	6935163	Mica schist	12	1.13	644459	7051600	Phyllite	17	0.46
544294	6930090	Phyllite	29	1.86	646254	7048778	Metasandstein	28	1.44
547533	6928148	Mica schist	163	2.8	593929	7044906	Greenstone	66	0.32
552681	7024343	Mica schist	53	1.72	589877	7041717	Metasandstein	53	1.65
606247	7038278	Carbonaceous phyllite	47	2.72	605036	7040702	Slate	18	3.22
590696	7032150	Mica schist	15	1.51	603968	7025311	Greenstone	24	0.18
595460	7018957	Greenstone	227	0.72	608304	7018480	Mica schist	74	2.23
540544	7044219	Greenstone	26	0.35	604696	7015717	Mica schist	68	1.85
544874	7037108	Granodioritic gneiss	8	3.92	590589	7023717	Greenstone	28	1.12
548317	7034320	Mica gneiss	19	3.68	588742	7012785	Carbonaceous phyllite	56	2.6
533388	7017160	Arkose	12	3.38	596262	7003841	Mica schist	44	1.2
613485	7094887	Greenschist	65	2.57	604906	7000827	Mica schist	40	3
609119	7091151	Greenschist	61	0.19	569731	7021750	Metagabbro	85	0.06
603698	7085791	Mica schist	22	1.76	572403	7009327	Greenschist	349	0.08
600460	7083602	Granite	0	2.95	607064	6989266	Migmatite	41	2.05
596978	7072270	Mica schist	69	2.03	644340	7117876	Rhyodacite	0	5.35
593387	7078490	Phyllite	64	2.23	648233	7119662	Rhyolite	5	4.85
580448	7067722	Mica schist	19	1.12	669836	7131945	Marble	0	0.015
584344	7064645	Mica schist	69	3.16	642622	7121754	Carbonaceous sandstone	0	0.19
563560	7048358	Mica schist	45	1.86	660457	7132490	Greenschist	82	0.1
611055	7114910	Granitic gneiss	0	5.95	645213	7122667	Sandstone	9	1.64
588300	7085144	Granodioritic gneiss	0	2.67	624066	7113046	Carbonaceous sandstone	12	2.02
601259	7103885	Diorite	11	1.95	625077	7111204	Carbonaceous sandstone	12	3.03
603140	7102075	Quartz sandstone	11	2.02	592594	6967789	Phyllite	50	0.58
628640	7092524	Quartz sandstone	33	4.39	591828	6968689	Phyllite	27	0.74
669130	7079120	Garben schist	77	4.15	586538	6974998	Mica schist	67	2.98
666562	7077103	Quartz sandstone	27	2.38	569538	6961611	Phyllite	77	1.64
662392	7079386	Phyllite	41	1.41	567452	6974063	Quartz mica schist	84	2.68
655598	7079165	Phyllite	57	2.74	574992	6956842	Mica schist	31	0.57
646429	7080942	Phyllite	31	1.81	525012	6956637	Quartz schist	6	3.82
643891	7085468	Rhyolite	0	5.89	607209	6958636	Gabbro	52	0.52
639722	7077692	Greenstone	23	0.6	607603	6964921	Gabbro	37	0.51
660168	7062329	Gabbro	31	1.22	611959	6967761	Phyllite	161	3.41
656335	7062564	Carbonaceous phyllite	69	2.73	652275	7093987	Greenstone	56	0.08
645463	7065972	Diorite	60	0.16	648437	7097519	Metadacite	0	4.83
622354	7097936	Metaarkose	11	4.41	631428	7098266	Mica schist	34	3.75
552847	6917668	Mica schist	102	1.3	633228	7111398	Greenschist	38	1.02
640005	7104785	Metarhyodacite	0	5.33					

Paper II

Faust, J.C., Knies, J., Milzer, G., Giraudeau, J., (in review). Terrigenous input to a fjord in central Norway records the environmental response to the North Atlantic Oscillation over the past 50 years. Submitted to The Holocene, 16.12.2013

Terrigenous input to a fjord in central Norway records the environmental response to the North Atlantic Oscillation over the past 50 years

Johan C. Faust [a, b, *], Jochen Knies [a], Gesa Milzer [d], Jacques Giraudeau [d]

[a] Geological Survey of Norway, 7491 Trondheim, Norway
[b] University of Tromsø, Department of Geology, 9011 Tromsø, Norway
[d] Universite Bordeaux 1 UMR CNRS 5805 EPOC, 33405 Talence cedex , France

*Corresponding author: Norges geologiske undersøkelse /Geological Survey of Norway (NGU), Marine Geology, Postboks 6315 Sluppen, 7491 Trondheim, Norway. Tel.: +47 7390 4000. E-mail address: Johan.Faust@ngu.no

Abstract

During the last century, both earth surface temperature and moisture transport towards high latitudes have increased rapidly. The response of the sub-arctic region to these changes in terms of weathering, transport and delivery of terrigenous material towards the coastal and deep ocean is both complex and poorly understood. Sediments accumulating in fjords offer an excellent opportunity for studying such land-ocean interactions and may provide ultra-high-resolution records of environmental response to short-term climate variability. As a basis for Holocene climate change studies modern sources, supply and distribution of particular sediment components in the Trondheimsfjord have been investigated and imply lithogenic elements as a promising proxy for terrigenous input and river discharge. To better understand the impact of atmospheric variability on central Norwegian environment, we examine instrumental time series and show that the dominant mode of the atmospheric circulation in the North Atlantic region, the North Atlantic Oscillation (NAO), has a strong impact on river discharge, temperature, and precipitation in central Norway. In addition, elemental composition analysis of a short sediment core reveals that from 1959 to 2010

winter precipitation and temperature changes are recorded by changes in the inorganic geochemical composition of Trondheimsfjord sediments. Elemental ratios of Al/Zr and K/Ni in the sediment core MC99-3 show a close relation to small scale, high frequency climate variations and large-scale changes in the Northern Hemisphere climate. This implies that terrigenous input and related erosional processes in the fjord hinterland are highly sensitive to atmospheric circulation variability in the North Atlantic region. By comparing our results with NAO records derived from ice accumulation rates of Norwegian glaciers, western Greenland ice sheets and river discharge anomalies in the Eurasian Arctic, we show that it is possible to reconstruct the NAO from sedimentary archives in central Norwegian fjords.

1. Introduction

The investigation of sub-Arctic environmental response to climate variability requires well-dated high resolution archives from climate sensitive regions. One such region is the Trondheimsfjord in central Norway (Fig. 1), which experienced relatively high sedimentation rates since the last deglaciation (approx. 0.3-0.5 cm/yr, Bøe et al., 2003; Rise et al., 2006a). These sediments represent a natural repository for dissolved and particulate material derived from terrestrial weathering and erosion. Apart from the relatively warm northward flowing North Atlantic Current, the Norwegian coastal climate is strongly influenced by the North Atlantic Oscillation (NAO) (e.g. Dickson et al., 2000; Hurrell, 1995; Cherry et al., 2005). This dominant mode of the atmospheric circulation is most pronounced during winter times (Dec-Mar) and swings between two phases: A positive (negative) NAO generates periods of warmer and wetter (colder and dryer) climate conditions in north-western Europe (e.g. Wanner et al., 2001). Changes in precipitation and temperature associated with NAO are assumed to alter the constitution of fluvial sediment flux from land towards ocean basins generated by weathering and erosion of bedrock and soils (e.g. Govin et al., 2012; Lamy et al., 2001; White and Blum, 1995). Moreover, several studies of sedimentary and mass-wasting processes in the Trondheimsfjord (Bøe et al., 2004; Bøe et al., 2003; Hansen et al., 2011; L'Heureux et al., 2011; L'Heureux et al., 2009; L'Heureux et al., 2010; Lysså et al., 2008; Rise et al., 2006b) imply Holocene climate variability as a potential trigger for geohazards. Exploring such a relationship between terrigenous input and changes in environmental conditions requires detailed knowledge of the transport mechanisms dominating particle supply (e.g. Zabel et al., 2001), although intricate fjord bathymetry combined with complex water circulation systems provides additional constraints on identifying climate proxies that pinpoint the terrigenous response to climate variability. In this study we examine the

inorganic geochemical record of the Trondheimsfjord sediments over the past 50 years (2010 - 1959). This data provides the possibility for a proxy calibration of selected sediment constituents to instrumental data of temperature, precipitation, river runoff and to large scale modes of climate variability such as the NAO. Thus, the existing relationship between climate and sediment composition can be quantified and the relative magnitude and impact of past changes can be better assessed. Previous investigations of Trondheimsfjord surface sediments and hinterland bedrocks have shown that the distribution of Al/Zr and K/Ni in the fjord sediments reflect regional sources of Al, Zr, K and Ni in the hinterland (Fig. 2). Thus, by studying the lithogenic elements Zr, K, Ni, Al in temporally well-constrained sediment records we may identify the causes, timing and extent of past changes in the erosion and weathering regime of the Trondheimsfjord catchment area associated with variable NAO modes.

In this paper we show that changes in Trondheimsfjord regional temperature, precipitation and river runoff are strongly related to variabilities in the winter NAO. Moreover, our terrigenous proxies record both small scale, high frequency, and large scale long term shifts in temperature and precipitation. This good relationships between regional sedimentary climatic proxies and key parameters of hydrological and atmospheric changes over the past 50 years potentially allows the reconstruction of long term NAO variations from Trondheimsfjord sediments. With regard to an expected future warming and associated overall increase in runoff (Gedney et al., 2006; Labat et al., 2004) this study will also help to better estimate the expected impact of climate change on geohazards due to weathering and erosion.

2. Study area

The temperate Trondheimsfjord is located in the central part of Norway (63°40´N, 09°45´E, 64°45´N, 11°30´E, Fig. 1). With a length of approximately 135 km, it is the third longest fjord in the country (Jacobson, 1983). Three sills, the Agdenes Sill at the entrance (max. 330 m water depth), the Tautra Sill in the middle section (max. 100 m water depth) and the Skarnsund Sill in the inner part (max. water depth 100 m), subdivide the Trondheimsfjord into three main basins: Seaward Basin, Middle Fjord and Beitstadfjord (Fig. 1). The total fjord volume is 235 km^3, total surface area 1420 km^2, average tide 1.8 m and the average water depth is 165 m (Sakshaug and Sneli, 2000: and references therein). The total drainage area is approximately 20 000 km^2 (Rise et al., 2006a) with a mean precipitation of about 1100 mm/year. Six main rivers enter the fjord from the South-East; four in the Seaward Basin (Gaula, Orkla, Nidelva, Stjørdalselva), one in the Middle Fjord (Verdalselva) and one in the Beitstadfjord (Steinkjerelva) (Fig. 1). The freshwater supply from these rivers decreases the surface salinity and initiates an estuarine circulation (Jacobson, 1983) with a brackish surface layer 5 to 15 m thick (Öztürk et al., 2002). Although the fjord reaches depths up to 620 m, in general water masses below the estuarine circulation cell can be described as an energetically low environment and the distribution of sediments within the fjord is, therefore, largely controlled by the circulation and particle load in the upper part of the water column (Syvitski, 1989a; Wendelbo, 1970). The temperature and salinity of Trondheimsfjord surface waters vary strongly with changes in insolation and river runoff (Jacobson, 1983). Due to the inflow of North Atlantic water, Trondheimsfjord deep water (below ca. 100 m), however, show stable temperature and salinity values of approximately 7.5°C and 34.8 PSU, respectively, throughout the year (Wendelbo, 1970).

3. Material and methods

3.1 Sediment cores: Sampling and preparation

A short sediment core MC99-3 (26 cm) (hereafter referred to as MC99) from the Trondheimsfjord Seaward Basin (water depth 504 m, 63°28'37"N, 10°11'37"E) was collected in April 2011 (Fig. 1). The multicore (5.5 cm diameter) was sliced in 1 cm intervals aboard the research vessel "RV Seisma" and samples were stored in plastic bags at -18°C. Prior to further analyses, all samples were freeze-dried and, except for grain size measurements, homogenised through gentle grinding. All analytical techniques applied in this study are described in detail by Faust J., Knies J., Slagstad T., Vogt C., Milzer G. and Giraudeau J,. Geochemical composition of Trondheimsfjord surface sediments: Sources and spatial variability of marine and terrigenous components. Continental Shelf Research (in review), hereafter referred to as (Faust et al., Paper I) and will be briefly summarised below.

3.2. Chronology

The chronology of the core is based on ^{210}Pb and ^{137}Cs content on neighbouring sediment core in the multi-corer rack (MC99-1). ^{210}Pb and ^{137}Cs measurements were made at EPOC, CNRS/University of Bordeaux 1, France. According to the age model of Milzer et al. (2013) (supplementary Tab. 1), the sedimentation rate of the MC99-1 is 0.49 cm/year and the core base age is 1959. The dating error increases gradually down core from ±0.07 to ±3.53 years.

3.3. Bulk elemental and grain size analyses

Sediment elemental composition was analysed at the ACME Ltd laboratory (Vancouver, Canada). Determination was performed by inductively coupled plasma atomic emission spectrometry (ICP-AES) following a four-acid digestion, which is considered to be a total

digestion method. The analytical quality was calculated by duplicate analyses of every 20 samples and further controlled by using the certified multi-element soil standard OREAS 45e and the certified multi-element basalt standard OREAS 24p. Grain size distribution was determined by laser diffraction using a Coulter LS 200 instrument. The analysis was carried out on material within a particle diameter range of 0.4–2000 µm.

3.4 Instrumental data

Seasonal and annual mean air temperature and precipitation records for the Trondheimsfjord region since 1900 were obtained from the Norwegian Meteorological Institute (www.eklima.no). Time series (1963-present) of river discharge for the six largest rivers entering the Trondheimsfjord, Gaula, Orkla, Nidelva, Stjørdalselva, Verdalselva and Steinkjerelva (Fig. 1) were obtained from the Norwegian Water Resource and Energy Directorate (www.nve.no). All data were collected at monitoring stations close to river outlets. The winter (December – March) PC-based NAO index (Hurrell, 1995) is based on the difference of normalised sea level pressure between Lisbon, Portugal and Stykkishomur, Iceland and the dataset was retrieved from https://climatedataguide.ucar.edu/climate-data/hurrell-north-atlantic-oscillation-nao-index-pc-based.

4. Results and discussion

4.1 Linkage between climate variability and terrigenous sediment supply

The inflow of relatively warm and saline Atlantic water keeps most of the Trondheimsfjord ice free during winter (Dec-Mar). However, the drainage areas of Trondheimsfjord experienced average winter air temperatures of -4.6°C over the last 50 years. Thus, precipitation in these regions occurs primarily as snow, rivers are often ice-

covered and freshwater inflow into the fjord is reduced. Annual precipitation and river discharge into the Trondheimsfjord are strongly correlated (Sakshaug and Sneli, 2000). Precipitation is highest in autumn and lowest in spring (Fig. 3). However, the highest runoff occurs in late April to May and is primarily caused by snow melt (Fig. 3). Thus, the major causes controlling the strength and duration of spring flooding events are: winter precipitation (P), air temperature (T) and the resulting amount of river runoff (R) in April/May. As shown in figure 4, winter-spring river runoff, winter temperature and winter precipitation are closely linked to each other on an annual basis (supplementary Tab. 2). Hence, we combined these parameters by normalising the instrumental data and show the aggregated annual mean as RTP record in figure 4. The strong relation between river runoff, temperature and precipitation (Fig. 4) indicates that these regional records are strongly influenced by larger scale atmospheric or oceanic processes, such as the NAO.

Numerous studies suggest that the NAO has a strong impact on the Norwegian climate. For example, Dickson et al. (2000) showed from spatial analysis of northern hemisphere winter precipitation that positive NAO periods are characterised by positive precipitation anomalies in Scandinavia. Moreover, Cherry et al. (2005) found 55 % of river discharge variation within Norway is associated with NAO variations. In accordance with these findings, our Trondheimsfjord regional RTP record shows a very good correlation to the winter NAO index (Fig. 4 and supplementary Tab. 2), confirming that regional temperature and precipitation in the Trondheimsfjord area are responding to changes in large-scale Northern Hemisphere climate patterns.

To date, the only detailed studies of sediment transport in Trondheimsfjord rivers are within the River Gaula, where between 1975 and 1976 more than 90 % of the annual

sediment transport occurred during spring floods (Bulgurlu, 1977). Although the total annual water runoff differed by only 13 %, a higher level and longer duration of spring flooding in 1976 generated a 68 % increase in the total sediment transport compared to 1975. Our working hypothesis is that the other main rivers entering the fjord show similar sediment transport behaviour. The latter is supported by (1) a similar vegetation and landscape of the entire Trondheimsfjord drainage area, (2) an up to 15 m thick brown brackish surface water layer often observed to cover the entire fjord in spring, and (3) concurrent snow melting in the whole Trondheimsfjord region. As drainage basin temperature and precipitation are primary controls on the intensity of terrestrial weathering and erosion (Syvitski, 2002; White and Blum, 1995), the elemental composition of the terrigenous material delivered into the Trondheimsfjord is likely able to record past NAO changes.

4.2 NAO as determinant of temporal variation in terrigenous material supply

Chemical and mechanical weathering fluxes depend on climate through changing temperature and runoff (e.g. Gislason et al., 2009; White et al., 1999). Bulk sediment elemental ratios can detect onshore weathering conditions and the intensity of the transport process such as freshwater discharge (e.g. Bertrand et al., 2012; Koinig et al., 2003; Zabel et al., 2001). Our previous study of numerous surface sediments provides evidence that Trondheimsfjord sediments are an excellent (recent) geochemical archive potentially reflecting the intensity of river discharge and therefore also the variability of the North Atlantic Oscillation (Faust et al., Paper I). To further validate these findings and gain a better understanding of the environmental response to climate variability within the Trondheimsfjord region we analysed the bulk geochemical composition of a short sediment core MC99 from the Trondheimsfjord Seward Basin (Fig. 1).

In the following we will (1) illustrate processes responsible for observed changes in elemental ratios of Al/Zr and Ni/K and (2) show their potential to detect NAO related regional changes in air temperature, winter precipitation and river discharge in Trondheimsfjord sediments. The high resolution record of the MC99 enables us to capture past-environmental variabilities that are comparable to the instrumental records. However, the sampling resolution of approximately two years is still too low to reveal strong interannual variations. Thus, we compare our proxy records to three point running averages of the RTP data.

Due to a sudden rise in the K concentrations, samples dated between 2010 and 1985 show much higher concentrations (16 % in average) compared to the samples between 1985 and 1959 (Fig. 5). However, no sedimentological (grain size, colour) difference between the upper and lower part of the core can be identified and a similar rise is not observed in any other elemental record. Since we cannot fully exclude an analytical problem or anthropogenic impact for this offset, we divide the K/Ni record into two sections (lower: 1959-1984, upper: 1984-2010) and individually compare the K/Ni records with RTP and NAO (Fig. 5). Still, K/Ni closely follows the winter RTP curve in the range of the dating error (≤ ±1 year) in the upper and lower record, implying K/Ni accurately records temporal changes in the supply of terrigenous material (Fig. 5). Furthermore, as expected from the good correlation between RTP and NAO, K/Ni shows a clear relation to the NAO over the investigated time span as illustrated by distinct K/Ni peaks during positive NAO phases (e.g. 1961, 1967, 1973 and 1992).

Recently, Faust et al. (Paper I) investigated the organic and inorganic composition of sixty evenly distributed surface sediment samples and revealed that the distribution of K/Ni in the

fjord sediments reflects regional geological bedrock pattern in the northern and southern hinterland, respectively (Fig. 1 and 2). Greenstones and metagreywackes located along the southern side of the fjord are the main Ni source in Trondheimsfjord sediments (Fig. 1). Thus, Ni enters the Trondheimsfjord mainly via the rivers Orkla, Gaula and Nidelva directly into the Seaward Basin. On the other hand, K originates largely from Precambrian felsic volcanic rocks related to a tectonic window called *Tømmerås anticline* (see Roberts, 1997: for details) in the north-eastern hinterland (Fig. 1 and Fig. 2). Hence, K enters the Trondheimsfjord primarily by the rivers Verdalselva and Steinkjerelva into the inner part of the fjord. We assume that the distribution of K and Ni rich material within the fjord takes place in the brackish surface current, above the halocline (Hoskin et al., 1978) because the water column below the estuarine circulation cell is a relatively low energy environment (Syvitski, 1989b). Moreover, during periods of high river discharge, the velocity of the fjord's surface currents is high, the water column is well stratified and the suspended material is transferred over longer distances. Hence, increased river discharge will strengthen surface water currents, and more K will be transported from the Middlefjord basin in the north across the Tautra sill into the Seaward basin in the south. Alternatively, hyperpycnal flows associated with sediment-laden river discharges and turbidity currents can also affect the distribution of terrigenous sediments in the Trondheimsfjord (Bøe et al., 2004: and refs. therein). However, the sediment core MC99 is composed of homogeneous very fine grained material. More than 90 % of the sediment grains are smaller than 63 µm and the grain size maximum is only 250 µm. Moreover, it has a linear sedimentation rate (0.49 cm/year). Hence, it seems very unlikely that the core position has been affected by strong and variable bottom currents during the past 50 years. Thus, we propose that the good relation between RTP and K/Ni in the MC99 can be explained by the variable strength and duration of the

annual spring floods. A strong (weaker) flooding event will generate higher (lower) surface velocity and transports more (less) K across the Tautra sill and causing an increase (decrease) in the K/Ni values. Finally, the annual spring floods are caused by snow melt and therefore, K/Ni is related to the NAO variability due to its impact on winter precipitation and winter temperature (Fig. 5).

The comparison of Al/Zr from the MC99 with NAO (DJFM) and the winter RTP in shown in figure 6. Similar to the K/Ni record, the Al/Zr ratio closely follows the winter RTP curve between 1959 and 2002. The temporal offset between relative maxima and minima of Al/Zr and RTP is less than the dating error. Due to very low and very high Al/Zr values in 2004 and 2008, respectively, the relation between RTP and Al/Zr in the period 2004 - 2010 is less clear. However, besides these two data points Al/Zr is shown to be sensitive to regional changes in winter precipitation, river discharge and temperature (as summarised by the winter RTP curve) which are in turn strongly related to the NAO. These findings indicate that large amounts of Al-rich (clay) minerals are transported into the fjord during the snow melt and the resulting spring flooding events. Due to a rapid Holocene glacioisostatic uplift of the Trondheimsfjord region (approximately 175 m) large onshore areas are dominated by fjord-marine and glacio-marine clays which contain high proportions of Al-rich illite and chloride (e.g. Hansen et al., 2011; Rise et al., 2006a; Lysså et al., 2008). Therefore, it is likely that these clays contribute considerably to the delivery of Al-rich material to the Trondheimsfjord especially during flooding events. It is generally assumed that an increase of Zr concentration in sediments points to enhanced physical weathering (e.g. Koinig et al., 2003). Bertrand et al. (2012) found Zr/Al to be well suited for estimating changes in the energy of terrestrial sediment supply in Chilean fjords. Zr is most often associated with the very dense minerals zircon ($ZrSiO_4$) and baddeleyite (ZrO_2). Thus, Zr is generally expected to be concentrated in

the coarse grain fraction (e.g. Ganeshram et al., 1999). As Zr, Al is a conservative element and due to its strong relation to the clay fraction it is often used as a normaliser to limit granulometric effects. As a result, lower (higher) Al/Zr values are assumed to occur during stronger (weaker) river discharge. However, as shown in Fig. 6, Al/Zr in this study correlates positive with RTP and NAO. One probable reason for this behaviour is that in the sediment core MC99, Al is positively correlated to the grain size fraction < 63 µm (r^2 = 0.55), while Zr shows no clear statistical relationship to any grain size fraction. Best regression for Zr was found with the grains size fraction < 63 µm (r^2 = 0.2). Moreover, Zr and Al are well correlated (r^2 = 0.6). This indicates that Zr in the MC99 originates rather from fine grained, heavily weathered, material and from Zr ions adsorbed to clay minerals. We thus consider that Zr/Al in this study is not related to grain size changes. Furthermore, previous investigations of fjord surface sediments (Faust et al., Paper I) reveal Al/Zr to increase from the inner part of the fjord (Beitstadfjord) towards the fjord entrance (Fig. 2). These points to either a Zr source in the northern- or an Al source in the southern hinterland. However, geochemical surveys of the Trondheimsfjord drainage area (see Faust et al., Paper I: for details) show that Al is ubiquitous in the fjord's hinterland. A distinct Zr source in the north could explain the affinity of Zr to the fine grain fraction in our core. Due to the large distance between the Zr source in the north and the position of the MC99, larger and heavy Zr rich grains might not be transported over such long distances. In fact, bedrock analyses suggest Precambrian rocks (same source rocks as for K) as a possible Zr source and a good relation between Zr and K (r^2 = 0.6) supports the suggestion. However, the relation between Zr and K is as good as between Zr and Al, and floodplain sediments (Ottesen et al., 2000) do not confirm a Zr anomaly in the northern drainage area. Further studies are needed to identify the Zr source in the sediments of the Seaward Basin.

5. Implications and Conclusions

With a global surface temperature increase of 0.6°C between 1975-2005 (Hansen et al., 2006) the time span discussed in this study corresponds to the most rapid recent global warming periods (e.g. Jones et al., 2001). Consequently, due to the direct link between temperature and weathering (e.g. West et al., 2005; White and Blum, 1995) overall weathering rates are expected to increase. In addition to the short term changes of K/Ni and Al/Zr, the Al/Zr record reveals a long term increasing trend with a shift towards a steeper gradient from approximately 1980 until today (Fig. 6). We assume that the overall increase of Al/Zr and the gradient shift is a response to an increase in weathering and erosion favouring the input of Al-rich clay minerals. This assumption is supported (a) by a strong agreement of Al/Zr with the Trondheimsfjord regional air temperature record (Fig. 6) and (b) by the course of the <63 µm fractions in the MC99 (Fig. 7). The air temperature from the Trondheimsfjord region overall decreases slightly from 1920 until approximately 1980 and then in accordance with the global surface temperature record (Hansen et al., 2006), it increases steeply until about 2005 (Fig. 6). Similar to the temperature record, the <63 µm fraction in the MC99 slightly decreases from 1960 (92.7 %) to 1983 (91.3 %) and afterwards increases to the highest value in the record in 2008 (95.3 %, Fig. 7). These findings show that Al/Zr in sediments of the Seaward Basin records two climatic processes: 1) a short term variability portably caused by changes in the seasonal strength and duration of spring floods and 2) a long term weathering development caused by an increase in the Al-rich clay fraction due to enhanced weathering and erosion.

The long term response of the hinterland to climate variability is not confirmed by the K/Ni due to the conciseness of both segments. However, the observed changes in the

chemical composition of the Trondheimsfjord sediments in close relation to the rapid variability of NAO and atmospheric temperatures (Fig. 5 and 6) suggest that weathering and erosion in the Trondheimsfjord hinterland responds very sensitive to climate change. Gravitational sedimentary processes in the Trondheimsfjord region are common today (e.g. L'Heureux et al., 2010), and a relation between periods of warm/wet climate and increased land slide activity during the Holocene in the Trondheimsfjord region was reported by Bøe et al. (2003). The ongoing increase in global surface temperatures and the related increase in the moisture transport from lower to higher latitudes are therefore likely to induce an increase in erosion and river sediment load of Trondheimsfjord rivers. Accelerated sedimentation and erosion is considered to be one of the main potential factors triggering slope failures, sub-marine mass movements (e.g. L'Heureux et al., 2013; Masson et al., 2006; L'Heureux et al., 2011) and quick-clay landslides in the Trondheimsfjord region (Hansen et al., 2011: and ref. therein). The risk for geohazards in future times can therefore be expected to increase in central Norway. Based on this assumption one might expect the MC99 to show an increase in the sedimentation rate for the last 50 years, which is not shown by the radiogenic isotope-based chronological framework (Milzer et al., 2013). While a change in the sedimentation rate could be masked by the dating error, we are highlighting that most sediments are probably transported to the position of the MC99 in a brackish surface water layer in a pulse during spring. This configuration possibly will limit the amount of material reaching the position of the MC99. Further studies of river load and sediment cores close to the river outlets are required to reveal the mechanism of the sediment transport in more detail.

The correspondence between NAO, RTP, K/Ni and Al/Zr suggest that the terrigenous input to the Trondheimsfjord responds to changes in large-scale Northern Hemisphere

climate patterns. In order to further investigate the reliability of the elemental composition of Trondheimsfjord sediments as climate proxy, we compared the continuous Al/Zr record with the following three NAO records from the circum-North Atlantic region (Fig. 8): (I) winter snow accumulation rates on a small glacier (*Ålfotbreen*) located near the coast approximately 300 km south-west of the Trondheimsfjord (Nesje et al., 2000). (II) Total annual discharge of the six largest Eurasian Arctic rivers (Yenisey, Lena, Ob, Kolyma, Pechora and Severnaya Dvina) (Peterson et al., 2002). (III) Normalised proxy NAO index based on western Greenland ice accumulation rates (Appenzeller et al., 1998).

Figure 8 shows a strong relation between the three point running average of the accumulation rate from the Ålfotbreen and the river runoff of the Eurasian Arctic rivers. Both records indicate the strong impact of the NAO on the precipitation patterns in Eurasia. The elemental ratio of Al/Zr in Trondheimsfjord sediments show a close relation to these records (Fig. 8) implying that terrigenous input and thus weathering and erosion in the central Norwegian hinterland, responds very sensitive to atmospheric circulation variability. Only the older part deviates slightly from the NAO pattern which might be related to the increasing dating error with core depth. The NAO index from Appenzeller et al. (1998) is less well related to any of the parameters in figure 8. Appenzeller et al. (1998) noted that the accumulation measurement of the top meters of the ice core is difficult due to uncertainties in the density measurements. Furthermore, Mosley-Thompson et al. (2005) analysed the same ice core data used by Appenzeller et al. (1998) and found a decrease in the correlation between NAO and the accumulation rate from $r^2 = 0.53$ in the period 1865-1925 towards $r^2 = 0.23$ in the period 1926-1994. Mosley-Thompson et al. (2005) assumed that this change is caused by the Arctic warming and related change in the NAO impact on precipitation variability in west-central Greenland. Nevertheless, the difference of the NAO index

provided by Appenzeller and the other records in Fig. 8 indicates that the temporal impact of the NAO in Greenland might be different as in Eurasia.

We conclude that the winter NAO is strongly related to changes in regional temperature, precipitation and river runoff in central Norway. Moreover, our terrigenous proxies recorded both small scale, high frequency, and large scale long term shifts in temperature and precipitation in the Northern Hemisphere over the past 50 years. By comparing our results with NAO records from the broader Atlantic-Arctic region, we show that it is possible to reconstruct a proxy NAO index from sedimentary archives in central Norwegian fjords on longer time scales.

Acknowledgments

We thank the captain Oddvar Longva, and the crew of the RV Seisma for their professional support during our expeditions. For their interest, stimulating discussions and many useful comments we thank our colleagues Ola Mange Sæther, Simone Sauer, Reidulv Bøe, Anne Dehls and John Naliboff. We also thank James Hurrell and the National Center for Atmospheric Research Staff for providing the NAO index data as well as Christof Appenzeller (ETH) for making his proxy NAO index available for us. This work is a contribution to the CASE Initial Training Network funded by the European Community's 7th Framework Programme FP7 2007/2013, Marie-Curie Actions, under Grant Agreement No. 238111.

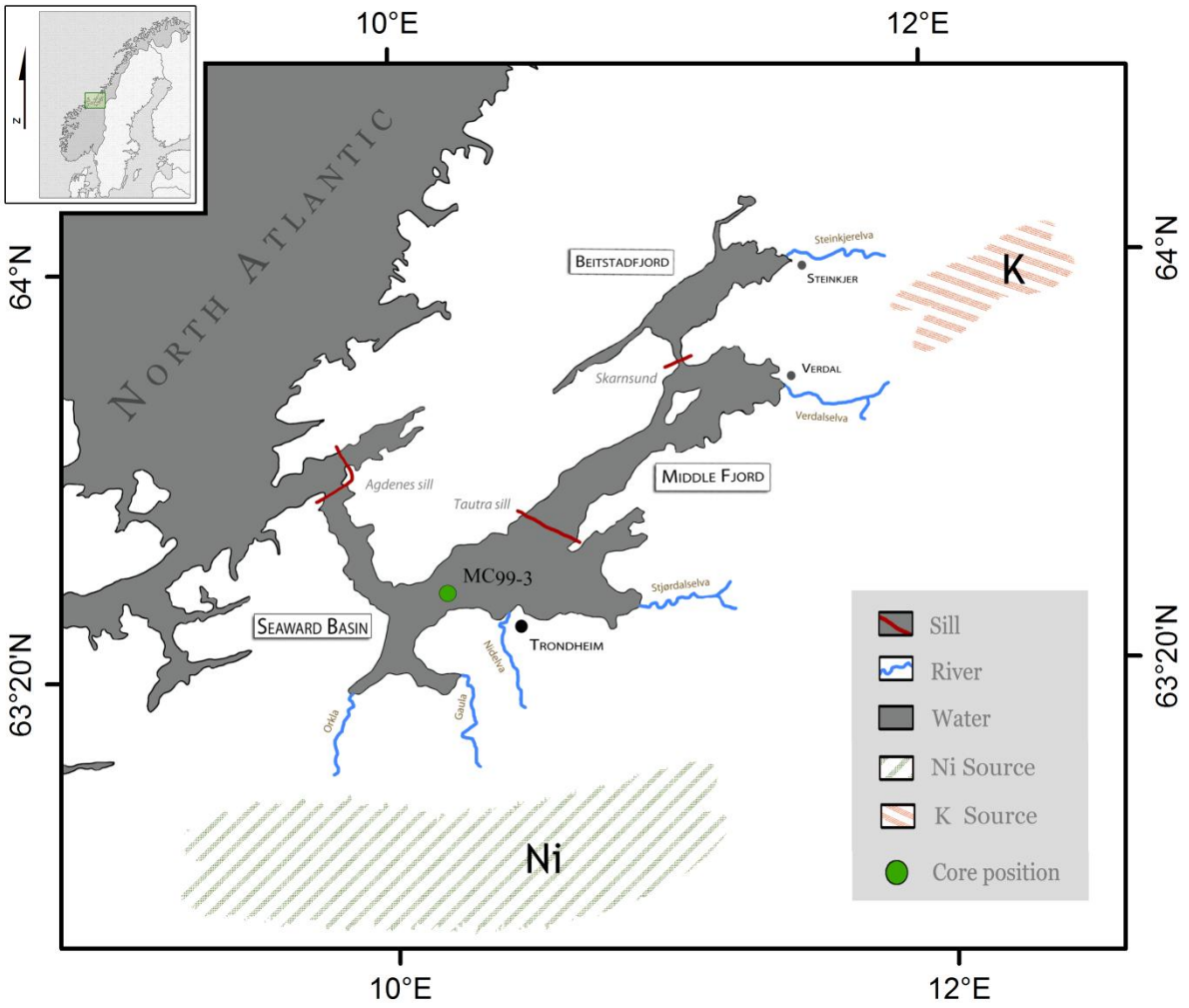

Figure 1: Location of the study area (upper left corner) and the Trondheimsfjord region with the core position of the MC99 (green circle) in the Seaward Basin. Three sills divide the fjord into three main basins and the six main rivers enter the fjord form the south-east. Regional sources for Ni and K in the hinterland bedrock are greenstones and metagreywakes in the southern and Precambrian volcanic rocks in the northern region, respectively (Faust et al., Paper I).

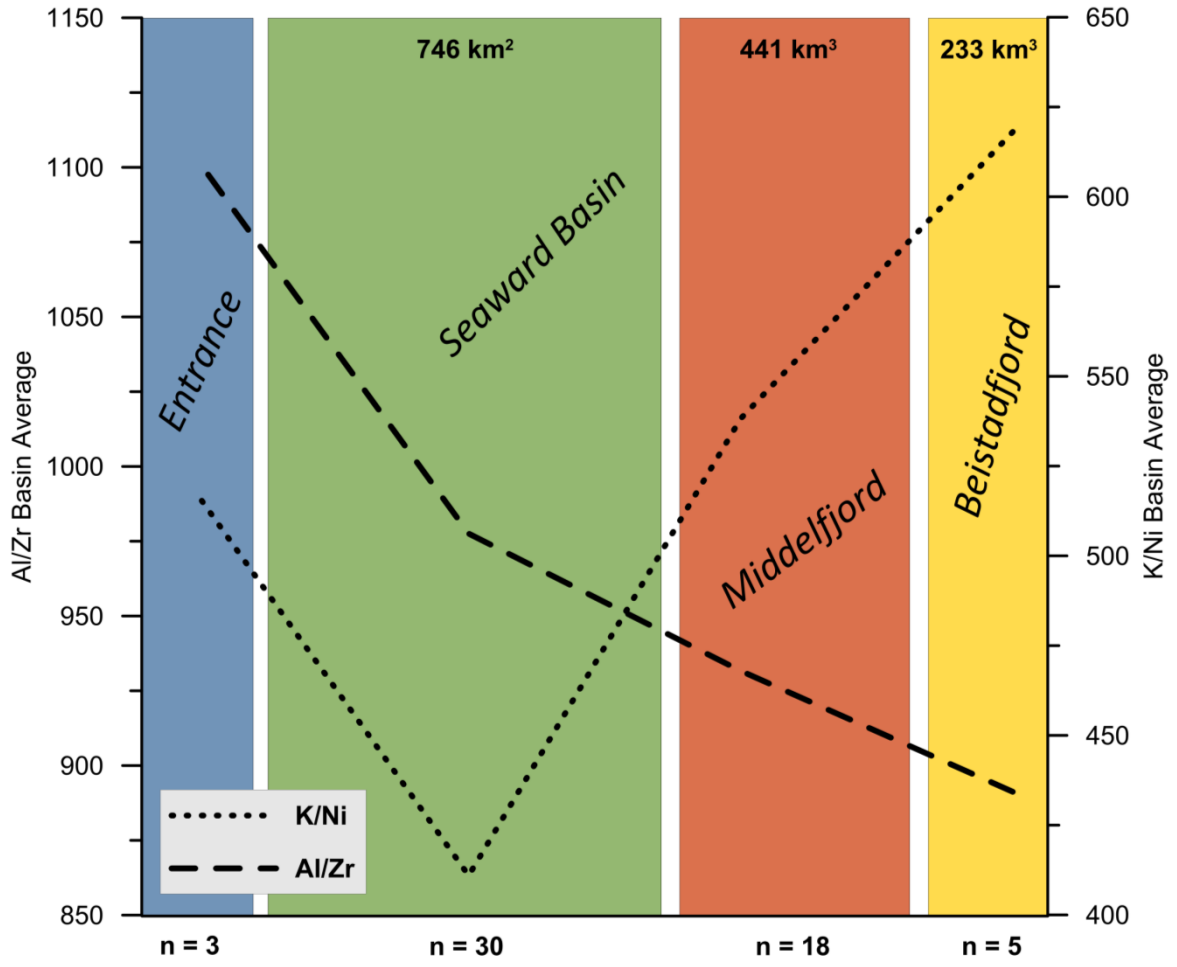

Figure 2: K/Ni and Al/Zr in Trondheimsfjord surface sediments (0-1 cm) shown as average values for each of the three main basins and the entrance area. Size of the basin areas is shown at the top and the number of samples for each basin is indicated below (see Faust et al., Paper I: for details).

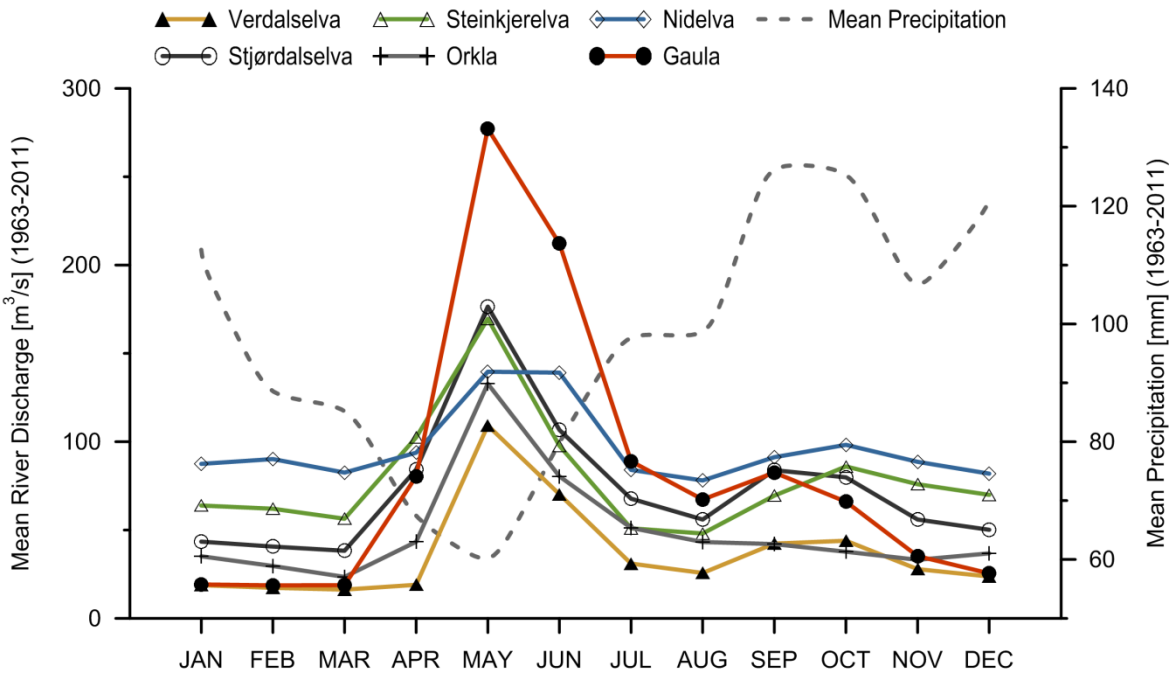

Figure 3: Monthly mean river discharge of the six main rivers entering the Trondheimsfjord and mean precipitation in the Trondheimsfjord region (1963-2011). During winter rivers are often ice covered, precipitation occurs as snow and the runoff is very low. Snowmelt causes spring floods, thus, annual river discharge is highest in May-June. Precipitation in the Trondheimsfjord region is highest in autumn but the effect on river discharge is small compared to the discharge in spring.

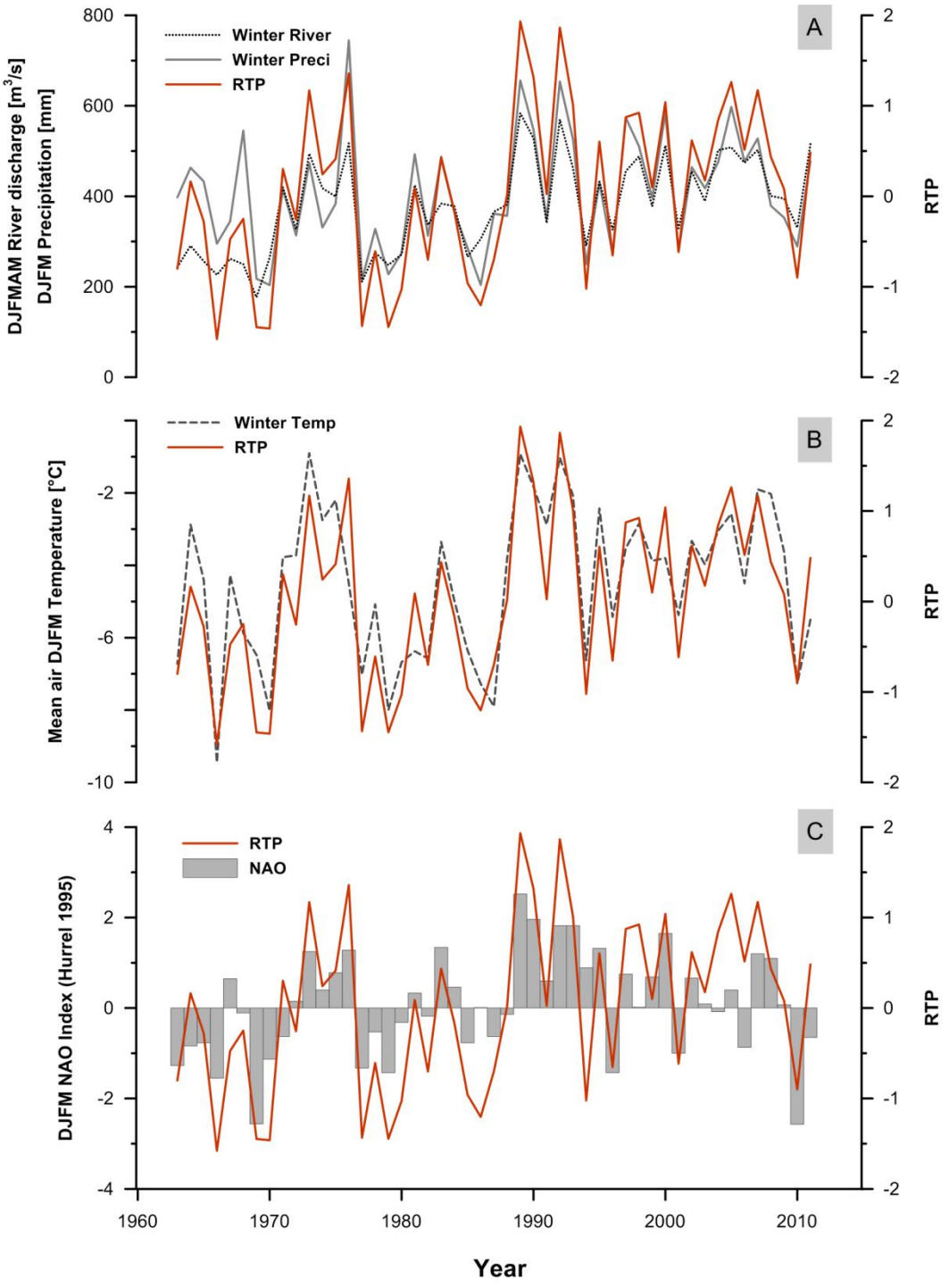

Figure 4: A) River discharge [DJFMAM] precipitation [DJFM] and RTP (the annual winter mean of normalised river discharge (R), air temperature (T) and precipitation (P)) since 1963. B) Air Temperature [DJFM] and RTP C) Comparison between RTP and the PC-based winter NAO index from http://climatedataguide.ucar.edu/guidance/hurrell-north-atlantic-oscillation-nao-index-station-based.

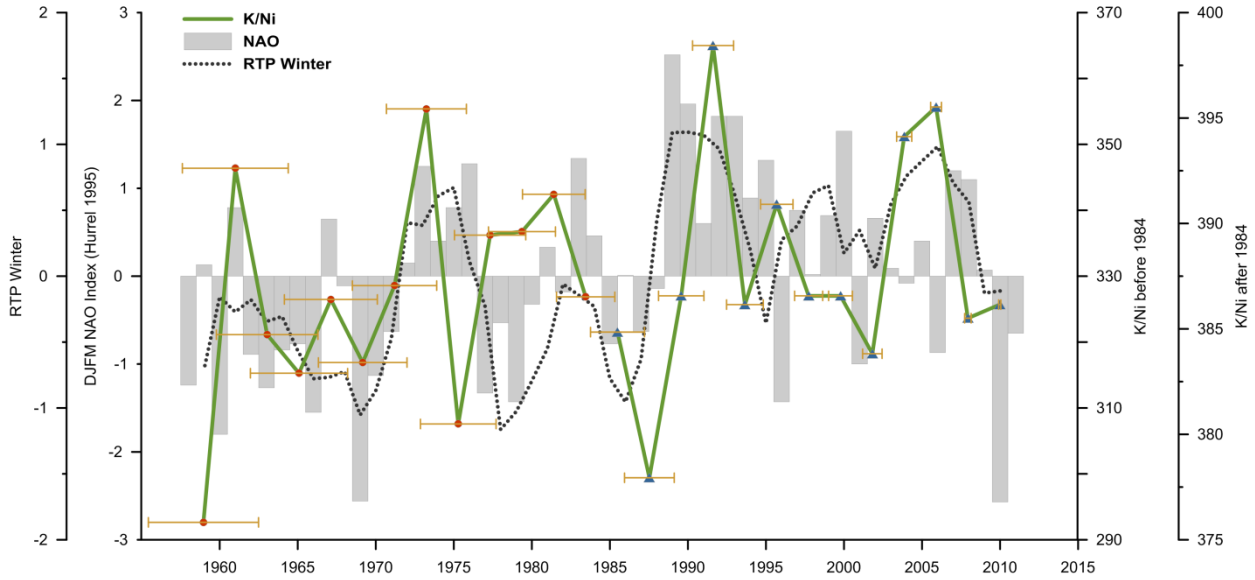

Figure 5: Comparison between K/Ni (supplementary Tab. 1) from the MC99, NAO (DJFM) and a three point running average of the winter RTP. Age error for each K/Ni measurement is indicated by yellow bars (supplementary Tab. 2). Note the different scale for the K/Ni record. Due to a leap in the K concentrations (see text for details) we divided the K/Ni record into a lower sections (green line with red circles) and an upper sections (green line with blue triangles) at 1984.

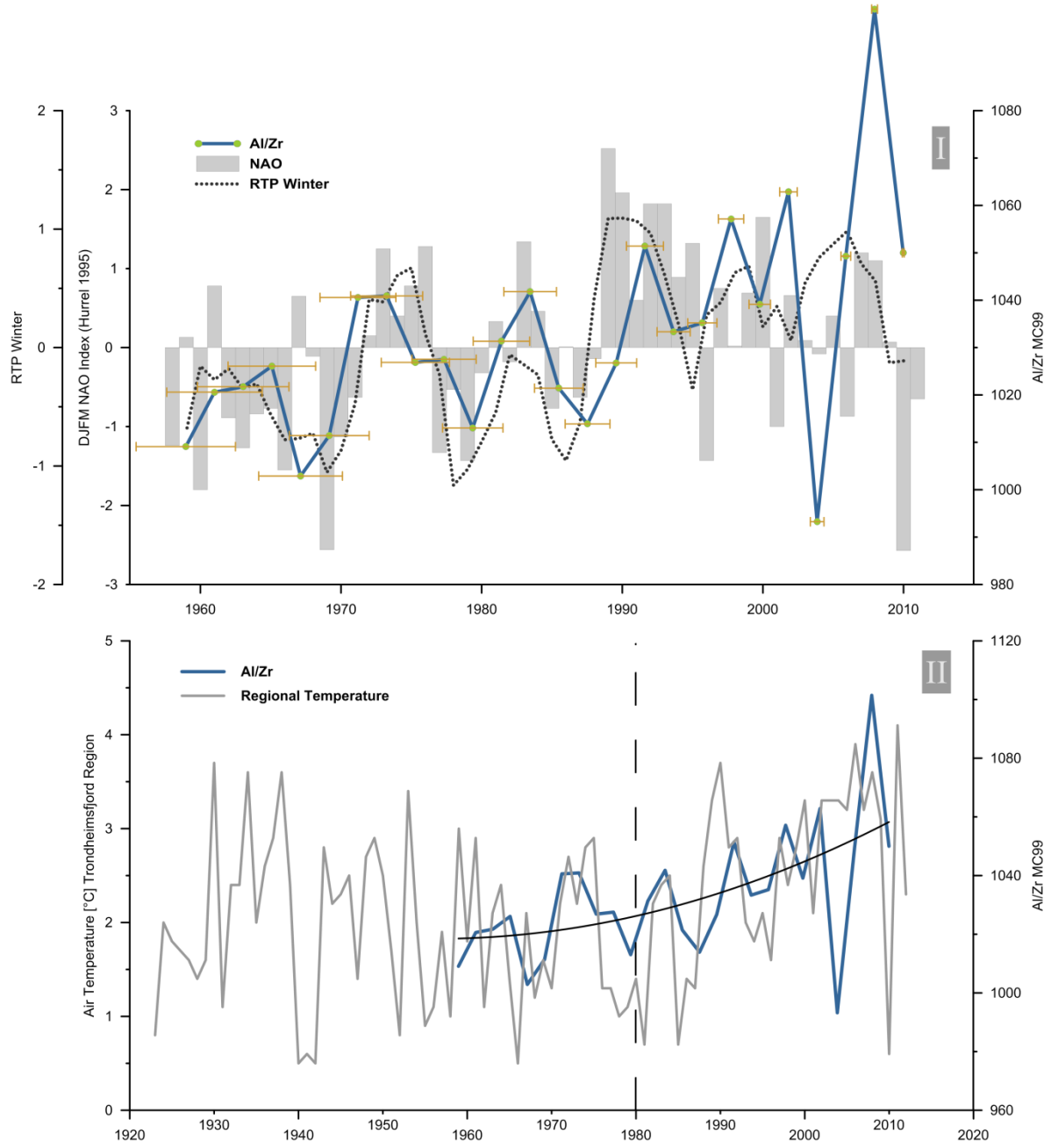

Figure 6: I) Comparison between Al/Zr (supplementary Tab. 1) from the MC99, NAO (DJFM) and a three point running average of the winter RTP. Age error for each Al/Zr measurement is indicated by yellow bars (supplementary Tab. 2). II) Comparison between Al/Zr and the air temperature in the Trondheimsfjord region. The dotted line indicates a gradient shift in the air temperature and in Al/Zr record at approximately 1980.

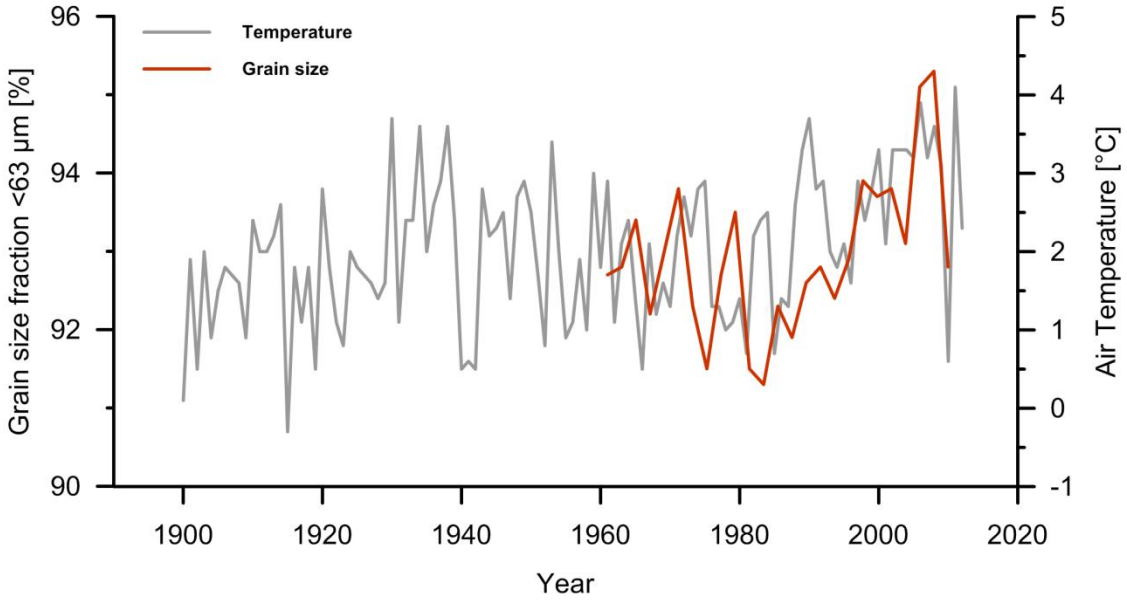

Figure 7: Comparison between the grain size fraction <63 µm (supplementary Tab. 1) and the air temperature in the Trondheimsfjord region.

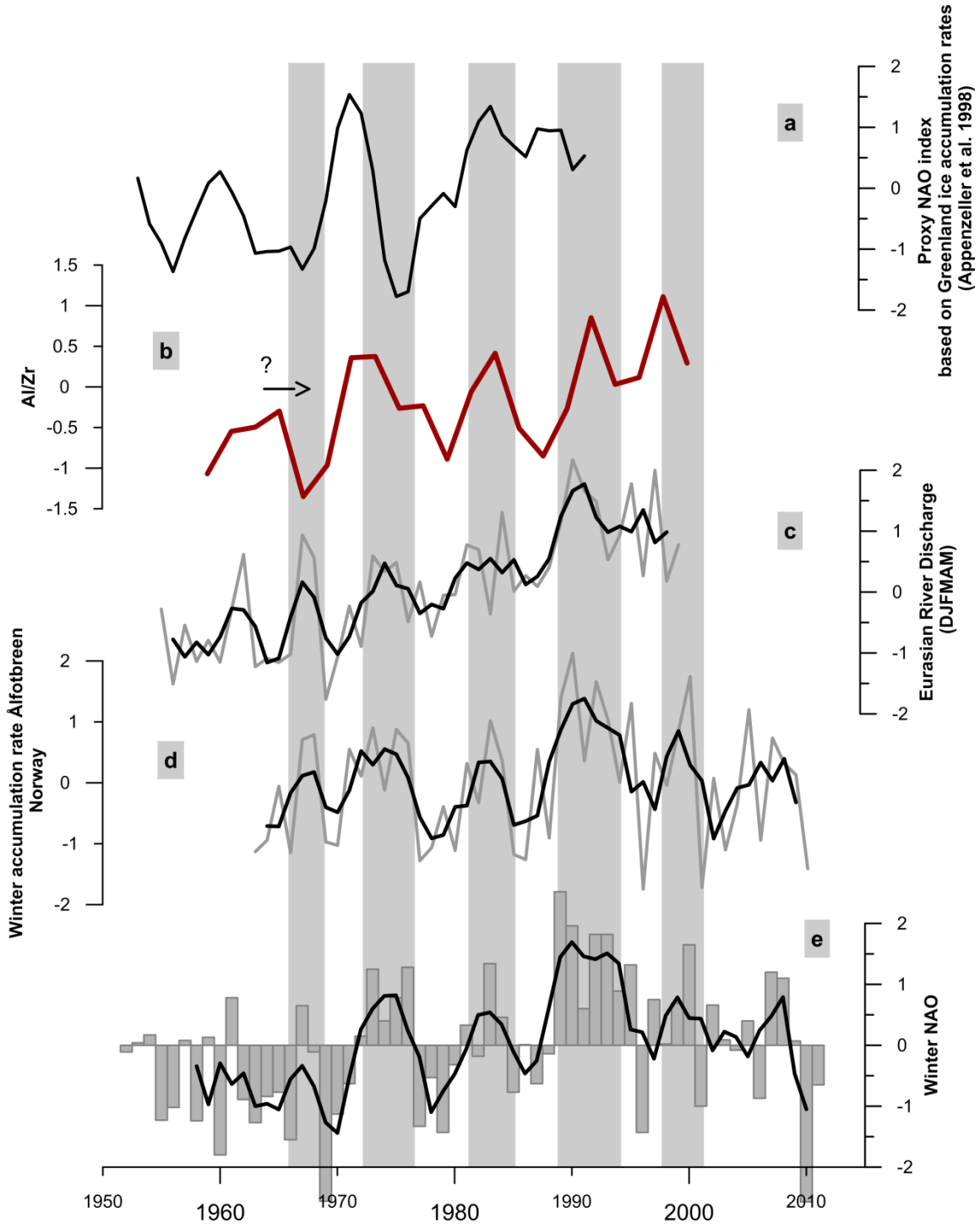

Figure 8: a) Normalised proxy NAO index based on western Greenland ice accumulation rates (see Appenzeller et al., 1998: for details) b) Normalised Al/Zr record between 1959 and 2002. Very high and low values in 2004 and 2008 were treated as outliers c) Combined and normalised Eurasian river discharge (DJFMAM) from the six largest arctic rivers: Yenisey, Lena, Ob, Kolyma, Kolymskoye, Pechora and Severnaya Dvina. We utilise the same river discharge data as Peterson et al. (2002) from the R-ArcticNet database, but only total

discharge values for the time period Dec-May, 1959-1999. In this period (Dec-May) discharge is much stronger related to the NAO (DJFM) ($r^2 = 0.46$) as the annual run of ($r^2 = 0.22$). The black line is the three point running average d) Normalised annual winter accumulation on the Norwegian glacier *Ålfotbreen* located approximately 300 km south-west of the Trondheimsfjord near the coast. Similar to the precipitation in the Trondheimsfjord area positive (negative) NAO periods corresponds to large (little) winter accumulation (see Nesje et al., 2000: for details). The black line is the three point running average e) Winter (DJFM) NAO index from https://climatedataguide.ucar.edu/climate-data/hurrell-north-atlantic-oscillation-nao-index-pc-based. The black line is the three point running average. Grey bars indicate five positive NAO phases (1: 1966-1968; 2: 1972-1976; 3: 1981-1985; 4:1989-1994; 5: 1998-2001)

References

Appenzeller C, Stocker TF and Anklin M. (1998) North Atlantic oscillation dynamics recorded in Greenland ice cores. *Science* 282: 446-449.

Bertrand S, Hughen KA, Sepulveda J, et al. (2012) Geochemistry of surface sediments from the fjords of Northern Chilean Patagonia (44-47°S): Spatial variability and implications for paleoclimate reconstructions. *Geochimica Et Cosmochimica Acta* 76: 125-146.

Bulgurlu B. (1977) A study of sediment transport in River Gaula. *Institutt for vassbygging.* Trondheim: Norges tekniske høgskole, NTH.

Bøe R, Bugge T, Rise L, et al. (2004) Erosional channel incision and the origin of large sediment waves in Trondheimsfjorden, central Norway. *Geo-Marine Letters* 24: 225-240.

Bøe R, Rise L, Blikra LH, et al. (2003) Holocene mass-movement processes in Trondheimsfjorden, Central Norway. *Norwegian Journal of Geology* 83: 3-22.

Cherry J, Cullen H, Visbeck M, et al. (2005) Impacts of the North Atlantic Oscillation on Scandinavian hydropower production and energy markets. *Water Resources Management* 19: 673-691.

Dickson RR, Osborn TJ, Hurrell JW, et al. (2000) The Arctic Ocean response to the North Atlantic oscillation. *Journal of Climate* 13: 2671-2696.

Faust JC, Knies J, Slagstad T, et al. (Paper I) Geochemical composition of Trondheimsfjord surface sediments: Sources and spatial variability of marine and terrigenous components. *Continental Shelf Research*.

Ganeshram RS, Calvert SE, Pedersen TF, et al. (1999) Factors controlling the burial of organic carbon in laminated and bioturbated sediments off NW Mexico: implications for hydrocarbon preservation. *Geochimica Et Cosmochimica Acta* 63: 1723-1734.

Gedney N, Cox PM, Betts RA, et al. (2006) Detection of a direct carbon dioxide effect in continental river runoff records. *Nature* 439: 835-838.

Gislason SR, Oelkers EH, Eiriksdottir ES, et al. (2009) Direct evidence of the feedback between climate and weathering. *Earth and Planetary Science Letters* 277: 213-222.

Govin A, Holzwarth U, Heslop D, et al. (2012) Distribution of major elements in Atlantic surface sediments (36°N–49°S): Imprint of terrigenous input and continental weathering. *Geochemistry, Geophysics, Geosystems* 13.

Hansen J, Sato M, Ruedy R, et al. (2006) Global temperature change. *Proceedings of the National Academy of Sciences of the United States of America* 103: 14288-14293.

Hansen L, L'Heureux JS and Longva O. (2011) Turbiditic, clay-rich event beds in fjord-marine deposits caused by landslides in emerging clay deposits - palaeoenvironmental interpretation and role for submarine mass-wasting. *Sedimentology* 58: 890-915.

Hoskin CM, Burrell DC and Freitag GR. (1978) Suspended sediment dynamics in Blue Fjord, western Prince William Sound, Alaska. *Estuarine and Coastal Marine Science* 7: 1-16.

Hurrell JW. (1995) Decadal Trends in the North-Atlantic Oscillation - Regional Temperatures and Precipitation. *Science* 269: 676-679.

Jacobson P. (1983) Physical oceanography of the Trondheimsfjord. *Geophysical & Astrophysical Fluid Dynamics* 26: 3-26.

Jones PD, Osborn TJ and Briffa KR. (2001) The evolution of climate over the last millennium. *Science* 292: 662-667.

Koinig KA, Shotyk W, Lotter AF, et al. (2003) 9000 years of geochemical evolution of lithogenic major and trace elements in the sediment of an alpine lake - the role of climate, vegetation, and land-use history. *Journal of Paleolimnology* 30: 307-320.

Koistinen T, Stephens MB, Bogatchev V, et al. (2001) *Geological Map of the Fennoscandian Shield, scale: 1: 2,000,000*: Geological Survey of Finland, Norway and Sweden and the North-West Department of Natural Resources of Russia.

L'Heureux JS, Glimsdal S, Longva O, et al. (2011) The 1888 shoreline landslide and tsunami in Trondheimsfjorden, central Norway. *Marine Geophysical Research* 32: 313-329.

L'Heureux JS, Hansen L and Longva O. (2009) Development of the submarine channel in front of the Nidelva River, Trondheimsfjorden, Norway. *Marine Geology* 260: 30-44.

L'Heureux JS, Hansen L, Longva O, et al. (2010) A multidisciplinary study of submarine landslides at the Nidelva fjord delta, Central Norway - Implications for geohazard assessment. *Norwegian Journal of Geology* 90: 1-20.

L'Heureux JS, Vanneste M, Rise L, et al. (2013) Stability, mobility and failure mechanism for landslides at the upper continental slope off Vesterålen, Norway. *Marine Geology* 346: 192-207.

Labat D, Godderis Y, Probst JL, et al. (2004) Evidence for global runoff increase related to climate warming. *Advances in Water Resources* 27: 631-642.

Lamy F, Hebbeln D, Rohl U, et al. (2001) Holocene rainfall variability in southern Chile: a marine record of latitudinal shifts of the Southern Westerlies. *Earth and Planetary Science Letters* 185: 369-382.

Lyså A, Hansen L, Christensen O, et al. (2008) Landscape evolution and slide processes in a glacioisostatic rebound area; a combined marine and terrestrial approach. *Marine Geology* 248: 53-73.

Masson DG, Harbitz CB, Wynn RB, et al. (2006) Submarine landslides: processes, triggers and hazard prediction. *Philosophical Transactions of the Royal Society a-Mathematical Physical and Engineering Sciences* 364: 2009-2039.

Milzer G, Giraudeau J, Schmidt S, et al. (2013) Qualitative and quantitative reconstruction of surface water characteristics and recent hydrographic changes in the Trondheimsfjord, central Norway. *Clim. Past Discuss.* 9: 4553-4598.

Mosley-Thompson E, Readinger CR, Craigmile P, et al. (2005) Regional sensitivity of Greenland precipitation to NAO variability. *Geophysical Research Letters* 32.

Nesje A, Lie Ø and Dahl SO. (2000) Is the North Atlantic Oscillation reflected in Scandinavian glacier mass balance records? *Journal of Quaternary Science* 15: 587-601.

Ottesen RT, Bogen J, Bølviken B, et al. (2000) *Geokjemisk atlas for Norge, del 1: Kjemisk sammensetning av flomsedimenter,* Trondheim: Geological survey of Norway (NGU), Norwegian Water Resources and Energy Directorate (NVE).

Peterson BJ, Holmes RM, McClelland JW, et al. (2002) Increasing river discharge to the Arctic Ocean. *Science* 298: 2171-2173.

Rise L, Boe R, Sveian H, et al. (2006a) The deglaciation history of Trondheimsfjorden and Trondheimsleia, Central Norway. *Norwegian Journal of Geology* 86: 415-434.

Rise L, Bøe R, Sveian H, et al. (2006b) The deglaciation history of Trondheimsfjorden and Trondheimsleia, Central Norway. *Norwegian Journal of Geology* 86: 415-434.

Roberts D. (1997) Geochemistry of Palaeoproterozoic porphyritic felsic volcanites from the olden and Tømmerås windows, central Norway. *GFF* 119: 141-148.

Sakshaug E and Sneli J-A. (2000) *Trondheimsfjorden,* Trondheim: Tapir Forlag.

Syvitski JPM. (1989a) On the Deposition of Sediment within Glacier-Influenced Fjords - Oceanographic Controls. *Marine Geology* 85: 301-329.

Syvitski JPM. (1989b) On the deposition of sediment within glacier-influenced fjords: Oceanographic controls. *Marine Geology* 85: 301-329.

Syvitski JPM. (2002) Sediment discharge variability in Arctic rivers: implications for a warmer future. *Polar Research* 21: 323-330.

Wanner H, Brönnimann S, Casty C, et al. (2001) North Atlantic Oscillation – Concepts And Studies. *Surveys in Geophysics* 22: 321-381.

Wendelbo PS. (1970) Hydrografiske forhold i Trondheimsfjorden 1963-66. *Institute of Geophysics.* Oslo: University of Oslo.

West AJ, Galy A and Bickle M. (2005) Tectonic and climatic controls on silicate weathering. *Earth and Planetary Science Letters* 235: 211-228.

White AF and Blum AE. (1995) Effects of Climate on Chemical-Weathering in Watersheds. *Geochimica Et Cosmochimica Acta* 59: 1729-1747.

White AF, Blum AE, Bullen TD, et al. (1999) The effect of temperature on experimental and natural chemical weathering rates of granitoid rocks. *Geochimica Et Cosmochimica Acta* 63: 3277-3291.

Zabel M, Schneider RR, Wagner T, et al. (2001) Late Quaternary climate changes in central Africa as inferred from terrigenous input to the Niger fan. *Quaternary Research* 56: 207-217.

Öztürk M, Steinnes E and Sakshaug E. (2002) Iron speciation in the Trondheim fjord from the perspective of iron limitation for phytoplankton. *Estuarine Coastal and Shelf Science* 55: 197-212.

Supplementary Paper II

Table 1: Chronology and dating error for the MC99-3 based on ^{210}Pb and ^{137}Cs measurement as well as geochemical and sedimentology data used in Figures 5, 6, 7 and 8.

Core Length [cm]	**Age** [year]	**Age Error** [year ±]	**Grain size** <63 µm [%]	**Al/Zr**	**K/Ni**
0.5	2010	0.1	92.8	1050.0	386.2
1.5	2008	0.2	95.3	1101.4	385.5
2.5	2006	0.3	95.1	1049.3	395.5
3.5	2004	0.5	93.1	993.2	394.1
4.5	2002	0.6	93.8	1062.9	383.8
5.5	2000	0.8	93.7	1039.1	386.6
6.5	1998	0.9	93.9	1057.1	386.6
7.5	1996	1.0	92.9	1035.2	390.9
8.5	1994	1.2	92.4	1033.3	386.2
9.5	1992	1.3	92.8	1051.4	398.4
10.5	1990	1.5	92.6	1026.8	386.6
11.5	1988	1.6	91.9	1013.9	377.9
12.5	1985	1.7	92.3	1021.4	384.8
13.5	1983	1.9	91.3	1041.8	326.9
14.5	1981	2.0	91.5	1031.3	342.4
15.5	1979	2.1	93.5	1013.0	336.8
16.5	1977	2.3	92.7	1027.5	336.2
17.5	1975	2.4	91.5	1026.9	307.6
18.5	1973	2.6	92.3	1040.9	355.4
19.5	1971	2.7	93.8	1040.6	328.6
20.5	1969	2.8	93.0	1011.4	316.9
21.5	1967	3.0	92.2	1002.9	326.5
22.5	1965	3.1	93.4	1026.1	315.3
23.5	1963	3.3	92.8	1021.7	321.1
24.5	1961	3.4	92.7	1020.6	346.4
25.5	1959	3.5	91.1	1009.1	292.6

Table 2: Correlation coefficients between winter NAO (DJFM) and Trondheimsfjord regional winter precipitation (P) (DJFM), temperature (T) (DJFM), river discharge (R) (DJFMAM) and RTP (the annual winter mean of normalized river discharge (R), air temperature (T) and precipitation (P)) for 1963-2011.

	NAO [DJFM]	R [DJFMAM]	T [DJFM]	P [DJFM]	RTP
NAO	-	0.49	0.54	0.43	0.60
R	0.49	-	0.52	0.63	0.86
T	0.54	0.52	-	0.41	0.77
P	0.43	0.63	0.41	-	0.81
RTP	0.60	0.86	0.77	0.81	-

Paper III

Faust, J.C., Fabian, K., Milzer, G., Giraudeau, J. Knies, J., (in prep.). North Atlantic Oscillation dynamics recorded in central Norwegian fjord sediments during the past 2800 years. To be submitted to Nature Geoscience

North Atlantic Oscillation dynamics recorded in central Norwegian fjord sediments during the past 2800 years

Johan C. Faust[a, b, *], Karl Fabian[a], Gesa Milzer[d], Jacques Giraudeau[d], Jochen Knies[a]

[a] Geological Survey of Norway, 7491 Trondheim, Norway
[b] University of Tromsø, Department of Geology, 9011 Tromsø, Norway
[d] Universite Bordeaux 1 UMR CNRS 5805 EPOC, 33405 Talence cedex , France

*Corresponding author: Norges geologiske undersøkelse /Geological Survey of Norway (NGU), Marine Geology, Postboks 6315 Sluppen, 7491 Trondheim, Norway. Tel.: +47 7390 4000. E-mail address: Johan.Faust@ngu.no

The North Atlantic Oscillation (NAO) is the leading mode of atmospheric circulation variability in the North Atlantic region[1]. Along the Norwegian coast it has a strong impact on precipitation, temperature and wind intensity changes, thereby affecting energy supply and demand, fisheries, agricultural, marine and terrestrial ecological dynamics[2-4]. Long term NAO reconstructions are crucial to better understand NAO variability in its response to climate forcing factors, and assess predictability and possible shifts associated with on-going global warming. However, existing records are rare and often inconsistent[5]. By comparing geochemical measurements with instrumental data we show that primary productivity recorded in central Norwegian fjord sediments is sensitive to NAO variability. This observation is used to calibrate paleoproductivity changes to a 500-year reconstruction of winter NAO[6] and to establish a high resolution NAO proxy record covering the past 2800 years. We find that NAO variability coincides with climatically associated changes in paleodemographics and Northern Hemisphere (NH) glacier advances. Furthermore, a strong volcanic eruption may have induced the onset of the Little Ice Age (LIA), which is marked by a rapid transition from a stable positive to a stable negative NAO phase.

Apart from the northward flowing North Atlantic Current (NAC), the climate in northern Europe is strongly influenced by the North Atlantic Oscillation (NAO)[1,7,8]. This dominant mode of atmospheric circulation is most pronounced during winter (Dec-Mar) and swings between two phases: a positive (negative) NAO generates periods of warmer and wetter (colder and dryer) climate conditions in north-western Europe[9].

Instrumental time series are too short to reveal NAO responses to internal and external climate forcing with confidence. Paleo-NAO records based on historical records, tree ring or ice core data are shorter than ~950 years[10], and have large uncertainties for the pre-industrial period[5,8,11]. General challenges for NAO reconstructions are its possible non-stationarity, and its strong alteration on very short time scales requiring high resolution (winter) paleoclimatic records. Only the latter can provide the essential knowledge for NAO prediction and quantification of possible anthropogenic changes.

The Norwegian coastal area is supposed to be consistently influenced by NAO variability over long time scales[8]. General high sedimentation in Norwegian fjords, together with the possibility to quantify environmental parameters such as water exchange and freshwater input, offer an excellent opportunity for studying local responses to short-term variability in the Earth's climate. Here we use the geochemical record of two sediment cores: the upper five meter of the piston core MD99-2292[12], and multi-core MC99-3 (hereafter referred to as MC99). They were recovered from the Trondheimsfjord, central Norway (Fig. S1, supplementary information), and have a temporal resolution of 1.8-3 years covering the past 2800 years.

The most important factors regulating primary productivity in fjords are light, temperature, wind-driven vertical mixing and freshwater runoff i.e. nutrient supply (e.g. Fe, N, P)[13-15].

Thus, the strong impact of the NAO on changes on physical climate parameters, such as wind, temperature and precipitation in Norway, influences ecological dynamics in marine and terrestrial systems and encompasses change in (e.g.) the phytoplankton production in terms of timing of reproduction and population dynamics[2,3,16]. In particular, the annual spring bloom, most likely the strongest primary productivity event in fjords, is triggered by the strength of spring river discharge due to snow melt[14,15]. During this period autotrophic production and heterotrophic consumption are uncoupled, resulting in dense phytoplankton population and large amounts of aggregated particles reaching the seafloor,[17] nourishing the benthic population[2].

Principle component analysis (PCA) indicates that for the last 50 years the three climate components of 1) winter-spring (DJFMAM) river discharge (R), 2) winter (DJFM) air temperature (T), and 3) precipitation (P) from the Trondheimsfjord area are strongly related. The first principal component (PCA1) explains 81 % of the variance (supplementary information, Tab. S3), and combines the three physical factors into a new RTP index (Fig. 1). The concurrent changes of the three climate components in the Trondheimsfjord region appear to be caused by changes in the large-scale atmospheric climate pattern as defined through the winter NAO index[1] (supplementary information, Fig. S4).

In accordance with investigations of Trondheimsfjord surface sediments[18] a strong connection ($r^2 = 0.8$) between marine derived organic matter and $CaCO_3$ retrieved from the short sediment core MC99 indicates carbonate marine productivity to be the main $CaCO_3$ source in Trondheimsfjord sediments during the past 50 years (supplementary information Fig. S2). Moreover, $CaCO_3$ variations are closely linked to the RTP index (Fig. 1 and S3), implying that the combined impact of air temperature, precipitation and river discharge on marine pro-

ductivity is directly reflected by the $CaCO_3$ concentrations in Trondheimsfjord sediments. Due to the insufficient resolution of the sediment record the available number of $CaCO_3$ measurements does not allow a reliable statistical comparison with the instrumental time series although, the $CaCO_3$ record from MC99 closely follows the winter NAO variation during the past fifty years. Temporal offsets between relative maxima and minima lie within chronological uncertainties (Fig. 1). Accordingly, winter NAO apparently is very well recorded by $CaCO_3$ in Trondheimsfjord sediments due to its impact on the annual spring bloom intensity, suggesting planktic and benthic carbonate productivity during spring as a promising proxy for NAO reconstruction.

In the sediment core MD99-2292, $CaCO_3$ percentages coincide closely with its high resolution (1.8 - 3.0 years) Ca/Si record (Fig. S5). This enables us to compare Ca/Si to reliable[11] winter (DJF) NAO reconstructions based on early instrumental and documentary proxy data covering the past 500 years (AD 1500-1990)[6]. A correlation of $r^2 = 0.8$ between Ca/Si and an averaged winter NAO index was achieved by adapting the depth-age relation of Ca/Si within its 1-sigma age error range to the Luterbacher [6] NAO using a dynamic time-warping algorithm (Fig. 2 and supplementary information). The derived linear calibration function was used to calculate a winter NAO_{TRD} proxy index for the past 2800 years (Fig. 3).

As previously proposed[10], but so far not completely recorded, the NAO_{TRD} reveals persistent positive values during the Medieval Climate Anomaly (MCA, ~950 to ~1250 A.D.)[19]. A rapid change towards a stable negative mode occurs at the LIA[20] onset followed by a much more variable behavior during the past 300 years. The only previous NAO reconstruction beyond 1000 A.D. (NAO_{PCA3})[21] suggests a similar overall paleo-NAO pattern (Fig. 3). However, the NAO_{TRD} varies more and does not contain the NAO_{PCA3} extended stable periods between

e.g. ~500 to ~350 B.C. and ~0 to ~200 A.D. In particular the longest persistent NAO_{PCA3} period (1100 - 1400 A.D.), originating from the calibration of the NAO_{PCA3}[10,21], differs from our record. The differences between the proxies are probably related to different response times of the proxies, dating uncertainties, and maybe also to changes in the stationarity of the NAO spatial pattern[8]. Nevertheless, spectral analysis of NAO_{TRD} reveals dominant periodicities of about 300 (±20), 170 (±10) and 66 (±2) years (Fig. S7, supplementary information), which are consistent with the cyclicities of the NAO_{PCA3}[21]. The occurrence of a 300-year climatic cycle, identified in NH meteorological observations and terrestrial climate archives, historically has been related to changes in solar activity[22,23], but to our knowledge this has not been confirmed. Although there might be an intrinsic atmospheric (NAO) periodicity driven by external forcing, the apparent 300-year cycle could also be a spurious periodicity of a red-noise climate process (Fig. S7, supplementary information).

It is noteworthy that climatically associated changes in central European paleodemographics[24] coincide with long and short term NAO_{TRD} variations (Fig. 3 and Tab. S4). Socio-economic crises, population migration, and settlement desertion intensified during negative NAO_{TRD} phases while positive NAO_{TRD} phases seem to heighten sustained demographic and economic growths. Moreover, a pronounced negative NAO_{TRD} overlaps with the collapse of the Classical Maya Civilization (~800 to ~1000 A.D.)[25] during an annual precipitation reduction of 40 %[25] in Mexico that is assumed to be caused by a shift of the Intertropical Convergence Zone (ITCZ)[26]. Within the same period glaciers advanced in Canada and Iceland[20] (Fig.3) as well as in the Alps, Alaska and Tibet[27]. The synchronicity of the central-American precipitation anomaly and widespread glacier advance in the NH suggest a common forcing promoting a negative NAO phase.

It is notable that transitions from positive to negative phases of the NAO_{TRD} are often rapid, whilst the increases back to positive values are more gradual. Possibly the spontaneous phase changes are related to threshold transitions triggered by internal or external forcing. For example, distinct positive to negative NAO_{TRD} shifts with subsequent advance of NH glaciers[20,27] occurred at the same time as the two major volcanic eruptions of the past 2800 years (536 and 1257 A.D.[20,28,29]) (Fig. 3). The rapid NAO_{TRD} MCA-LIA transition in the mid to late 13th century differs from the NAO reconstruction based on tree rings and speleothems (NAO_{ms}[10], Fig. 3), but is consistent with ice-cap development reconstructed in Canada[20] (Fig. 3). Associated climate modeling shows that volcanic-induced cooler climate conditions can continue after the aerosols are removed by sea-ice/ocean feedbacks over long time scales[20]. This scenario could explain the long negative NAO_{TRD} phase from 1250-1450 A.D.. Furthermore, periods of "volcanic-solar downturns"[30] seem to correspond with negative NAO_{TRD} phases (Fig. 3). Nevertheless, many phase changes in the NAO_{TRD} record are unaffected by volcanic activity, and other forcing factors such as internal atmospheric dynamical processes[31] may be responsible for NAO variability.

Compared to other paleoclimate records the LIA onset occurs relatively early in the NAO_{TRD}. We propose that this difference reflects different response times between the ocean and the atmosphere to internal or external forcing on short time scales. A positive NAO, as during the MCA, is generally associated with stronger eastward air-flow towards northern Europe supporting a strengthening of the North Atlantic Current (NAC) and Meridional Overturning Circulation[32]. The rapid NAO reversal at ~1250 A.D. may have decreased heat and moisture transport towards northern latitudes, whilst the buffering effect of the ocean may have prevented an immediate temperature drop in northern Europe. By

following Miller [20], we propose that the onset of the LIA occurred around 1250 A.D. when volcanic activity triggered large changes in the atmospheric circulation. A delayed LIA appearance by 100 years or so and a slower MCA-LIA transition in other records[30] is likely the result of the delayed response of the oceanic circulation to atmospheric forcing. Similar scenarios may also hold true for other periods of rapid NAO_{TRD} shifts.

The here presented first high-resolution winter NAO reconstruction from marine sediments (Fig. 3) reveals a strong connection between NH climate history and NAO regional impact in central Norway. Persistent positive and negative NAO phases are in accordance with cooler and warmer climate periods during the late Holocene, such as MCA and LIA. Rapid phase transitions related to large volcanic eruptions indicate the existence of internal atmospheric thresholds and instabilities in the atmospheric circulation pattern. Ongoing climate change and global warming requires improved physical modeling of the NAO to gain better knowledge of the feedback mechanisms involved in these changes to answer the important questions of which processes are potential triggers, and which are the main amplifiers of large scale climatic changes. Compared to the historic NAO variability over the last 300-400 years, the NAO_{TRD} proxy record shows comparable amplitudes over the last 2800 years, but also indicates that positive and negative phases are typically more persistent.

Material and Methods

The data presented here were obtained from two sediment cores, MD99-2292 and MC99, recovered at the same site in the Trondheimsfjord Seaward Basin (Fig. S1). The 31 m long sediment core MD99-2292 (water depth 486 m, 63°28'62"N, 10°11'63"E) was taken by the research vessel “Marion Dufresne” in 1999. Prior to sediment sampling the elemental composition of the first five meters were measured in 0.5 cm steps using an Avaatech X-ray

fluorescence (XRF) core scanner. Additional X-ray images using the SCOPIX system were taken at EPOC, CNRS/University of Bordeaux 1, France. Subsequently sediment slices (1 cm deep, 1.5 cm wide, 7 cm long) were taken in 4 cm intervals. The short (26 cm) multicore MC99 (5.5 cm diameter) was collected by the research vessel “Seisma” in April 2011 (water depth 504 m, 63°28'37"N, 10°11'37"E). The core was sliced in 1 cm intervals aboard the research vessel, and samples were stored in plastic bags at -18°C. Prior to further analyses, all samples (MD99-2292 and MC99) were freeze-dried and, except for grain size measurements, homogenised through gentle grinding.

Total carbon (TC) and total organic carbon (C_{org}) measurements were performed at the Geological Survey of Norway (NGU). C_{org} and TC were determined with a LECO SC-444. Prior to the C_{org} analysis, sediment subsamples (ca. 200 mg) were treated with 10 % (vol.) hydrochloric acid at 60°C, and subsequently washed 10 times with distilled water to remove inorganic carbon (carbonate). Carbonate content was calculated as $CaCO_3 = (TC- C_{org}) \times 8.33$.

Total nitrogen (N_{tot} in wt%) was determined using an elemental analyzer isotope ratio mass spectrometer (EA-IRMS) at EPOC, CNRS/University of Bordeaux 1, France. The inorganic nitrogen (N_{inorg}) content was analysed on 20 mg sediment subsamples treated with KOBr-KOH solution to remove organic nitrogen (see Knies [33] for details) using an EA-IRMS (Iso-Analytical Ltd., UK). The organic proportion of the total nitrogen content was calculated by subtracting the N_{inorg} fraction from N_{tot}. Stable carbon isotopes of the C_{org} fraction ($\delta^{13}C_{org}$) were measured on decarbonated (10 % HCl) aliquots using an EA-IRMS (Iso-Analytical Ltd., UK). $\delta^{13}C_{org}$ values are given in per mil vs. Vienna-PDB.

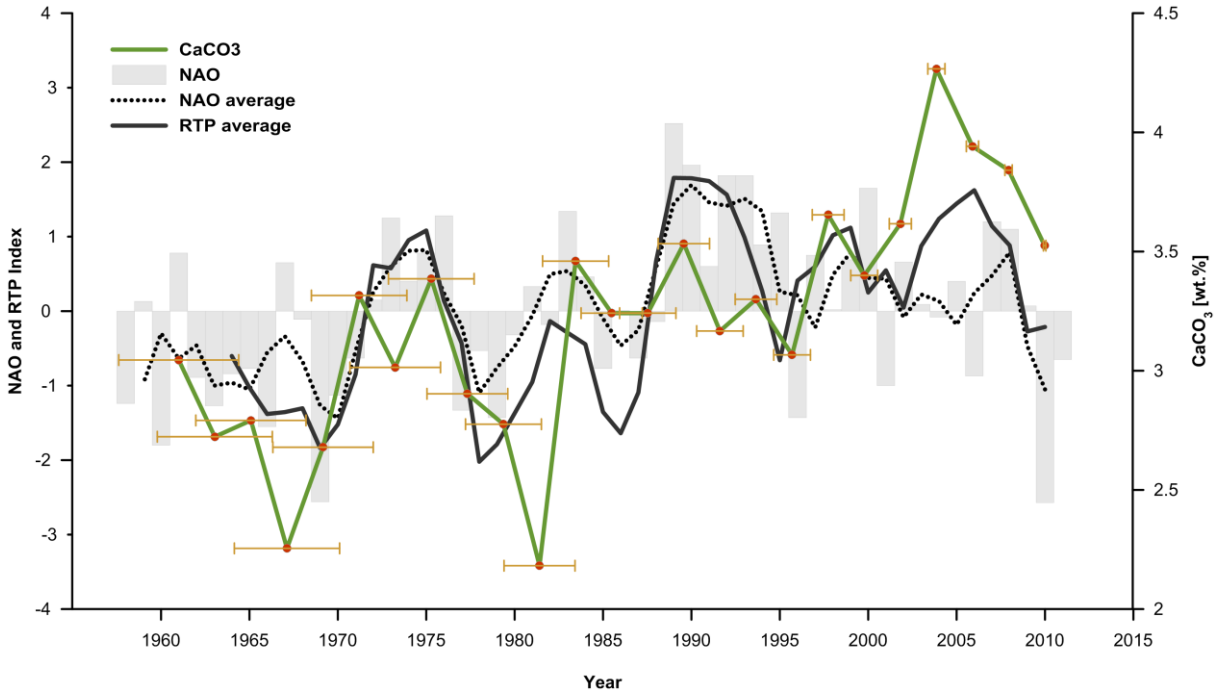

Figure 1: Comparison of instrumental data with $CaCO_3$ over the past 50 years. 3 point running average of RTP index (black line) combines instrumental records of winter-spring (DJFMAM) river discharge (R), winter (DJFM) air temperature (T) and precipitation (P) from the Trondheimsfjord area since 1963 (supplementary information). Grey bars are the annual winter NAO index[1] and dotted line is a 3 point running average. $CaCO_3$ concentration from MC99 (green line) follows the course of the averaged instrumental data in the range of the dating error (yellow bars).

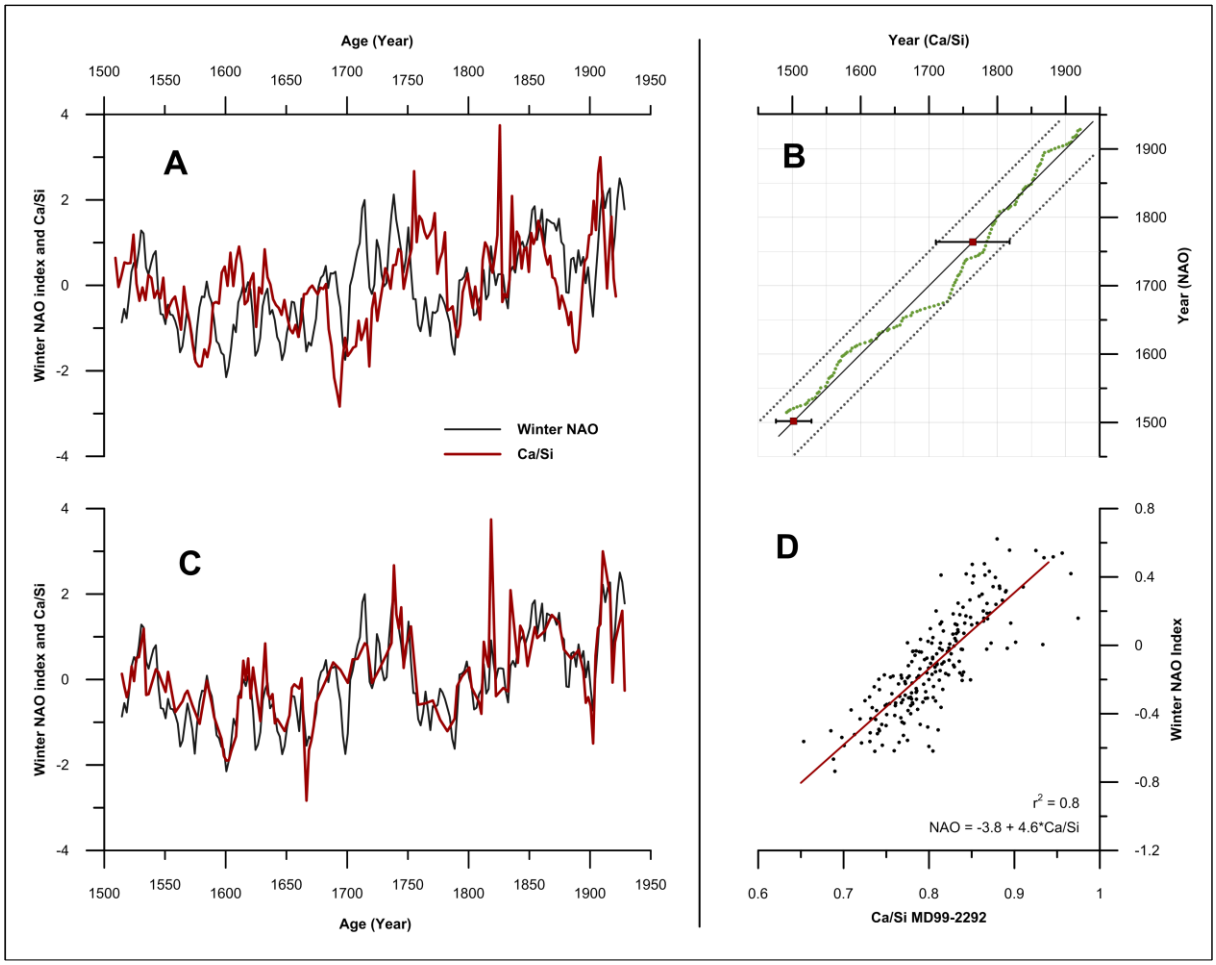

Figure 2: NAO_{TRD} calibration using a DTW fit A) Comparison between Ca/Si (MD99-2292) and averaged winter NAO index.[6] B) DTW fit between Ca/Si and averaged winter NAO index[6]. Red squares indicate ^{14}C ages (MD99-2292) with age error sigma 1 (Tab. S1). Dotted lines indicate ±50 year deviation. C) DTW fitted Ca/Si and averaged winter NAO index[6]. D) Calibration curve (r^2 = 0.8) based on Ca/Si winter NAO in C).

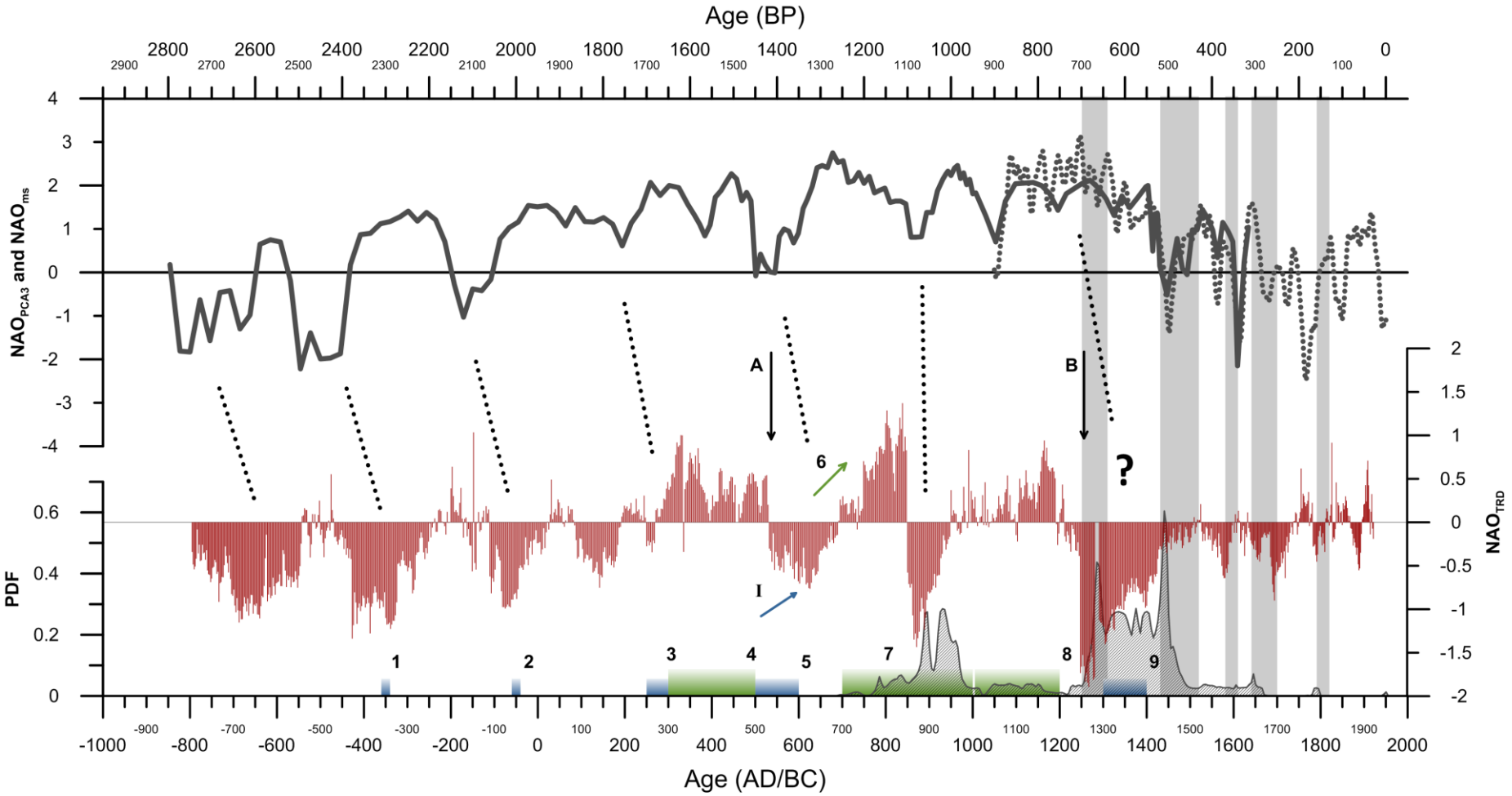

Fig. 3: Comparison between NAO_{TRD} and NH paleo-climate records. Longest NAO reconstruction (NAO_{PCA3})[21] available to date (black line) calibrated on a NAO record based on tree ring and speleothems (NAO_{ms})[10] (dotted black line). Black arrows: major volcanic eruptions in A) 536 A.D.[28] and B) 1257 A.D.[29]. European paleo-demographic climatic associated development[24] (Tab. S4) indicated by: blue squares (political turmoil, culture change, population instability) and green arrow/squares (demographic expansion, economic prosperity). Filled grey plot: ice cap expansion in Arctic Canada as probability density functions (PDF) of snow line depression[20]. Blue arrow (I) NH glacier advances during the 6th century[27]. Vertical grey bars: Periods of "Volcanic-Solar downturns" as defined by Pages 2k [30].

Acknowledgments

For their interest, stimulating discussions and many useful comments we thank our colleagues Simone Sauer and Benjamin Snook. This work is a contribution to the CASE Initial Training Network funded by the European Community's 7th Framework Programme FP7 2007/2013, Marie-Curie Actions, under Grant Agreement No. 238111.

References

1. Hurrell JW. Decadal Trends in the North-Atlantic Oscillation - Regional Temperatures and Precipitation. *Science* 1995, **269**(5224)**:** 676-679.
2. Drinkwater KF, Belgrano A, Borja A, Conversi A, Edwards M, Greene CH*, et al.* the response of marine ecosystems to climate variability associated with the North Atlantic Oscillation. *The North Atlantic Oscillation: Climatic Significance and Environmental Impact*, vol. 134. AGU: Washington, DC, 2003, pp 211-234.
3. Ottersen G, Planque B, Belgrano A, Post E, Reid P, Stenseth N. Ecological effects of the North Atlantic Oscillation. *Oecologia* 2001, **128**(1)**:** 1-14.
4. Hurrell JW, Kushnir Y, Ottersen G, Visbeck M. *The North Atlantic Oscillation: climatic significance and environmental impact*, vol. 134. American Geophysical Union, 2003.
5. Pinto JG, Raible CC. Past and recent changes in the North Atlantic oscillation. *Wires Clim Change* 2012, **3**(1)**:** 79-90.
6. Luterbacher J, Xoplaki E, Dietrich D, Jones PD, Davies TD, Portis D*, et al.* Extending North Atlantic Oscillation reconstructions back to 1500. *Atmos Sci Lett* 2001, **2**(1-4)**:** 114-124.
7. Nesje A, Lie Ø, Dahl SO. Is the North Atlantic Oscillation reflected in Scandinavian glacier mass balance records? *Journal of Quaternary Science* 2000, **15**(6)**:** 587-601.
8. Lehner F, Raible CC, Stocker TF. Testing the robustness of a precipitation proxy-based North Atlantic Oscillation reconstruction. *Quaternary Sci Rev* 2012, **45:** 85-94.
9. Wanner H, Brönnimann S, Casty C, Gyalistras D, Luterbacher J, Schmutz C*, et al.* North Atlantic Oscillation – Concepts And Studies. *Surveys in Geophysics* 2001, **22**(4)**:** 321-381.
10. Trouet V, Esper J, Graham NE, Baker A, Scourse JD, Frank DC. Persistent Positive North Atlantic Oscillation Mode Dominated the Medieval Climate Anomaly. *Science* 2009, **324**(5923)**:** 78-80.
11. Schmutz C, Luterbacher J, Gyalistras D, Xoplaki E, Wanner H. Can we trust proxy-based NAO index reconstructions? *Geophys Res Lett* 2000, **27**(8)**:** 1135-1138.
12. Bøe R, Rise L, Blikra LH, Longva O, Eide A. Holocene mass-movement processes in Trondheimsfjorden, Central Norway. *Norw J Geol* 2003, **83**(1)**:** 3-22.
13. Wassmann P, Svendsen H, Keck A, Reigstad M. Selected aspects of the physical oceanography and particle fluxes in fjords of northern Norway. *Journal of Marine Systems* 1996, **8**(1–2)**:** 53-71.
14. Öztürk M, Steinnes E, Sakshaug E. Iron speciation in the Trondheim fjord from the perspective of iron limitation for phytoplankton. *Estuar Coast Shelf S* 2002, **55**(2)**:** 197-212.
15. Sakshaug E, Myklestad S. Studies on the phytoplankton ecology of the trondheimsfjord. III. Dynamics of phytoplankton blooms in relation to environmental factors, bioassay experiments and parameters for the physiological state of the populations. *Journal of Experimental Marine Biology and Ecology* 1973, **11**(2)**:** 157-188.
16. Belgrano A, Lindahl O, Hernroth B. North Atlantic Oscillation primary productivity and toxic phytoplankton in the Gullmar Fjord, Sweden (1985-1996). *P Roy Soc B-Biol Sci* 1999, **266**(1418)**:** 425-430.
17. Kristiansen S, Farbrot T, Naustvoll LJ. Spring bloom nutrient dynamics in the Oslofjord. *Mar Ecol Prog Ser* 2001, **219:** 41-49.

18. Faust JC, Knies J, Slagstad T, Vogt C, Milzer G, Girausdeau J. Geochemical composition of Trondheimsfjord surface sediments: Sources and spatial variability of marine and terrigenous components. *Cont Shelf Res* Paper I.
19. Mann ME, Zhang ZH, Rutherford S, Bradley RS, Hughes MK, Shindell D*, et al.* Global Signatures and Dynamical Origins of the Little Ice Age and Medieval Climate Anomaly. *Science* 2009, **326**(5957)**:** 1256-1260.
20. Miller GH, Geirsdottir A, Zhong YF, Larsen DJ, Otto-Bliesner BL, Holland MM*, et al.* Abrupt onset of the Little Ice Age triggered by volcanism and sustained by sea-ice/ocean feedbacks. *Geophys Res Lett* 2012, **39**.
21. Olsen J, Anderson NJ, Knudsen MF. Variability of the North Atlantic Oscillation over the past 5,200 years. *Nat Geosci* 2012, **5**(11)**:** 808-812.
22. Clough H. Synchronous variations in solar and terrestrial phenomena. *The Astrophysical Journal* 1905, **22:** 42.
23. Kingsmill T. A 300-Year Climatic and Solar Cycle. *Nature* 1906, **73:** 413-414.
24. Büntgen U, Tegel W, Nicolussi K, McCormick M, Frank D, Trouet V*, et al.* 2500 Years of European Climate Variability and Human Susceptibility. *Science* 2011, **331**(6017)**:** 578-582.
25. Medina-Elizalde M, Rohling EJ. Collapse of Classic Maya Civilization Related to Modest Reduction in Precipitation. *Science* 2012, **335**(6071)**:** 956-959.
26. Haug GH, Gunther D, Peterson LC, Sigman DM, Hughen KA, Aeschlimann B. Climate and the collapse of Maya civilization. *Science* 2003, **299**(5613)**:** 1731-1735.
27. Wanner H, Beer J, Butikofer J, Crowley TJ, Cubasch U, Fluckiger J*, et al.* Mid- to Late Holocene climate change: an overview. *Quaternary Sci Rev* 2008, **27**(19-20)**:** 1791-1828.
28. Larsen LB, Vinther BM, Briffa KR, Melvin TM, Clausen HB, Jones PD*, et al.* New ice core evidence for a volcanic cause of the AD 536 dust veil. *Geophys Res Lett* 2008, **35**(4).
29. Lavigne F, Degeai JP, Komorowski JC, Guillet S, Robert V, Lahitte P*, et al.* Source of the great A.D. 1257 mystery eruption unveiled, Samalas volcano, Rinjani Volcanic Complex, Indonesia. *P Natl Acad Sci USA* 2013, **110**(42)**:** 16742-16747.
30. Pages 2k C. Continental-scale temperature variability during the past two millennia. *Nat Geosci* 2013, **6**(6)**:** 339.
31. Jung T, Vitart F, Ferranti L, Morcrette JJ. Origin and predictability of the extreme negative NAO winter of 2009/10. *Geophys Res Lett* 2011, **38**.
32. Trouet V, Scourse JD, Raible CC. North Atlantic storminess and Atlantic Meridional Overturning Circulation during the last Millennium: Reconciling contradictory proxy records of NAO variability. *Global Planet Change* 2012, **84-85:** 48-55.
33. Knies J, Brookes S, Schubert CJ. Re-assessing the nitrogen signal in continental margin sediments: New insights from the high northern latitudes. *Earth Planet Sc Lett* 2007, **253**(3-4)**:** 471-484.

Supplementary Paper III

Study area

The temperate Trondheimsfjord is located in the central part of Norway (Fig. S1) and, with a length of approximately 135 km, it is the third longest fjord in the country[2]. Three sills (the Agdenes Sill at the entrance (max. 330 m water depth), the Tautra Ridge in the middle section (max. 100 m water depth) and the Skarnsund in the inner part (max. water depth 100 m)) divide the Trondheimsfjord into four main basins: Stjørnfjord, Seaward basin, Middle fjord and Beistadfjord (Fig. S1) (for detailed maps of bathymetry and topography of the drainage area, we refer to http://kart.statkart.no). The average tide in the Trondheimsfjord is 1.8 m, the average water depth is 165 m and the maximum water depth (620 m) is found at the mouth of the Seaward basin [3].

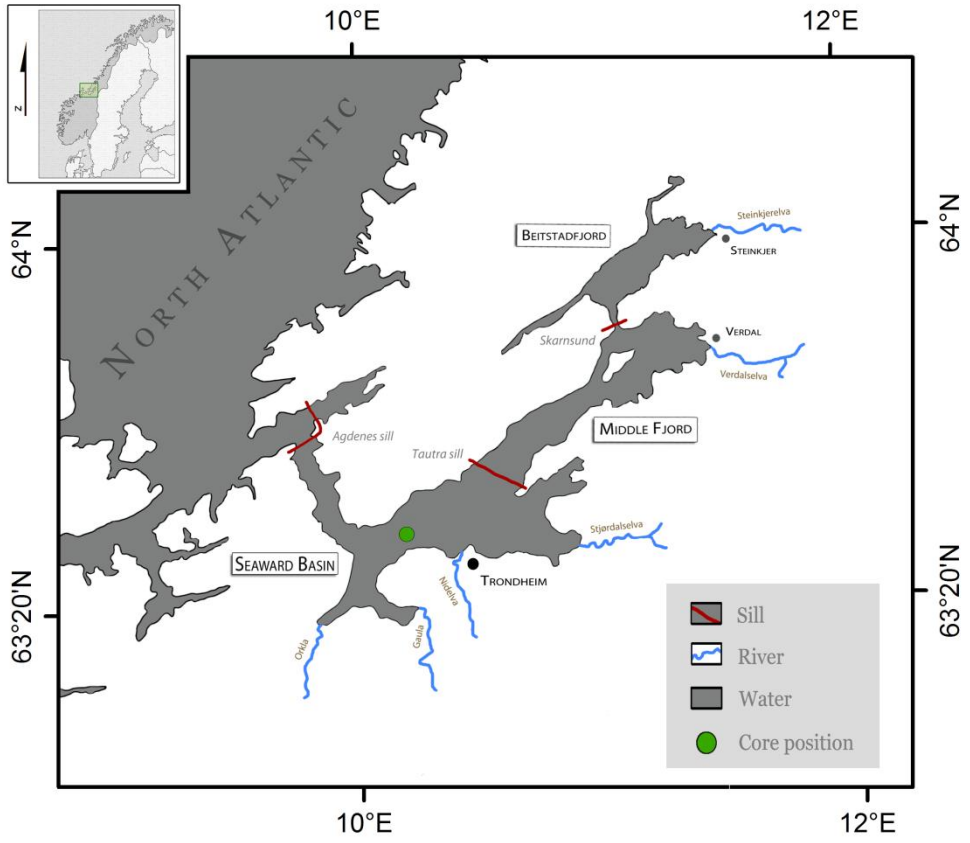

Figure S1: A) Location of the study area (upper left corner) and map of the Trondheimsfjord with the position of the sediment core MD99-2292 and MC99 (green circle). Three sills divide the fjord into three main basins and the six main rivers enter the fjord from the south-east.

Origin of organic matter

On the basis of sixty evenly distributed surface sediment samples around the entire Trondheimsfjord an index for the variable input of marine versus terrigenous organic matter (MT index) was generated by Faust et al (Paper I): MT index = $16.68 - 0.034 * F_{terr} + 0.65 * \delta^{13}C_{org}$. F_{terr} is the fraction of terrestrial organic carbon, which is calculated from the N_{org}/C_{org} ratio[4]. To calculate F_{terr}, the lowest and highest N_{org}/C_{org} ratios (0.052 and 0.113) revealed from the surface sediment analysis (Faust et al Paper I) were used to define the marine and terrestrial end members, respectively. Thus, MT index variations (Fig. S2) in the sedimentary record discussed in this study is tied to the modern environmental conditions in the fjord and positive (negative) MT index values indicate higher (lower) marine organic matter input.

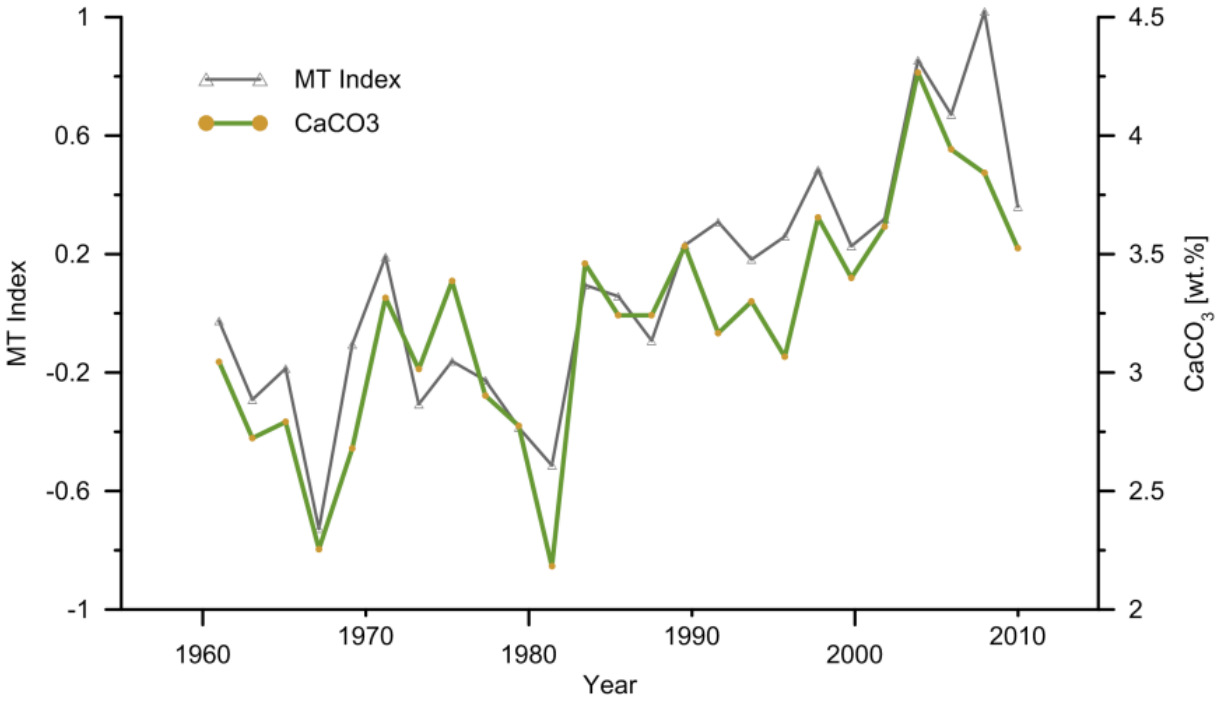

Figure S2: A strong connection between positive (negative) MT index values indicate higher (lower) marine organic matter input and $CaCO_3$ retrieved from the short sediment core MC99 indicates carbonate marine productivity to be the main $CaCO_3$ source in Trondheimsfjord sediments during the past 50 years.

Instrumental Data: NAO versus temperature, precipitation and river discharge

Seasonal and annual mean air temperature and precipitation records for the Trondheimsfjord region since 1900 were obtained from the Norwegian Meteorological Institute (www.eklima.no). Time series (1963-present) of river discharge for the six largest rivers entering the Trondheimsfjord, Gaula, Orkla, Nidelva, Stjørdalselva, Verdalselva and Steinkjerelva (Fig. S1) were obtained from the Norwegian Water Resource and Energy Directorate (www.nve.no). All data were collected at monitoring stations close to river outlets. The winter (December – March) PC-based NAO index[5] is based on the difference of normalised sea level pressure between Lisbon, Portugal and Stykkishomur, Iceland and the dataset was retrieved from https://climatedataguide.ucar.edu/climate-data/hurrell-north-atlantic-oscillation-nao-index-pc-based. Annual precipitation and river discharge into the Trondheimsfjord are strongly correlated[3]. However, the highest runoff occurs in late April to May and is primarily caused by snow melt (winter precipitation). As winter-spring river runoff, winter temperature and winter precipitation are closely linked to each other 81 % of the variance is explained by score of the first axis of principal component analysis (Tab. S3).

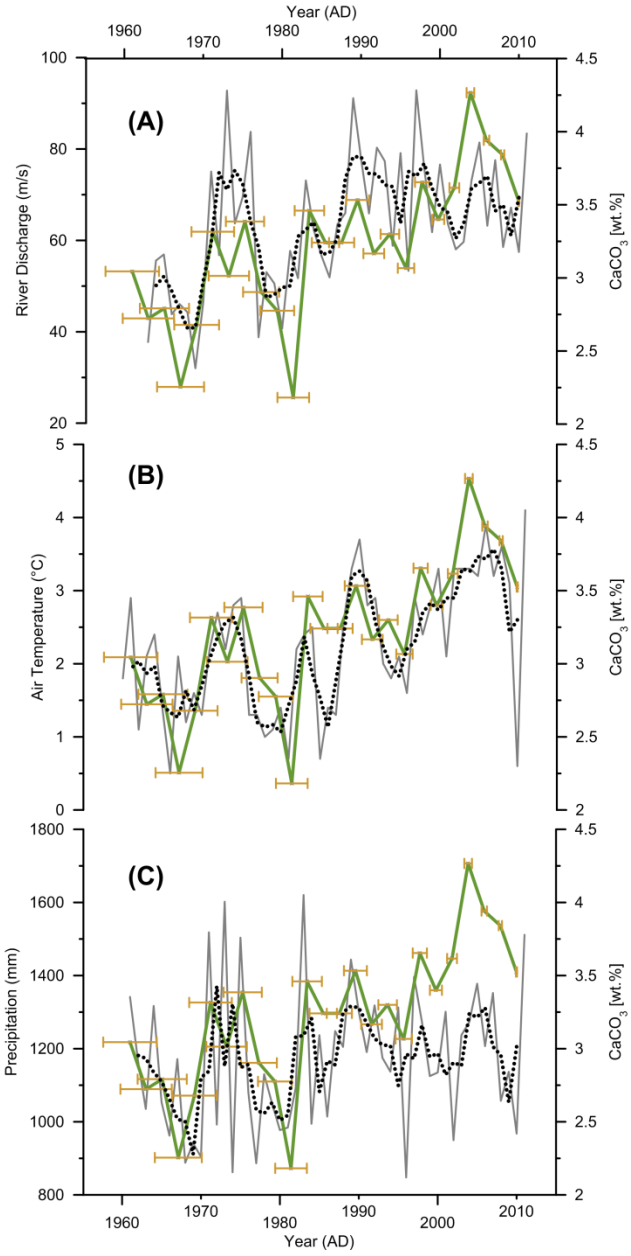

Figure S3: $CaCO_3$ from the sediment core MC99 compared to Trondheimsfjord regional variations of A) winter-spring (DJFMAM) river discharge B) winter (DJFM) air temperature and C) winter (DJFM) precipitation. Dotted black line is a 3 point running average.

Our Trondheimsfjord regional RTP record (PCA1) shows a very good correlation to the winter NAO index ($r^2 = 0.6$, Fig. S4), confirming that regional temperature and precipitation in the Trondheimsfjord area are responding to changes in large-scale Northern Hemisphere climate patterns.

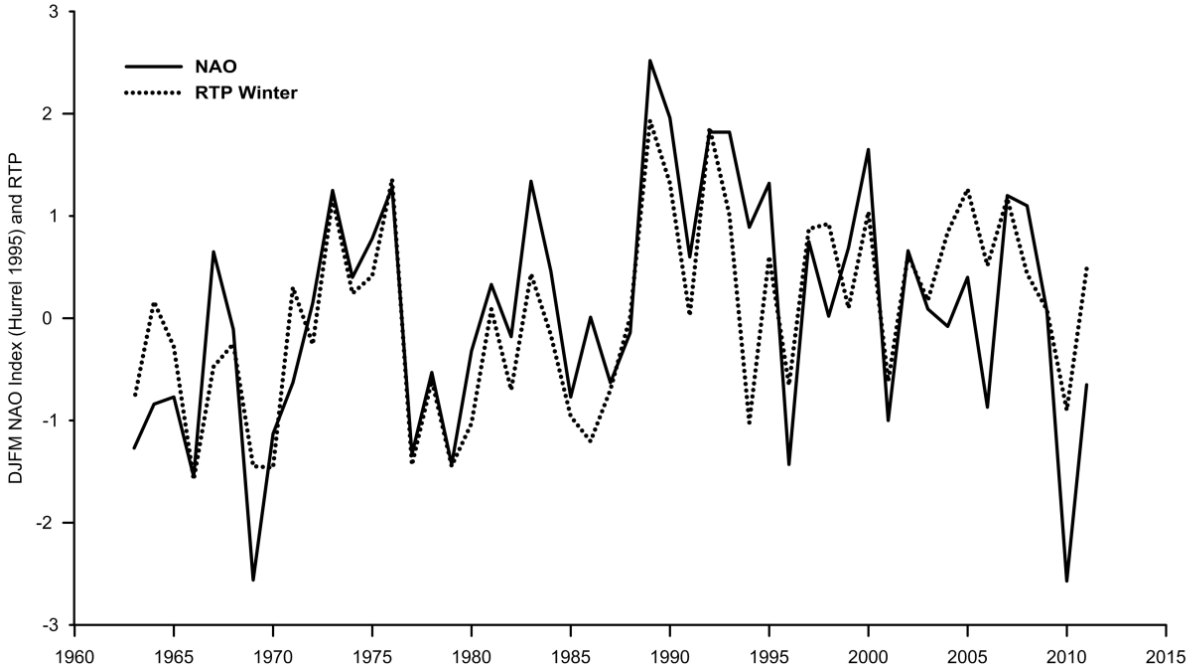

Figure S4: Winter NAO index[5] versus RTP index since 1963.

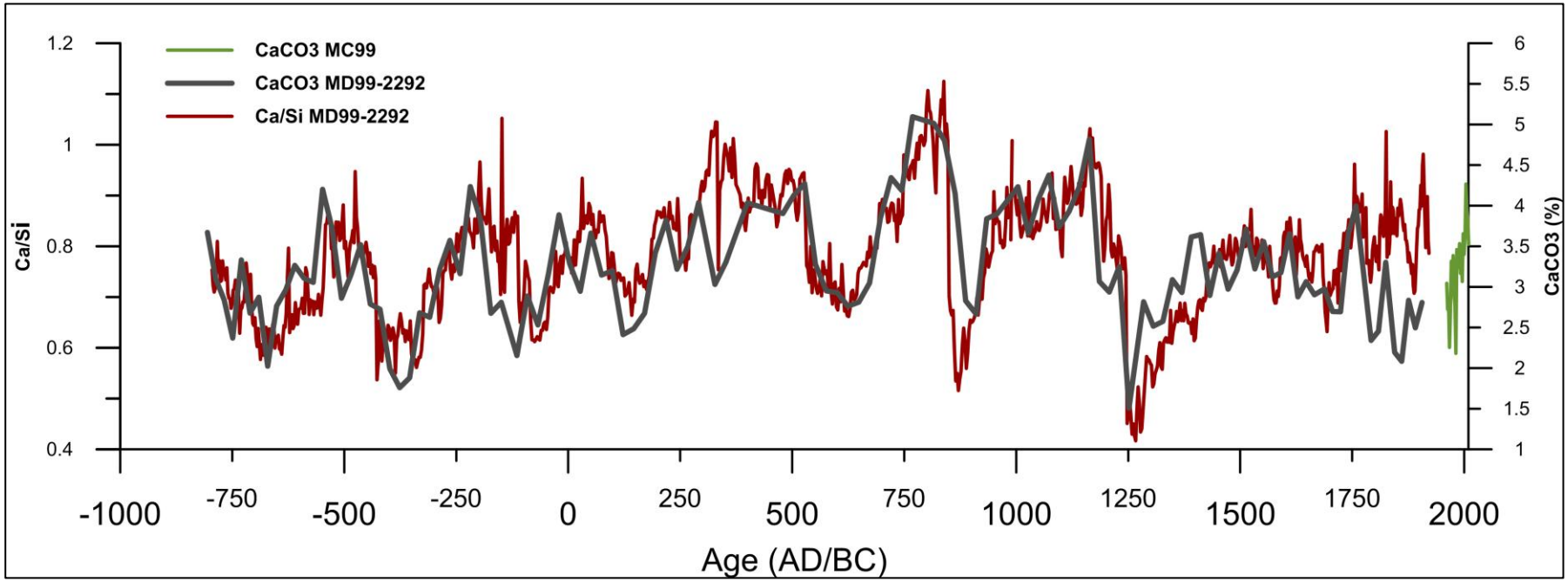

Figure S5: $CaCO_3$ in the gravity core MD99-2292 is in correspondence with $CaCO_3$ variations in the MC99. The ultra high resolution Ca/Si record closely resembles the $CaCO_3$ percentage in the MD99-2292.

NAO_{TRD} calibration

To convert Ca/Si ratios from MD99-2292 to estimates of the winter NAO index for the last 2800 years, the upper part (containing about 200 measurements between 1500 and 1930 A.D.) was fitted to a smoothed version of the winter NAO index of Luterbacher [1].

The smoothing kernel used,

$$\mathrm{Ker}(L,t) := \begin{cases} \max\left(0{,}1 - \frac{t}{2}\right), & t \geq 0 \\ \exp\left(\frac{2L}{t}\right), & t \leq 0 \end{cases}$$

takes into account both exponential mixing during sedimentation and linear averaging of the XRF sensor over its footprint area. Its only free parameter, the exponential decay constant, was chosen such that the variability of the smoothed record best resembled the Ca/Si variability (Fig. S6).

Because MD99-2292 contains only two ^{14}C ages in the time interval 1500 to 1930 A.D., its interpolated age model was modified to achieve an optimal fit of the Ca/Si signal to the smoothed winter NAO index, while keeping the dated sediment layers within their 1 sigma error range. This was performed using a dynamic time-warping (DTW) algorithm as described by Hofmann [6] and results in the transfer function between the two time scales shown in Fig. 2B. The suggested fit (Fig. 2C) shows that after alignment the two standardized signals agree very well, although near 1700 A.D. there is an alternative signal alignment. After alignment, the original Ca/Si measurement is plotted against the matching smoothed NAO index value of Luterbacher [1] in Fig. 2D. A robust linear fit (neglecting 10% of the data points furthest away from an initial fit) results in a clear ($r^2 = 0.8$) linear relation, whereby

$$smoothed\ NAO = 4.6\frac{Ca}{Si} - 3.8$$

The fit quality related to all data points is $r^2 = 0.7$. This relation was used to calibrate the Ca/Si record from MD99-2292 over the full time interval of 2,800 years.

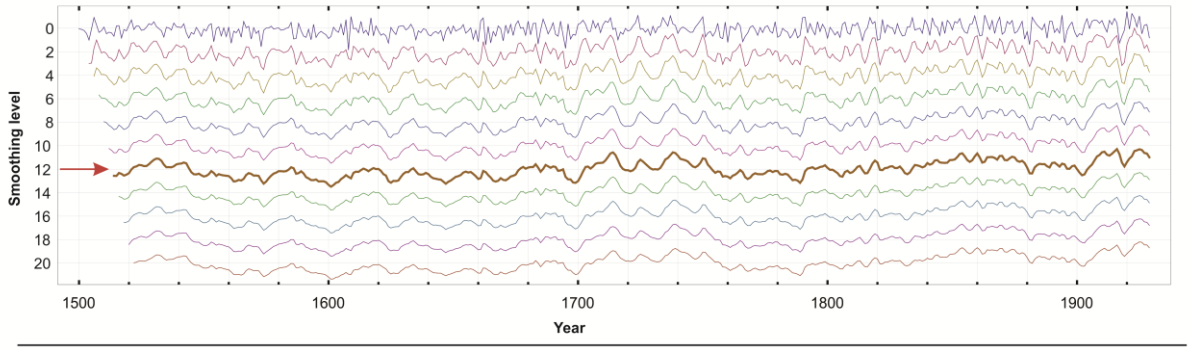

Figure S6: Smoothing of the NAO index[1] required to correctly account for delays in the transport and sedimentary deposition processes, as well as averaging during measurement, due to the finite overlapping footprints of the XRF sensor. Above) Original record (0) and increasingly smoothed versions (2-20) of the NAO index[1]. Right) Smoothing kernel (12) visually chosen to represent the high-frequency reduction observed in the Ca/Si record from the MD99-2292. Note that Ca/Si signal can only serve as a proxy for an accordingly smoothed NAO index.

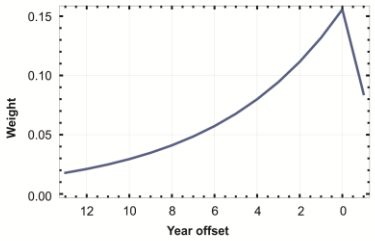

Spectral Analysis

The Ca/Si record from the sediment core MD99-2292 was analyzed for periodicities using Fourier transforms of length 512 with Welch overlapping windows (WOSA, overlap 384). The WOSA periodogram shows spectral peaks at frequencies corresponding to about 300 ±20, 170 ±10 and 66 ±2 years (Fig. S7). None of these peaks is statistically significant as a climatic periodicity. To confirm this we created random sequences $(r_n)_{n=1\ldots1002}$ of AR(1) processes based on white noise $(w_n)_{n=1\ldots1002}$ with standard deviation $\sigma = 0.45$ according to $r_0 = 0$, $\rho=0.92$, and

$$r_{n+1} = \rho\, r_n + w_n.$$

These sequences were smoothed by the same smoothing kernel as used for the NAO data and finally analyzed by the WOSA periodogram[7]. While the average periodogram corresponds to the known theoretical red noise spectrum each individual random record shows distinct peaks at varying frequencies. Within the first 50 trials we already found a spectrum closely resembling the one obtained from the observed Ca/Si record.

It is therefore impossible to relate the observed periodicities to true eigenfrequencies of the climate system. Yet, because they originate from the NAO signal, these frequencies may

be observed in other related time series covering the same time interval even if they are spurious.

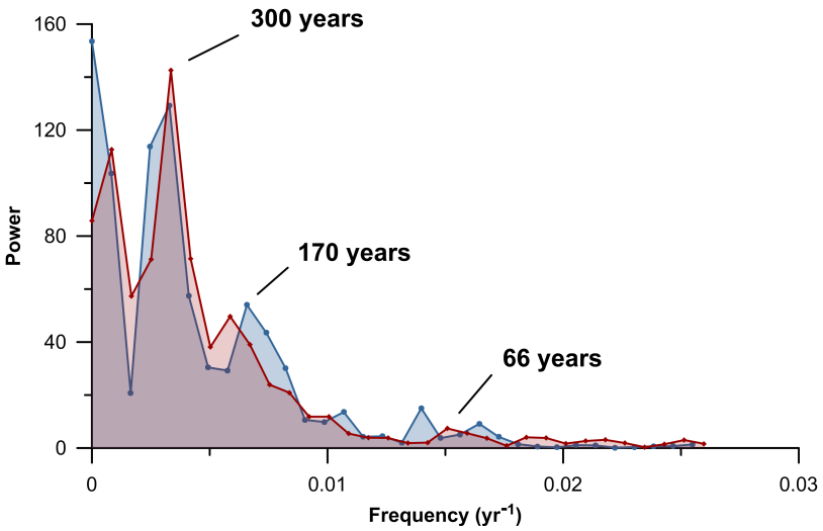

Figure S7: One out of 50 random AR(1) processes (blue) shows a WOSA periodogram similar to the observed signal (red).

Chronology

The chronology of the core MC99 is based on ^{210}Pb and ^{137}Cs content on neighbouring sediment core in the multi-corer rack (MC99-1). ^{210}Pb and ^{137}Cs measurements were made at EPOC, CNRS/University of Bordeaux 1, France. According to the age model of Milzer [8] (Fig. S8), the sedimentation rate of the MC99-1 is 0.49 cm/year and the core base age is 1959. The dating error increases gradually down core from ±0.07 to ±3.53 years.

The age model of the upper five meters of the MD99-2292[9] is based on eight ^{14}C-AMS dates and polynomial regression between these dates (Fig. S8). The ^{14}C-AMS dates were determined on shell material at the Leibniz Laboratory (University of Kiel, Germany) and at the Laboratoire de Mesure du Carbone 14 (Gif sur Yvette Cedex, France) (Tab. S1). We applied a reservoir correction of 400 years (ΔR = 0) and converted the radiocarbon dates into calibrated years with the Calib 6.0.1 software[10]. Six sand layers between 3-8 cm thick in various core depths (Tab. S2) were identified as gravitational mass movement and therefore as short

term sedimentation events. The depth of the six slides (in total 35 cm) were subtracted from the total core depth prior to the construction of the age model.

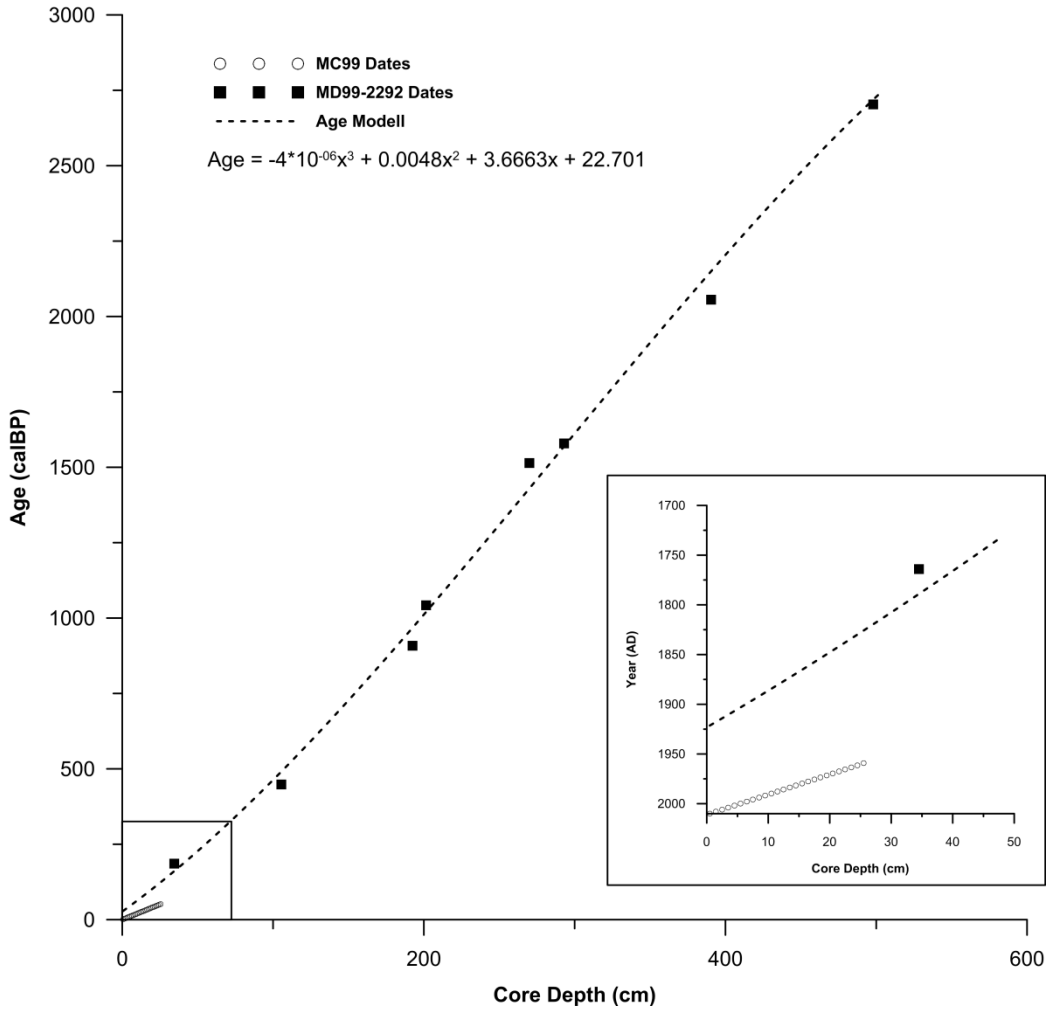

Figure S8: Age model for the MD99-2292. Black squares represent calibrated ^{14}C dates from core MD99-2292 and open circles are ^{210}Pb dates from core MC99[8]. Dashed line represents the age model for the MD99-2292. Equation of the 3rd order polynomial regression is shown at the upper left side. The inlayed graph on the lower right side is the magnification of the past~300 years marked by the square at the lower left corner.

References

1. Luterbacher J, Xoplaki E, Dietrich D, Jones PD, Davies TD, Portis D*, et al.* Extending North Atlantic Oscillation reconstructions back to 1500. *Atmos Sci Lett* 2001, **2**(1-4)**:** 114-124.
2. Jacobson P. Physical oceanography of the Trondheimsfjord. *Geophysical & Astrophysical Fluid Dynamics* 1983, **26**(1-2)**:** 3-26.
3. Sakshaug E, Sneli J-A. *Trondheimsfjorden*. Tapir Forlag: Trondheim, 2000.
4. Perdue EM, Koprivnjak JF. Using the C/N ratio to estimate terrigenous inputs of organic matter to aquatic environments. *Estuar Coast Shelf S* 2007, **73**(1-2)**:** 65-72.
5. Hurrell JW. Decadal Trends in the North-Atlantic Oscillation - Regional Temperatures and Precipitation. *Science* 1995, **269**(5224)**:** 676-679.
6. Hofmann DI, Fabian K, Schmieder F, Donner B, Bleil U. A stratigraphic network across the Subtropical Front in the central South Atlantic: Multi-parameter correlation of magnetic susceptibility, density, X-ray fluorescence and delta O-18 records. *Earth Planet Sc Lett* 2005, **240**(3-4)**:** 694-709.
7. Percival DB. *Spectral analysis for physical applications*. Cambridge University Press, 1993.
8. Milzer G, Giraudeau J, Schmidt S, Eynaud F, Faust J. Qualitative and quantitative reconstruction of surface water characteristics and recent hydrographic changes in the Trondheimsfjord, central Norway. *Clim Past Discuss* 2013, **9**(4)**:** 4553-4598.
9. Bøe R, Rise L, Blikra LH, Longva O, Eide A. Holocene mass-movement processes in Trondheimsfjorden, Central Norway. *Norw J Geol* 2003, **83**(1)**:** 3-22.
10. Stuiver M, Reimer PJ. Extended 14C data base and revised CALIB 3.0 14C age calibration program. *Radiocarbon* 1993, **35**(1)**:** 215-230.
11. Büntgen U, Tegel W, Nicolussi K, McCormick M, Frank D, Trouet V*, et al.* 2500 Years of European Climate Variability and Human Susceptibility. *Science* 2011, **331**(6017)**:** 578-582.

Table S1: Chronological information

Core	Depth [cmbsf]	Lab code [a)]	Material	^{14}C Age BP (uncorrected)	Model Age [BP] [b)]	Sedimentation rate (cm/a)
MD99-2292	34.5	SacA23876	Shell fragment	550±35	186±54	0.2
MD99-2292	105.5	KIA-38731	Shell (Modiolaria)	800±25	448±26	0.2
MD99-2292	192.5	SacA 19110	Shell fragment	1360±30	908±36	0.2
MD99-2292	201.5	SacA23879	Shell fragment	1495±30	1042±50	0.2
MD99-2292	270	KIA-38732	Shell (Abra alba)	1960±25	1514±43.5	0.2
MD99-2292	293	SacA 19111	Shell fragment	2015±30	1579±46	0.2
MD99-2292	390.5	SacA 19112	Shell fragment	2420±30	2056±49	0.2
MD99-2292	498	KIA-38734	Shell fragment	2915±35	2703±32	0.2

[a)] KIA: Leibniz Laboratory (University of Kiel, Germany); SacA: Laboratoire de Mesure du Carbone 14 (Gif sur Yvette Cedex, France)
[b)] Ages with 1 sigma range were determined using Calib 6.0.1[10]

Table S2: Depth of six slides subtracted from the total core depth

Slide Num-ber	Core Depth	Slide Length (cm)
1	23-26	3
2	40-44	4
3	67-70	3
4	157-165	8
5	305-310	5
6	326-332	6
7	407-413	6

Table S3: PCA Analysis

			Loadings		
	Eigenvalue	Variance (%)	R[DJFMAM][a)]	T[DJFM][b)]	P[DJFM][c)]
PCA1	2.44	81.2	0.92	0.71	0.97
PCA2	0.37	12.3	0.4	0.18	-0.24
PCA3	0.19	6.5	0	0.69	0

[a)] River discharge (m/s)
[b)] Temperature (°C)
[c)] Precipitation (mm)

Table S4: European paleo-demographic climatic associated development shown in Fig. 3. All data are from Büntgen [11]

Number in Fig. 3	Period	Histroical Event	Climate summer conditions
1	~350 B.C.	Celtic Expansion, followed by the Late Iron Age	Colder Temperatures
2	~50 B.C.	Roman Conquest followed by the Roman Empire	Colder Temperatures
3	250-300 A.D.	Crisis in the West Roman Empire marked by barbarian invasion	Distinct drier conditions
4	300-500 A.D.	Dynasties of Constantine and Valentinian	Relative stable conditions
5	500-600 A.D.	Frequent epidemics, disrupt food production of agrarian societies	Sharp drop in precipitation in the first half of the 6th century, NH cooling
6	End 600 - 800 A.D.	Societal consolidation of new kingdoms that developed in the former West Roman Empire	Increase in temperature and precipitation
7	700-1000 A.D.	Sustained demographic growth in the northwest European countryside, establishment of colonies in Iceland and Greenland	Stable wet and warm conditions
8	1000-1200 A.D.	Peak medieval demographic and economic growth	Stable wet and warm conditions
9	1300-1400 A.D.	Widespread famine across central Europe, desertion of Greenland settlements	Colder Temperatures

Table S5: Ca/Si values from the MD99-2292 and calculated NAO_{TRD}

Age AD/BC	Ca/Si	NAO_{TRD}	Age AD/BC	Ca/Si	NAO_{TRD}	Age AD/BC	Ca/Si	NAO_{TRD}	Age AD/BC	Ca/Si	NAO_{TRD}
1921	0.79	-0.19	1764	0.88	0.23	1583	0.71	-0.53	1382	0.66	-0.76
1920	0.81	-0.07	1762	0.89	0.30	1580	0.69	-0.64	1379	0.67	-0.74
1918	0.90	0.33	1760	0.90	0.33	1578	0.69	-0.64	1376	0.69	-0.64
1916	0.85	0.12	1757	0.86	0.16	1575	0.69	-0.61	1374	0.65	-0.80
1914	0.80	-0.14	1755	0.96	0.62	1573	0.72	-0.50	1371	0.67	-0.71
1912	0.86	0.15	1753	0.85	0.12	1571	0.75	-0.36	1368	0.65	-0.80
1910	0.92	0.43	1751	0.84	0.05	1568	0.77	-0.27	1366	0.69	-0.64
1909	0.98	0.71	1749	0.82	-0.05	1566	0.80	-0.13	1363	0.66	-0.75
1907	0.96	0.60	1747	0.80	-0.14	1563	0.74	-0.40	1361	0.65	-0.81
1905	0.88	0.24	1745	0.85	0.10	1561	0.77	-0.28	1358	0.67	-0.72
1903	0.92	0.43	1742	0.85	0.12	1558	0.79	-0.19	1355	0.65	-0.80
1901	0.87	0.21	1740	0.83	0.02	1556	0.78	-0.21	1353	0.64	-0.85
1899	0.87	0.20	1738	0.83	0.01	1554	0.77	-0.26	1350	0.63	-0.91
1898	0.84	0.06	1736	0.80	-0.14	1551	0.76	-0.33	1347	0.61	-1.01
1896	0.84	0.04	1734	0.82	-0.06	1549	0.81	-0.07	1345	0.67	-0.71
1894	0.80	-0.13	1731	0.83	-0.01	1546	0.78	-0.20	1342	0.61	-1.00
1892	0.75	-0.35	1729	0.80	-0.12	1544	0.79	-0.15	1339	0.62	-0.96
1890	0.71	-0.53	1727	0.78	-0.23	1541	0.78	-0.20	1337	0.61	-1.00
1888	0.71	-0.55	1725	0.75	-0.35	1539	0.81	-0.07	1334	0.62	-0.96
1886	0.72	-0.48	1723	0.79	-0.17	1536	0.82	-0.05	1331	0.62	-0.98
1884	0.76	-0.29	1721	0.77	-0.27	1534	0.78	-0.21	1329	0.61	-1.00
1883	0.75	-0.37	1718	0.69	-0.64	1532	0.80	-0.13	1326	0.56	-1.24
1881	0.76	-0.29	1716	0.75	-0.33	1529	0.78	-0.22	1323	0.56	-1.22
1879	0.78	-0.23	1714	0.74	-0.42	1527	0.80	-0.11	1321	0.61	-1.00
1877	0.79	-0.18	1712	0.73	-0.47	1524	0.87	0.21	1318	0.59	-1.08
1875	0.77	-0.27	1710	0.75	-0.35	1522	0.83	0.03	1315	0.56	-1.21
1873	0.80	-0.13	1707	0.72	-0.51	1519	0.83	0.02	1313	0.56	-1.25
1871	0.81	-0.07	1705	0.71	-0.52	1517	0.83	0.03	1310	0.55	-1.28
1869	0.81	-0.07	1703	0.71	-0.55	1514	0.82	-0.06	1307	0.53	-1.37
1867	0.84	0.07	1701	0.70	-0.57	1512	0.80	-0.13	1305	0.52	-1.40
1865	0.83	0.02	1698	0.73	-0.46	1509	0.84	0.06	1302	0.57	-1.20
1863	0.84	0.08	1696	0.69	-0.61	1507	0.82	-0.03	1299	0.57	-1.19
1861	0.86	0.17	1694	0.63	-0.90	1504	0.81	-0.06	1296	0.58	-1.16
1859	0.88	0.25	1692	0.65	-0.80	1502	0.79	-0.18	1294	0.58	-1.15
1858	0.89	0.30	1689	0.67	-0.71	1499	0.78	-0.23	1291	0.58	-1.13
1856	0.87	0.19	1687	0.72	-0.51	1497	0.78	-0.23	1280	0.44	-1.78
1854	0.86	0.15	1685	0.74	-0.40	1494	0.79	-0.16	1278	0.43	-1.81
1852	0.88	0.22	1683	0.80	-0.11	1492	0.81	-0.08	1275	0.49	-1.55
1850	0.82	-0.03	1680	0.80	-0.14	1489	0.82	-0.05	1272	0.52	-1.40
1848	0.86	0.13	1678	0.80	-0.13	1487	0.79	-0.17	1269	0.48	-1.61
1846	0.85	0.11	1676	0.79	-0.18	1484	0.77	-0.27	1267	0.42	-1.89
1844	0.83	-0.01	1674	0.80	-0.15	1482	0.76	-0.30	1264	0.43	-1.84
1842	0.87	0.20	1671	0.80	-0.12	1479	0.78	-0.21	1261	0.45	-1.74
1840	0.88	0.23	1669	0.80	-0.14	1477	0.82	-0.03	1259	0.43	-1.83
1838	0.83	-0.01	1667	0.79	-0.17	1474	0.80	-0.12	1256	0.47	-1.66
1836	0.93	0.46	1665	0.79	-0.17	1472	0.78	-0.20	1253	0.50	-1.53
1834	0.81	-0.08	1662	0.75	-0.35	1469	0.77	-0.25	1250	0.47	-1.66
1832	0.79	-0.19	1660	0.73	-0.45	1467	0.78	-0.22	1248	0.45	-1.73
1830	0.79	-0.17	1658	0.75	-0.37	1464	0.78	-0.24	1245	0.74	-0.39
1828	0.78	-0.23	1655	0.73	-0.43	1462	0.81	-0.07	1242	0.78	-0.23
1826	1.03	0.92	1653	0.74	-0.40	1459	0.79	-0.17	1239	0.76	-0.33
1824	0.87	0.21	1651	0.76	-0.32	1456	0.76	-0.31	1237	0.76	-0.32
1822	0.84	0.08	1648	0.78	-0.21	1454	0.79	-0.16	1234	0.80	-0.14
1820	0.82	-0.04	1646	0.76	-0.31	1451	0.78	-0.24	1231	0.81	-0.08
1818	0.83	0.03	1644	0.77	-0.26	1449	0.78	-0.23	1228	0.82	-0.03
1816	0.85	0.13	1642	0.77	-0.24	1446	0.75	-0.35	1226	0.75	-0.34
1814	0.86	0.16	1639	0.78	-0.21	1444	0.77	-0.28	1223	0.77	-0.24
1812	0.84	0.05	1637	0.80	-0.11	1441	0.80	-0.12	1220	0.80	-0.15
1810	0.75	-0.34	1635	0.81	-0.07	1439	0.78	-0.23	1217	0.80	-0.10
1808	0.77	-0.24	1632	0.85	0.11	1436	0.77	-0.28	1215	0.78	-0.22
1806	0.80	-0.13	1630	0.79	-0.17	1433	0.76	-0.31	1212	0.79	-0.16
1804	0.77	-0.26	1628	0.80	-0.13	1431	0.77	-0.28	1209	0.89	0.27
1801	0.79	-0.17	1625	0.74	-0.39	1428	0.76	-0.31	1206	0.92	0.43
1799	0.82	-0.04	1623	0.82	-0.04	1426	0.74	-0.42	1204	0.86	0.16
1797	0.81	-0.10	1621	0.81	-0.09	1423	0.70	-0.59	1201	0.85	0.11
1795	0.79	-0.16	1618	0.78	-0.22	1421	0.69	-0.62	1198	0.80	-0.13
1793	0.75	-0.37	1616	0.78	-0.24	1418	0.70	-0.60	1195	0.77	-0.26
1791	0.73	-0.45	1613	0.83	0.02	1415	0.67	-0.71	1192	0.82	-0.02
1789	0.75	-0.38	1611	0.86	0.13	1413	0.68	-0.69	1190	0.94	0.51
1787	0.77	-0.25	1609	0.84	0.04	1410	0.69	-0.61	1187	0.95	0.59
1785	0.77	-0.27	1606	0.80	-0.12	1408	0.69	-0.62	1184	0.96	0.63
1783	0.77	-0.28	1604	0.85	0.09	1405	0.68	-0.68	1181	0.96	0.62
1781	0.88	0.22	1602	0.80	-0.12	1402	0.65	-0.80	1179	0.95	0.58
1779	0.85	0.10	1599	0.83	0.00	1400	0.62	-0.96	1176	0.96	0.60
1776	0.84	0.05	1597	0.82	-0.04	1397	0.61	-0.98	1173	0.97	0.64
1774	0.82	-0.04	1595	0.78	-0.24	1395	0.66	-0.79	1170	1.01	0.86
1772	0.90	0.35	1592	0.78	-0.23	1392	0.63	-0.92	1167	0.98	0.71
1770	0.88	0.25	1590	0.78	-0.24	1389	0.65	-0.82	1165	1.03	0.94
1768	0.87	0.21	1587	0.72	-0.49	1387	0.65	-0.83	1162	1.01	0.83
1766	0.87	0.19	1585	0.70	-0.58	1384	0.65	-0.82	1159	0.99	0.75

Table S5: Continued

Age AD/BC	Ca/Si	NAO_{TRD}	Age AD/BC	Ca/Si	NAO_{TRD}	Age AD/BC	Ca/Si	NAO_{TRD}	Age AD/BC	Ca/Si	NAO_{TRD}
1156	0.95	0.59	921	0.70	-0.61	683	0.79	-0.18	435	0.91	0.38
1153	0.92	0.42	918	0.69	-0.62	680	0.78	-0.24	432	0.88	0.24
1151	0.93	0.45	915	0.66	-0.75	677	0.78	-0.20	429	0.91	0.38
1148	0.88	0.23	912	0.70	-0.59	674	0.82	-0.04	426	0.90	0.31
1145	0.86	0.15	909	0.67	-0.73	671	0.78	-0.23	423	0.96	0.59
1142	0.90	0.35	906	0.66	-0.78	668	0.79	-0.18	420	0.96	0.62
1139	0.92	0.45	903	0.65	-0.81	665	0.76	-0.31	417	0.95	0.58
1137	0.89	0.27	900	0.65	-0.82	662	0.77	-0.29	414	0.88	0.24
1134	0.88	0.26	897	0.65	-0.80	659	0.77	-0.27	411	0.88	0.24
1131	0.89	0.31	895	0.63	-0.89	656	0.76	-0.30	408	0.88	0.24
1128	0.89	0.27	892	0.59	-1.10	653	0.76	-0.32	405	0.87	0.19
1125	0.93	0.46	889	0.56	-1.23	650	0.76	-0.33	402	0.90	0.31
1122	0.96	0.60	886	0.61	-0.99	647	0.75	-0.37	399	0.86	0.14
1120	0.92	0.43	883	0.64	-0.87	644	0.71	-0.56	396	0.83	0.02
1117	0.89	0.30	880	0.60	-1.03	641	0.70	-0.60	393	0.85	0.10
1114	0.88	0.26	877	0.55	-1.26	638	0.69	-0.61	390	0.89	0.27
1111	0.91	0.40	874	0.54	-1.33	635	0.71	-0.52	387	0.88	0.23
1108	0.94	0.50	871	0.52	-1.44	632	0.71	-0.54	384	0.90	0.34
1106	0.88	0.22	868	0.55	-1.28	629	0.68	-0.69	381	0.91	0.37
1103	0.78	-0.22	865	0.53	-1.35	626	0.66	-0.76	378	0.92	0.41
1100	0.80	-0.15	862	0.60	-1.07	623	0.66	-0.76	375	0.92	0.43
1097	0.85	0.09	859	0.67	-0.71	620	0.68	-0.70	371	0.98	0.68
1094	0.84	0.04	856	0.66	-0.75	617	0.67	-0.71	368	1.01	0.85
1091	0.83	0.03	853	0.67	-0.71	614	0.71	-0.53	365	0.94	0.50
1088	0.83	0.03	850	0.70	-0.58	611	0.76	-0.29	362	0.99	0.77
1086	0.90	0.31	847	1.01	0.83	608	0.69	-0.63	359	0.95	0.56
1083	0.85	0.13	844	1.04	0.99	605	0.72	-0.51	356	0.97	0.67
1080	0.94	0.54	841	1.00	0.82	602	0.67	-0.70	353	0.99	0.74
1077	0.91	0.38	838	1.12	1.37	599	0.68	-0.68	350	1.00	0.80
1074	0.90	0.34	835	1.06	1.08	596	0.73	-0.45	347	0.98	0.69
1071	0.87	0.21	833	1.09	1.20	593	0.73	-0.47	344	0.93	0.48
1069	0.85	0.09	830	1.05	1.00	590	0.69	-0.65	341	0.93	0.46
1066	0.86	0.16	827	1.02	0.88	587	0.71	-0.54	338	0.91	0.38
1063	0.87	0.20	824	1.02	0.90	584	0.81	-0.10	335	0.75	-0.34
1060	0.89	0.30	821	0.91	0.36	581	0.72	-0.50	332	1.04	1.00
1057	0.86	0.16	818	0.95	0.57	578	0.75	-0.35	329	1.04	1.00
1054	0.84	0.06	815	1.01	0.82	575	0.75	-0.38	326	1.02	0.89
1051	0.83	0.02	812	1.04	0.97	572	0.75	-0.33	323	1.02	0.87
1048	0.84	0.05	809	1.06	1.09	569	0.77	-0.26	320	1.03	0.92
1046	0.85	0.10	806	1.07	1.11	566	0.70	-0.58	317	1.00	0.78
1043	0.83	0.01	803	1.11	1.29	563	0.74	-0.42	314	0.94	0.52
1040	0.83	-0.01	800	1.07	1.14	559	0.71	-0.52	311	0.95	0.57
1037	0.82	-0.06	797	1.01	0.83	556	0.71	-0.55	308	0.95	0.55
1034	0.86	0.15	794	1.00	0.79	553	0.72	-0.50	305	0.92	0.41
1031	0.82	-0.03	791	1.01	0.84	550	0.74	-0.39	302	0.91	0.38
1028	0.93	0.46	788	1.02	0.88	547	0.75	-0.34	299	0.93	0.46
1026	0.82	-0.03	785	1.02	0.87	544	0.71	-0.55	296	0.91	0.39
1023	0.90	0.31	782	0.97	0.66	541	0.80	-0.13	293	0.88	0.26
1020	0.84	0.07	779	1.00	0.81	538	0.73	-0.45	290	0.89	0.27
1017	0.84	0.06	776	0.98	0.70	535	0.76	-0.33	287	0.86	0.15
1014	0.83	0.00	773	0.93	0.49	532	0.76	-0.30	284	0.86	0.16
1011	0.82	-0.04	770	0.97	0.65	529	0.87	0.20	281	0.84	0.07
1008	0.84	0.06	767	0.96	0.62	526	0.95	0.54	278	0.84	0.06
1005	0.89	0.29	764	0.96	0.60	523	0.94	0.53	275	0.86	0.16
1002	0.86	0.16	761	0.93	0.48	520	0.94	0.51	271	0.86	0.14
1000	0.88	0.26	758	0.94	0.51	517	0.93	0.48	268	0.78	-0.24
997	0.91	0.36	755	0.95	0.59	514	0.87	0.19	265	0.78	-0.21
991	1.01	0.83	752	0.97	0.66	511	0.85	0.11	262	0.75	-0.34
988	0.81	-0.07	749	0.98	0.70	508	0.87	0.20	259	0.78	-0.23
982	0.86	0.13	746	0.86	0.16	505	0.92	0.41	256	0.77	-0.26
979	0.92	0.41	743	0.86	0.13	502	0.93	0.47	253	0.78	-0.21
976	0.84	0.07	740	0.84	0.08	499	0.93	0.47	250	0.77	-0.28
973	0.80	-0.12	737	0.89	0.30	496	0.95	0.56	247	0.84	0.05
971	0.80	-0.14	734	0.81	-0.08	493	0.95	0.57	244	0.89	0.31
968	0.81	-0.07	731	0.86	0.15	490	0.92	0.44	241	0.83	0.02
965	0.81	-0.10	728	0.85	0.11	487	0.95	0.56	238	0.84	0.08
962	0.85	0.10	725	0.88	0.25	484	0.94	0.53	235	0.84	0.04
959	0.85	0.10	722	0.89	0.27	481	0.92	0.43	232	0.86	0.15
956	0.86	0.14	719	0.88	0.22	478	0.90	0.33	229	0.85	0.13
953	0.84	0.08	716	0.85	0.10	475	0.90	0.34	226	0.89	0.27
950	0.91	0.37	713	0.85	0.09	472	0.88	0.24	223	0.85	0.10
947	0.79	-0.17	710	0.88	0.22	469	0.85	0.11	220	0.85	0.10
944	0.79	-0.19	707	0.87	0.21	466	0.84	0.05	217	0.85	0.09
941	0.77	-0.25	704	0.87	0.20	463	0.87	0.21	214	0.88	0.22
938	0.76	-0.31	701	0.89	0.30	453	0.92	0.43	211	0.86	0.16
936	0.78	-0.21	698	0.87	0.19	450	0.88	0.23	208	0.86	0.14
933	0.79	-0.15	695	0.88	0.26	447	0.94	0.52	205	0.87	0.18
930	0.75	-0.36	692	0.83	0.02	444	0.94	0.53	202	0.86	0.16
927	0.74	-0.41	689	0.80	-0.14	441	0.93	0.47	199	0.87	0.19
924	0.70	-0.61	686	0.79	-0.15	438	0.90	0.32	196	0.85	0.11

Table S5: Continued

Age AD/BC	Ca/Si	NAO_{TRD}	Age AD/BC	Ca/Si	NAO_{TRD}	Age AD/BC	Ca/Si	NAO_{TRD}	Age AD/BC	Ca/Si	NAO_{TRD}
193	0.84	0.07	-46	0.66	-0.77	-277	0.75	-0.35	-497	0.81	-0.08
190	0.82	-0.05	-49	0.64	-0.88	-280	0.75	-0.38	-500	0.80	-0.14
187	0.81	-0.06	-52	0.65	-0.81	-283	0.68	-0.66	-502	0.88	0.25
184	0.77	-0.26	-55	0.65	-0.83	-285	0.66	-0.78	-505	0.85	0.08
181	0.74	-0.39	-57	0.63	-0.89	-288	0.65	-0.82	-507	0.82	-0.06
178	0.73	-0.45	-60	0.63	-0.89	-291	0.71	-0.53	-510	0.81	-0.07
175	0.71	-0.52	-63	0.62	-0.98	-294	0.73	-0.44	-513	0.85	0.09
172	0.73	-0.44	-66	0.62	-0.97	-297	0.71	-0.52	-515	0.82	-0.01
169	0.72	-0.49	-69	0.62	-0.95	-299	0.71	-0.56	-518	0.85	0.09
166	0.74	-0.38	-72	0.62	-0.97	-302	0.72	-0.50	-521	0.77	-0.25
163	0.74	-0.41	-75	0.61	-0.99	-305	0.72	-0.49	-523	0.74	-0.40
160	0.73	-0.46	-78	0.62	-0.97	-308	0.73	-0.44	-526	0.79	-0.16
157	0.74	-0.42	-81	0.62	-0.98	-311	0.76	-0.33	-529	0.80	-0.15
154	0.76	-0.29	-84	0.66	-0.79	-314	0.73	-0.43	-531	0.86	0.14
151	0.75	-0.34	-87	0.73	-0.44	-316	0.72	-0.50	-534	0.86	0.14
148	0.69	-0.63	-90	0.74	-0.40	-319	0.73	-0.47	-537	0.86	0.16
145	0.70	-0.61	-93	0.76	-0.31	-322	0.72	-0.48	-539	0.85	0.08
142	0.66	-0.75	-96	0.77	-0.26	-325	0.63	-0.92	-542	0.84	0.07
139	0.70	-0.59	-98	0.71	-0.54	-328	0.60	-1.07	-544	0.77	-0.25
136	0.73	-0.46	-101	0.68	-0.68	-330	0.58	-1.13	-547	0.72	-0.50
133	0.71	-0.52	-104	0.69	-0.64	-333	0.58	-1.13	-550	0.69	-0.61
130	0.71	-0.56	-107	0.65	-0.82	-336	0.57	-1.18	-552	0.66	-0.75
127	0.70	-0.58	-110	0.69	-0.62	-339	0.56	-1.23	-555	0.68	-0.66
124	0.74	-0.41	-113	0.86	0.15	-341	0.58	-1.16	-557	0.71	-0.56
121	0.74	-0.42	-116	0.85	0.10	-344	0.57	-1.17	-560	0.68	-0.68
118	0.73	-0.44	-119	0.87	0.19	-347	0.57	-1.18	-563	0.68	-0.69
115	0.75	-0.38	-122	0.83	0.00	-350	0.59	-1.10	-565	0.69	-0.63
112	0.75	-0.37	-125	0.86	0.13	-353	0.65	-0.80	-568	0.67	-0.75
109	0.74	-0.42	-128	0.84	0.06	-355	0.62	-0.97	-570	0.69	-0.62
106	0.73	-0.46	-131	0.81	-0.09	-358	0.63	-0.91	-573	0.68	-0.66
103	0.76	-0.31	-133	0.80	-0.11	-361	0.63	-0.89	-576	0.69	-0.61
100	0.79	-0.19	-136	0.85	0.12	-364	0.61	-0.99	-578	0.67	-0.74
97	0.79	-0.18	-139	0.83	-0.01	-366	0.64	-0.88	-581	0.71	-0.55
94	0.74	-0.40	-142	0.71	-0.54	-369	0.63	-0.92	-583	0.75	-0.36
91	0.74	-0.42	-145	0.73	-0.47	-372	0.65	-0.81	-586	0.76	-0.32
88	0.78	-0.21	-148	1.05	1.04	-375	0.67	-0.74	-589	0.67	-0.73
85	0.82	-0.04	-151	0.71	-0.56	-378	0.65	-0.81	-591	0.67	-0.73
82	0.83	0.02	-154	0.77	-0.27	-380	0.62	-0.93	-594	0.70	-0.60
79	0.86	0.15	-157	0.77	-0.26	-383	0.62	-0.97	-596	0.68	-0.68
76	0.86	0.15	-160	0.81	-0.08	-386	0.55	-1.28	-599	0.68	-0.69
73	0.85	0.10	-162	0.79	-0.16	-389	0.63	-0.93	-601	0.68	-0.70
70	0.87	0.19	-165	0.84	0.06	-391	0.64	-0.87	-604	0.65	-0.83
67	0.83	0.00	-168	0.84	0.04	-394	0.62	-0.94	-607	0.67	-0.74
64	0.83	0.02	-171	0.79	-0.18	-397	0.61	-0.98	-609	0.69	-0.64
61	0.82	-0.05	-174	0.84	0.04	-400	0.64	-0.87	-612	0.64	-0.84
58	0.82	-0.02	-177	0.91	0.40	-402	0.64	-0.84	-614	0.64	-0.87
55	0.86	0.16	-180	0.88	0.22	-405	0.62	-0.96	-617	0.67	-0.75
52	0.84	0.07	-183	0.84	0.08	-408	0.61	-1.02	-619	0.65	-0.83
49	0.88	0.23	-186	0.85	0.12	-410	0.62	-0.93	-622	0.63	-0.91
46	0.88	0.26	-188	0.86	0.14	-413	0.61	-0.98	-624	0.80	-0.14
43	0.85	0.08	-191	0.85	0.12	-416	0.57	-1.17	-627	0.74	-0.41
40	0.86	0.15	-194	0.89	0.30	-419	0.63	-0.92	-629	0.67	-0.73
37	0.85	0.12	-197	0.97	0.64	-421	0.65	-0.80	-632	0.64	-0.86
34	0.84	0.04	-200	0.91	0.39	-424	0.57	-1.18	-635	0.64	-0.85
31	0.93	0.49	-203	0.83	0.00	-427	0.54	-1.34	-637	0.62	-0.96
28	0.85	0.09	-206	0.83	-0.01	-430	0.74	-0.42	-640	0.59	-1.11
25	0.81	-0.08	-209	0.85	0.12	-432	0.76	-0.31	-642	0.60	-1.06
22	0.83	0.01	-211	0.80	-0.14	-435	0.74	-0.41	-645	0.60	-1.06
19	0.80	-0.12	-214	0.82	-0.04	-438	0.76	-0.30	-647	0.62	-0.93
16	0.76	-0.30	-217	0.83	-0.01	-440	0.75	-0.37	-650	0.62	-0.96
13	0.81	-0.07	-220	0.83	0.01	-443	0.79	-0.19	-652	0.62	-0.95
10	0.76	-0.31	-223	0.86	0.13	-446	0.76	-0.31	-655	0.60	-1.05
8	0.75	-0.37	-226	0.86	0.15	-449	0.79	-0.17	-657	0.65	-0.84
5	0.78	-0.23	-229	0.86	0.14	-451	0.81	-0.09	-660	0.65	-0.83
2	0.78	-0.24	-231	0.80	-0.11	-454	0.80	-0.14	-662	0.62	-0.93
-1	0.78	-0.24	-234	0.80	-0.11	-457	0.78	-0.20	-665	0.59	-1.07
-4	0.81	-0.09	-237	0.84	0.05	-459	0.77	-0.26	-667	0.64	-0.88
-7	0.78	-0.20	-240	0.82	-0.01	-462	0.78	-0.22	-670	0.60	-1.02
-10	0.78	-0.21	-243	0.81	-0.06	-465	0.79	-0.16	-672	0.62	-0.94
-13	0.75	-0.37	-246	0.79	-0.17	-467	0.79	-0.17	-675	0.64	-0.86
-16	0.78	-0.22	-249	0.82	-0.01	-470	0.84	0.05	-677	0.62	-0.97
-19	0.76	-0.29	-251	0.78	-0.22	-473	0.86	0.14	-680	0.59	-1.11
-22	0.72	-0.49	-254	0.75	-0.36	-475	0.95	0.55	-682	0.59	-1.11
-25	0.74	-0.42	-257	0.76	-0.30	-478	0.81	-0.09	-684	0.61	-1.02
-28	0.79	-0.17	-260	0.74	-0.42	-481	0.83	0.02	-687	0.58	-1.15
-31	0.72	-0.49	-263	0.75	-0.34	-484	0.81	-0.06	-689	0.61	-1.01
-34	0.71	-0.55	-266	0.79	-0.18	-486	0.81	-0.10	-692	0.64	-0.87
-37	0.71	-0.52	-268	0.80	-0.12	-489	0.79	-0.18	-694	0.60	-1.04
-40	0.72	-0.50	-271	0.79	-0.18	-492	0.74	-0.40	-697	0.62	-0.96
-43	0.71	-0.53	-274	0.75	-0.34	-494	0.78	-0.24	-699	0.66	-0.77

Table S5: Continued

Age AD/BC	Ca/Si	NAO_{TRD}
-702	0.64	-0.85
-704	0.65	-0.83
-707	0.69	-0.65
-709	0.74	-0.38
-711	0.70	-0.58
-714	0.73	-0.47
-716	0.74	-0.39
-719	0.77	-0.28
-721	0.72	-0.49
-724	0.69	-0.63
-726	0.69	-0.63
-728	0.68	-0.69
-731	0.68	-0.70
-733	0.63	-0.92
-736	0.70	-0.57
-738	0.70	-0.59
-741	0.73	-0.46
-743	0.73	-0.43
-745	0.72	-0.51
-748	0.71	-0.52
-750	0.69	-0.65
-753	0.68	-0.69
-755	0.70	-0.60
-757	0.70	-0.60
-760	0.71	-0.55
-762	0.76	-0.32
-764	0.73	-0.43
-767	0.75	-0.35
-769	0.75	-0.36
-772	0.77	-0.26
-774	0.73	-0.44
-776	0.73	-0.44
-779	0.77	-0.26
-781	0.75	-0.36
-783	0.81	-0.08
-786	0.74	-0.42
-788	0.72	-0.51
-790	0.71	-0.54
-793	0.72	-0.49
-795	0.75	-0.34